UiT
THE ARCTIC
UNIVERSITY
OF NORWAY

Faculty of Science and Technology

Department of Physics and Technology

Investigation of the ion composition in the topside ionosphere at solar maximum using incoherent scatter technique

—

Maryna Shulha

FYS-3900 Master thesis in Physics May 2016

Investigation of the ion composition in the topside ionosphere at solar maximum using incoherent scatter technique

A Thesis Submitted by:

Maryna Shulha

Master in Physics

Faculty of Science and Technology

UiT The Arctic University of Norway

Supervised by:

Dr. Dmytro Kotov

National Technical University

"Kharkiv Polytechnic Institute"

Ukraine

Prof. Björn Gustavsson

UiT The Arctic University of Norway

Acknowledgments

I would like to thank my supervisor Prof. Björn Gustavsson, for his cooperation and helpful professional advice, which are important to me, as well as for his understanding and patience.

I express my sincere and deep gratitude to my second supervisor Dr. Dmytro Kotov, for the continuous help, which he has given me throughout my work with this thesis, for having shared his extensive knowledge with me, and for the useful tips during the data processing.

I would like to thank the University of Tromsø and all the University staff for the opportunity to study here and for providing me all the facilities that I need in the educational process. In addition, I want to thank all the professors that I met here, for useful and interesting lectures.

Finally, I want to thank my family for their continued support and for believing in me.

Contents

Abstract

The aim of this study was to investigate the altitudinal and diurnal variations of light ion densities in the topside ionosphere during the 23rd and 24th solar maximums. This made it possible to understand the behavior of the ion composition after extended solar minimum and compare how it differs from the preceding solar maximum. The observed variations are compared with estimates of empirical (IRI) and physical (SAMI3) models. All necessary data were obtained at Kharkiv Ionospheric Observatory for the summer solstices during the 23rd and 24th solar cycles.

The observations showed that there are more helium than hydrogen ions in the daytime during the 23rd solar maximum compared to 24th. The relative concentration of H^+ decreases with increasing of solar activity. The O^+ have an opposite behavior to H^+ and He^+ ions: at increasing solar activity, the O^+ concentration increases. The dynamic processes have an effect on the variations of light ions in the upper ionosphere. It is found that variations in the mixing ratio of the three main topside ion species above Ukraine differ both qualitatively and quantitatively from the model variations. The experimental relative concentrations of H^+ and He^+ were much higher than empirical and physical model estimates. There is a somewhat better agreement in the case of O^+ densities. The results obtained in this work can be useful in predicting of variations the relative concentration of H^+, He^+ and O^+ in the upper ionosphere over the Central Europe region.

Chapter 1

Introduction

We live in the period of rapid scientific and technological development. Humans give considerable attention to using of near-Earth space. This stimulates scientists to study near-Earth space, since knowledge about its current state and predictions of its properties is essential for the normal functioning of space technology as well as terrestrial and satellite radio communication. Research of the ionosphere as one of the scientific experiments leads to further development of our understanding the solar-terrestrial relations and near space.

There are large amount works about the theoretical description of processes that occur in the ionospheric plasma and its interaction with the neutral atmosphere and space (e.g. *Akasofu*, 1972; *Brekke*, 2013; *Brunelli*, 1988; *Schunk and Nagy*, 2009; *Ratcliffe,* 1972). As well as about the experimental studies (e.g. *Kotov et.al*., 2012, 2013 and 2015; *King*, 1965; *Bauer*, 1965; *Taran,* 2001; *Truhlik et.al*., 2014; *Bilitza* et.al., 2014; *Huba,* 2008; and many others). The results of these studies contribute to the creation of a global system for monitoring the ionosphere. In this system, ionospheric measurements coordinated with the help of special radar facilities from various regions of the world (see chapter 4).

One of the powerful methods of radio physics is the method of incoherent scattering (IS). This technique uses radio waves with frequency much higher than typical ionospheric plasma frequencies. This makes possible to obtain information from the ionosphere both at low altitudes and at heights above 1000 km. At high altitudes, the study of altitudinal and temporal variations of light ion densities in the plasma become important. The results of such investigations lead to better understanding of the interaction between the ionosphere and the plasmasphere (*Krinberg*, 1984) which has a significant effect on the state and behavior of the ionosphere and the Earth-atmosphere-ionosphere-magnetosphere system as a whole (*Chernogor*, 2007).

The hydrogen ions, H^+, play an important role in the processes that have an effect on the state of the ionosphere. These are the lightest ions (their weight is 16 times less than mass of atomic oxygen ions O^+ and 4 times less than the mass of helium ions, He^+). Further, their altitudinal and temporal variations are significantly affected by dynamic processes (ambipolar diffusion, neutral winds), which are responsible for plasmasphere - ionosphere interaction (see chapter 3). In addition to dynamic processes, chemical processes in the ionosphere also have significant effects. Further, one of the most important interaction processes in the ionosphere - plasmasphere system is the process of charge exchange between oxygen ions (atoms) and hydrogen atoms (ions). The vertical

distribution of electron density N_e is affected by all processes, which have a noticeable effect on the ion composition near the height of peak electron density and above. Therefore, reliable results about an experimental observation of variations O^+ and H^+ are important. These results make it possible obtain a qualitative assessment of the effectiveness of chemical and dynamical processes in the upper ionosphere under different space weather conditions (*Brunelli*, 1988; *Kotov et al*., 2012).

The study of altitudinal, latitudinal, and temporal variations of helium ions is also an important and interesting. A lot of attention was devoted to the investigation of He^+ in the following works: *Craven et al.,* 1995; *Wilford*, 2001; *Raitt, Schunk and Banks*, 1978; *Taylor et al*., 1969, and *Bauer*, 1965. As a result, of these studies, some explanations were suggested for the effect of helium ions on the temperature in the topside ionosphere and plasmasphere. Further, the changes of temperature in the ionosphere can significantly affect the profile variation of electron density. Thus, the electrons and the main ions of the upper ionosphere He^+, O^+, H^+ are coupled. Therefore, reliable information about the ion composition is important, not only for creating of models the ion composition, but also for creating a model of the electron density in the ionosphere.

There are global models of ion composition developed by *Triskova et al.*, 2003 which are based on a wide range of ground-based and satellite data. Those models are good in a statistical sense but for any given time the deviation from true values might be significant (about a factor of 2 for F-region). As a result, estimates of ion concentrations will be obtained with significant errors. Thus, the reliability of the data is low and remains a subject of discussion (*Kotov et al.,* 2012 and 2015). Here, it is also worth to note that the results of many experimental studies using measurements from satellites and incoherent scatter radars reveal a significant dependence of ion composition in the upper ionosphere with not only the season, time of day or changes in solar activity but also with a location (latitude and longitude). For high-latitude, midlatitude and equatorial upper ionosphere, the main characteristics of ion composition can vary significantly. As a result, in the analysis even small averaging over latitude will observe completely different processes that occur in the ionosphere. Thus, the experimental study of spatial and temporal variations the relative concentrations H^+, He^+ and O^+ in the midlatitude region of the ionosphere and scientific explanation of these variations are relevant.

The current solar maximum follows the last prolonged and extreme solar minimum of 2006 – 2009, which led to significant changes in the geospace environment (*Heelis et.al.*, 1990 and *Aponte et al.,* 2013). During this period, the upper atmosphere was notably cooled (*Solomon et al.,* 2010). Additionally, the current solar maximum is remarkably less than it was during the preceding solar maximum. It is interesting to compare the observed altitudinal and diurnal variations in the fractions of O^+, H^+, and He^+ during the 23rd and 24th solar maximums. This will make possible to understand how, after extended solar minimum, the behavior of ion composition differs from the variations at preceding solar maximum.

Thus, the objective of this project is the investigation of diurnal and seasonal variations in the fractions of the three main topside ion species (atomic oxygen, O^+, hydrogen, H^+, and helium, He^+) using Kharkiv incoherent scatter radar (KISR) data for the 23rd and 24th solar maximums, comparative study of these variations with empirical

(IRI) and physical (e.g., SAMI3) models, and attempting to find the explanation of the possible differences between observations and models.

The objects of investigation are processes in the ionospheric plasma in the altitude range of 300 - 1000 km above Ukraine.

The subject of investigation is the daily variation of the relative concentrations H^+, He^+ and O^+ during the 23rd and 24th solar cycles.

The method of investigation includes performing ion composition measurements using ISR of Institute of Ionosphere (Kharkiv, Ukraine), data processing, and analyzing the observations. The data for both 23rd and 24th solar maximums have been processed by the specialized software package 'UPRISE' developed in Institute of Ionosphere (*Bogomaz*, 2013). Additionally, in the calculations was used the mathematical editor Matchad, and for visualization of the experimental results was used the graphic software package SigmaPlot. During data processing from the physical model SAMI3 was used the Matlab script (see appendix A), which was written to get color plots of daily variations the relative concentrations of He^+, H^+, and O^+. The empirical (IRI) and physical (SAMI3) models have been used for calculations, which aimed to the better understanding features of observation results.

The results of this work show that characteristics of ion composition above Ukraine significantly differ from estimates of modern ionospheric models. Thus, the obtained results can be used for creating of regional model of ion composition of the upper ionosphere. This model will much better explain the real state of the ionosphere for the mid-latitude region.

Chapter 2

Background

2.1 The importance of ionospheric research

A lot of attention is given to investigation the ionosphere as a component of the solar-terrestrial system, which also includes the Sun, solar wind, magnetosphere, and atmosphere. This is due to the rapid development of radio satellite communication, GPS navigation systems, exploration of space and radio astronomy. The development of scientific research and communication equipment allows us to study the ionosphere on a qualitatively new level. The object of this thesis is not only ionosphere as a medium of radio wave propagation, but also as a medium wherein there are many various physical processes.

The ionosphere is very sensitive to magnetic and electric fields as well as to effects of particle flows. Under the influence of solar radiation, cosmic rays and particles from the radiation belts of the magnetosphere, ionization occurs in the upper atmosphere, which leads to plasma formation. Its main composition, density and temperatures depend on the time of day, season, altitude, solar activity, state of the magnetosphere and geographic coordinates. Therefore, the ionosphere can be used for diagnostic surveillance and monitoring of not only external cosmic effects but also internal processes, which have a terrestrial, causes (anthropogenic effects).

Due to the above-mentioned processes, the ionosphere is a dynamic and variable region of the atmosphere. Depending on its state the absorption and refraction radio waves are changed, and others effects that may have an impact on modern communication system, mobile communication, navigation, and satellite systems (*Hargreaves*, 1995).

The ionosphere is the ionized region of Earth's upper atmosphere, which extends from 50 km (where the plasma starts to have a significant influence on the propagation radio waves) to about 1000 km (which is the somewhat arbitrary transition to the magnetosphere). Its behavior and composition primarily depend on the daily cycle of solar electromagnetic radiation at short wavelengths, which cause ionization, and, at high latitudes depend on dissipation of energy from the magnetosphere (*NASA,* 1980). The ions, which are produced by chemical reactions with neutral atoms and recombine with electrons, are carried to higher or lower altitudes by transport mechanisms such as neutral winds and diffusion. Especially, the transports processes strongly depend on the Earth's magnetic field (*Schunk and Nagy*, 2009).

2.2 The general structure of the ionosphere

The ionosphere is typically separated into several layers (see Fig. 2.1). The F-layer is highest, with the highest electron density. It starts at 150 km, extends to ~1000 km where it transitions to the plasmasphere, and is the focus of this report thesis. The *F-region* is partly ionized because at these altitudes the neutral density is still significant and it has the peak electron density at altitudes of 150 − 250 km (F_1-region) and 250 − 500 km (F_2-region).

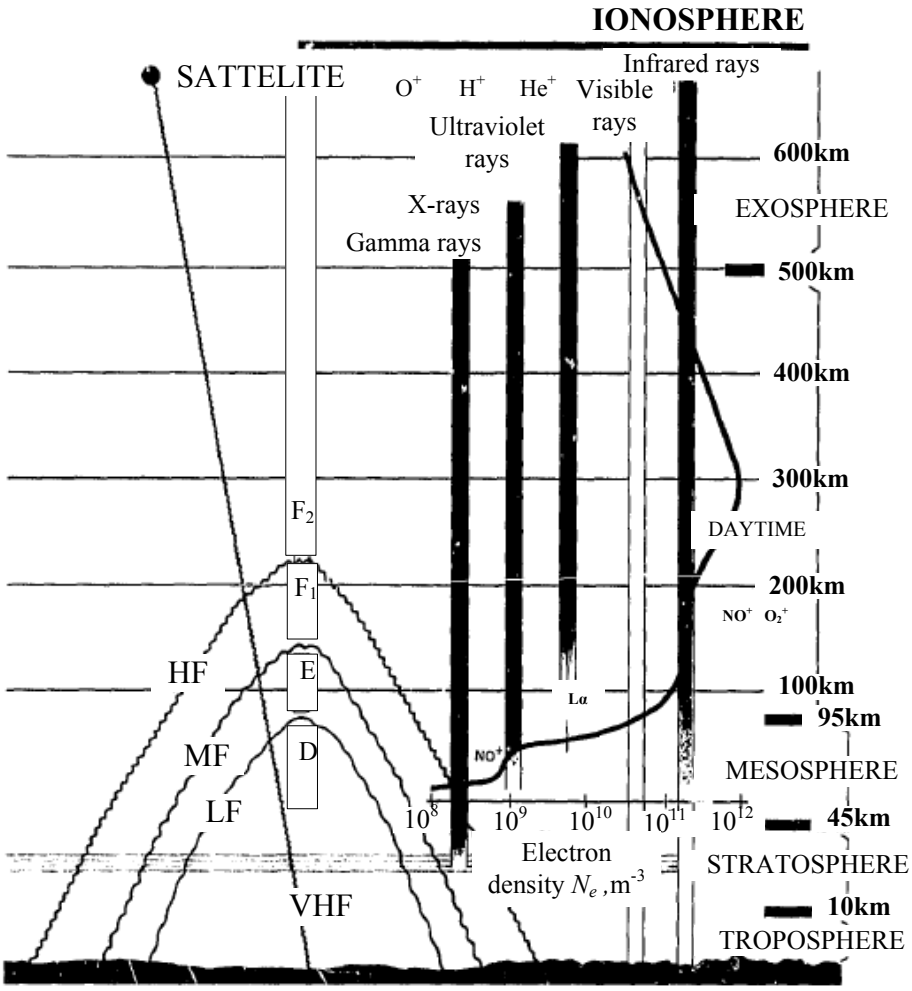

Figure 2.1 Ionospheric layers associated with the altitude profile of the electron density in the (Figure from *NASA*, 1980).

The first maximum (F_1-region) is clearly observed only in the daytime during the summer months, the concentration of electrons there reaches about 10^{11} m^{-3}. Here, in addition to photochemical reactions the density and composition are affected by charge exchange between ions and atoms. Gradually toward higher altitudes, transport processes affect them. The maximum electron density in the F_2-region is about 10^{12} m^{-3} and the neutral density is about 10^{14} m^{-3} (*Schunk and Nagy*, 2009). In this region, the competing processes of photo-ionization, chemical losses and plasma transport determine the height

of peak electron density and its decrease toward higher altitudes. Usually, F_2-region has larger electron density than F_1-region. At night, F_1-region disappears, but F_2-region remains. The plasma produced around the F-region peak is transported up and down by diffusion and drift, so the highest concentration of electrons and ions are concentrated at the altitudes of 250 − 400 km. In addition, the ion composition of F-region depends on solar activity. For example, the role of He^+ becomes dominant during high solar activity, while under low activity the main components of the ionospheric plasma above the electron concentration maximum are O^+ and H^+ (*Gonzalez et al*., 1992).

The topside ionosphere starts at the F-region peak. Above 150 km, atomic oxygen ions, O^+, are more abundant and may dominate even up to 600 km and higher. However, this will depend on magnetospheric and solar conditions (*Brekke*, 2013). Continuing upward, we come to the photosphere or plasmasphere where hydrogen ions, H^+, are the dominant species and there are small amounts of helium ions He^+. Transport processes control the plasma density profiles in this region (*Schunk and Nagy*, 2009).

One of the important features of the F-region is its ability to reflect radio waves, which makes it possible to transmit short-wave radio signals over long distances. The temperature of the ionosphere is mainly controlled by the absorption of solar radiation in the thermosphere. During the ionization of molecules and atoms, photoelectrons have high energy and heat the ambient electrons. Since electrons have lower mass than ions, they will have a larger mobility and heat conductivity and their elastic electron-ion and electron-neutral collisions practically lead to no loss energy. Ions are heavier and collide with neutral particles, thereby giving them most of their energy. As a result, the temperature of electrons, T_e, will be higher than neutral atoms, T_n, and less mobile ions, T_i (*Brekke*, 2013). Also worth to mention, that due to the strong dependence on solar radiation, the ion and electron temperatures strongly vary by day, season and solar activity.

The *E-region* is located at an altitude range 100−150 km and plays an essential role in the propagation of short and medium waves. In this region, the electron density increase to 10^{11} m^{-3} during daytime. The main source of ionization is the EUV radiation. The recombination of ions in this region is very fast and, at night, the ion density decreases. To this process counteract, at first, the diffusion of charged particles from the F-region where the ion concentration during this period is still relatively high and secondly, sources of the nighttime ionization (these include the geocoronal scattering of solar radiation, meteors, and cosmic rays). Dominant ions in this region are NO^+, O_2^+, and N_2^+.

The *D-region* is lowest and located at altitude range 60 − 90 km. Ionization here occurs mainly due to an impact of the solar X-rays, as well as additional weak ionization sources: cosmic rays and meteors. This region is characterized by a sharp decrease of ionization at night. During daytime, the electron concentration reaches $10^8 - 10^9$ m^{-3} and at night this region disappears. There are dominant molecular ions in this region NO^+, O_2^+ and neutral particles N_2, O_2, and O. Additionally, there are negative ions, whose concentration can exceed the concentration of electrons lower than 75 km).

To summarize this section it can be noted that the ionospheric research is important. Since in order to understand the evolution of the atmosphere we need to know how it is

coupled to the ionosphere, likewise, we need to understand the coupling between the ionosphere and the magnetosphere to understand the physics of the inner magnetosphere (and both require improved understanding of the ionosphere). A global network of incoherent scatter radar has been developed by which has made it possible to observe spatial and temporal variations of ion composition, temperature and plasma flow at the altitude range of 100 − 1000 km.

Near-Earth Space also can be studied by satellite, sounding rockets, and radio-propagation methods. The scientific output from such observations is increased when complemented with observations from incoherent scatter radars due to spatial and temporal coverage. An example of this is that in the latest decades, data about the topside ionosphere have become demanded in practical purposes because of rapid development global models of the near-Earth environment, which describe and predict the state of "space weather". Here it is worth to mention the development of international models for the neutral atmosphere, MSIS, and ionosphere, IRI. They are based on the results of satellite measurements and data of incoherent scatter radars from all over the world. At the same time, information about composition and dynamics of the ionosphere that was obtained more than for 30 year history of measurements by the incoherent scatter radars constantly exposed to a new analysis with the aim of identification the global long-term variations of parameters the ionosphere above the electron density peak.

Chapter 3

Effects of dynamic and chemical processes on the distribution of O^+, H^+, and He^+

3.1 The dynamics of the ionosphere

A lot of attention is given to theoretical and experimental studies of dynamic processes through programs of geophysical and space research. Such knowledge about dynamics of ionized and neutral components is necessary both for constructing models of the upper atmosphere and for determining the physical nature of the interaction between atmospheric layers, and further, for solving such applied objectives as radio wave propagation and design of the aerospace equipment.

In particular, it should be noted that interaction of neutral and ionized components determines features of the ionosphere dynamic. The presence of even a few ions causes noticeable "ion deceleration" of neutral particles motion that, in its turn, affects the spatial and temporal distribution of ionization (*Kazymyrovsky*, 1973). Therefore, a joint solution both transport and continuity equations lead to the explanation of many phenomena in the ionosphere.

The complexity and variability of the dynamic processes and ambiguous interpretation of observation results lead to the fact that our knowledge about the upper ionosphere is far from complete. Therefore, for improvement our understanding of the topside ionosphere it is important to study features of dynamic processes such as neutral winds, a drift of ionized components of ionospheric plasma, and the ambipolar diffusion.

3.2 The effects of neutral winds in the ionosphere

Ionospheric winds usually refer to the movement of the neutral atmosphere. Time-scales of large-scale neutral wind patterns range from a few hours to several days. It depends on variability processes of uneven heating and cooling of the atmosphere The possible impact of diurnal variations the electron density and ion composition on F - region neutral winds was first addressed by (*King* et al., 1965).

The main parameters that determine nature of the neutral wind are pressure distribution and temperature changes of atmospheric gases. Due to the presence of differential pressure, which is caused by the uneven solar heating of two region of the atmosphere, occurs transfer process of air from the high-pressure area to the low-pressure region. There are both vertical and horizontal movements of the

neutral gas. In the ionosphere, it leads to plasma transfer by neutral wind (V_n), since there is significant coupling between the neutral particles are trapped and electrons (*Akasofu*, 1972).

Numerous observations by incoherent scatter radars (e.g. *Salah et al.,* 1974) have shown that meridional horizontal wind in the daytime (and partly zonal due to the differences in geographic and magnetic poles), usually is directed toward the poles (forcing the plasma) but at night toward the equator (see Fig 3.1). On the night side, the wind velocity can reach 200 – 300 m/s. On the dayside, it decreases due to large plasma density since the neutral particles lose energy in collisions. The wind velocity in this period typically reaches 50 – 100 m/s (*Akasofu*, 1972).

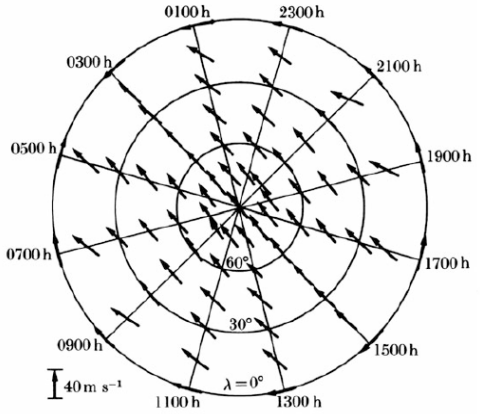

Figure 3.1 The inferred wind system at altitude 300 km, which is based on the temperature distribution by *King et al.,* 1965.

The neutral wind also has an effect on the vertical motion of plasma. Neutral particles transfer horizontal momentum to the charged particles (predominantly ions). This leads to vertical drift up or down (3.1) since the charged particles gyrate around the Earth's magnetic field lines (see Fig. 3.2).

$$V_{d.up(down)} = V_n \cdot \cos I \tag{3.1}$$

Here, V_n is the neutral wind velocity, I is angle to the horizontal plane (*Evans*, 1975).

Figure 3.2 shows that during daytime the neutral winds create a vector component of motion charged particles, which is directed downwards, where there are larger loss rates. Herewith a height of peak electron density is also shifted downwards to the area with high loss rates of O^+ ions. At nighttime, a component of vector motion due to horizontal neutral winds is directed upward where recombination is reduced. Further, in the F_2-region ion-molecular reactions including O^+ are much slower than at low altitudes. Thus, the daytime F_2-region is lowered by winds, while the nighttime F_2-region is raised. This mechanism is essential for the maintenance of the nighttime F_2-region (*Salah et al.,* 1974).

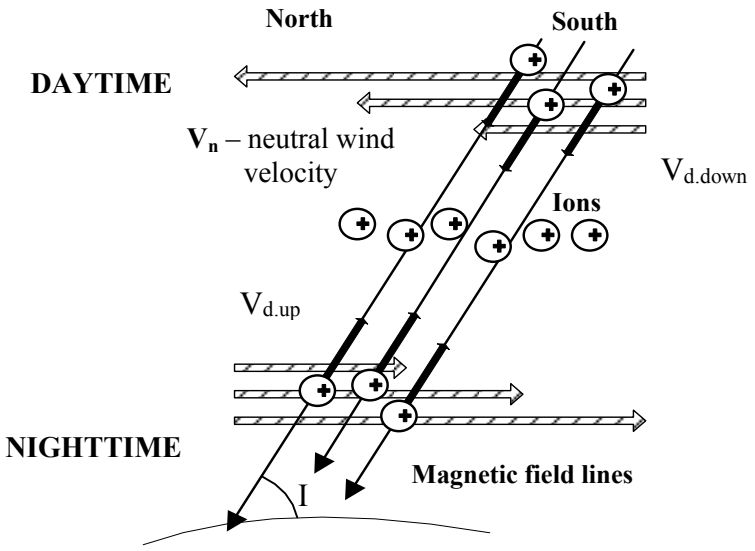

Figure 3.2. The influence of the neutral wind velocity V_n on the ion drifts along the magnetic field lines (during daytime and nighttime).

To summarize this section, note that neutral winds play an important role for the diurnal variation of the F_2-region as well as for the existence of the ionosphere after sunset. In addition to that, changes in density and chemical composition of the neutral atmosphere, which have an influence on the ion composition and electron density in the ionosphere, also have an influence on the behavior of neutral and charged particles in the plasmasphere and magnetosphere. This underlines the fact that knowledge about various features (diurnal variation, for example) of neutral winds are essential and valuable for an explanation behavior of charged particles in the ionosphere (including investigated in this work light ions) as well as for understanding of dynamic processes and improvements in the results of modeling the F-region.

3.3 Effect of the diffusion process on the ionospheric parameters

Mid-latitude ionospheric plasma transport is caused both by convection and by diffusion. At altitudes below of 200 km, all charged components are in photochemical equilibrium that leads to a continuous increase of charged particles with height. However, above 200 km, the photochemical reaction rates decreases and diffusion increases. At some altitudes, diffusion and photochemistry are comparable but with further increase of altitude, the diffusion process is the dominant mechanism. Depending on which process dominates, the height of maximum electron density shifts downward or upward. During daytime, it shifts downward closer to Earth and at night moves upward (see Fig. 3.3).

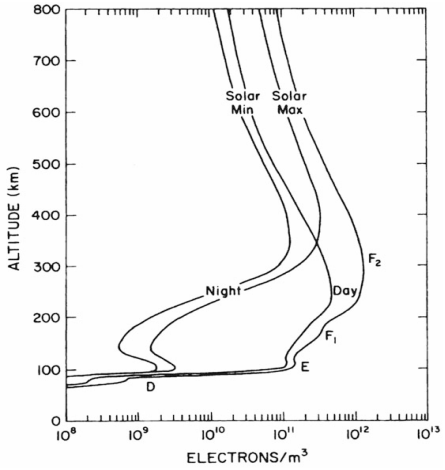

Figure 3.3. Typical mid-latitude ionospheric electron density profiles for sunspot maximum and minimum conditions at daytime and nighttime. The different altitude regions in the ionosphere are labeled with the appropriate nomenclature by *Richmond*, 1987 (Figure from *Brekke,* 2013).

3.3.1 Ambipolar diffusion

Ambipolar diffusion in the ionosphere is a joint diffusion of oppositely charged particles in weakly ionized plasma with a significant density gradient toward the region of low density. This process is negligible at altitudes below 200 km. In this region (if we consider the steady state), the chemical time constant for ions is determined by reaction of loss rates l_i:

$$\tau_{\text{chem}} = \frac{n_i}{l_i} \tag{3.2}$$

where n_i is the ion concentration constituent. Then, the diffusion time constant for ions will be:

$$\tau_{dif} = \frac{H^2}{D_i} \tag{3.3}$$

where H is the scale height representing the ion constituent and D_i is the diffusion coefficient, which depends inversely on the collision frequency v (*Bauer*, 1965).

At higher altitudes, the diffusion rate is very dependent on the density of neutral particles in the atmosphere. The diffusion rate increases with decreasing neutral density. Due to lower l_i at these altitudes, τ_{chem} will increase with altitude, whereas τ_{dif}, which depends directly on the collision frequency of ions with neutral particles, will decrease with altitude. At some height, the characteristic time of diffusion is equal to photochemical reactions and at higher altitudes diffusion dominates. Therefore, below this height, the ionosphere is in a chemical equilibrium, and above, in a diffusive equilibrium.

3.3.2 Dynamics of plasma diffusion without and with effect of magnetic field

For the ionosphere at steady state, there will be no net acceleration of plasma, so momentum equations for ions and electrons are:

$$n_i m_i \frac{\partial w_i}{\partial t} = -\frac{\partial p_i}{\partial h} - n_i m_i g + n_i eE - n_i m_i \nu_i w_i = 0 \tag{3.4}$$

$$n_e m_e \frac{\partial w_e}{\partial t} = -\frac{\partial p_e}{\partial h} - n_e m_e g + n_e eE - n_e m_e \nu_e w_e = 0 \tag{3.5}$$

where ν_i and ν_e are the electron and ion collision frequencies with the neutrals, respectively, w_i and w_e – are vertical ion and electron velocities (these velocities describe motion of charged particles which is caused by charge separation of electrons and ions). Summing equations (3.4) and (3.5), moving the collision terms on the left-hand side, and taking to account the ideal gas law ($p = n_j \cdot k_B \cdot (T_i + T_e)$):

$$n_e(m_i\nu_i + m_e\nu_e)w = -k_B(T_e + T_i) \cdot \frac{\partial n_e}{\partial h} - n_e(m_i + m_e)g = 0 \tag{3.6}$$

Here, T_e and T_i are temperatures of electrons and ions respectively; k_B is the Boltzmann constant; w is the plasma flux; m_i and m_e are massed of ions and electrons respectively; h is a height; g is the gravitational constant.

Since the mass of ions is greater than the mass of electrons ($m_i >> m_e$) we can solve for flux of plasma:

$$n_e w = -\frac{k_B(T_e + T_i)}{(m_i\nu_i + m_e\nu_e)}\left(\frac{\partial n_e}{\partial h} + \frac{n_e m_i g}{k_B(T_e + T_i)}\right) \tag{3.7}$$

Here, the first factor on the right-hand side of (3.7) is the plasma *ambipolar diffusion coefficient* D_a. At steady state, there is no net vertical flux of plasma, so equation (3.7) should be equal to 0. That can be achieved if: $\frac{\partial n_e}{\partial h} = -\frac{n_e m_i g}{k_B(T_e + T_i)}$, where the plasma scale height is:

$$H_p = \frac{k_B(T_e + T_i)}{m_i g} \tag{3.8}$$

For $m_i\nu_i >> m_e\nu_e$ using the approximation $T_e \simeq T_i$ and assumption $n_i \simeq n_e$, the diffusion coefficient D_a a factor of 2 larger than the neutral diffusion coefficient. And velocity of joint diffusion is determined generally by the less mobile ions (see 3.9). However, if $T_e \neq T_i$, plasma diffusion will strongly depend on the electron-ion temperature ratio.

$$D_a = \frac{k_B(T_e + T_i)}{(m_i \nu_i + m_e \nu_e)} \approx 2D_i \qquad (3.9)$$

Due to quasi-neutrality of plasma ($n_e \approx n_i$), ions and electrons can not diffuse independently. Minor deviations from quasi-neutrality lead to charge separation and large electric fields $\vec{E}$, which prevent further separation of charges. Since, the mass of electrons m_e is much smaller than ions m_i, the speed of their thermal motion V_e will be higher than V_i. Consequently, the slow and heavy particles reduce the motion of faster particles and move upwards together in the direction of decreasing density (see Fig.3.4).

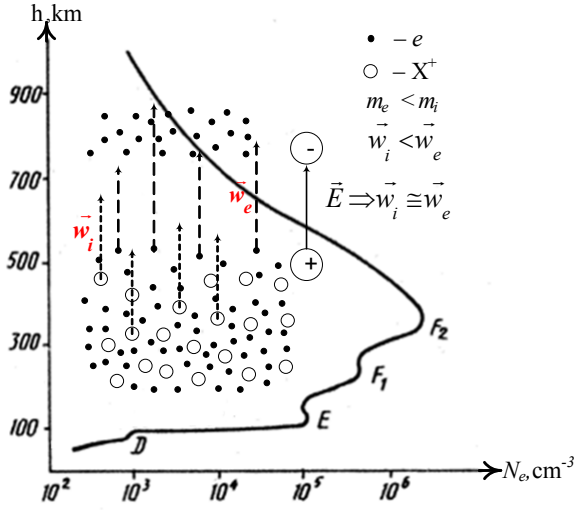

Figure 3.4. The scheme of appearance the ambipolar diffusion process.

If diffusion coefficients of particles with opposite charges are very different, the deceleration of fast electrons by slow ions leads to faster diffusion than the slowly diffusing particles, and slower diffusion than the diffusion of fast particles. In the case of no magnetic field or parallel to $\vec{B}$, we get (3.9). For diffusion transverse to the magnetic field, the ion diffusion coefficient is much larger (because of the larger cyclotron radius) and ambipolar diffusion coefficient is equal to two times the diffusion coefficient of electrons (*Frank-Kamenetzky*, 1975).

The magnetic field has a weak effect on the plasma motion along of it. Diffusion rate parallel to $\vec{B}$ typically much larger than transversally. Interestingly that ambipolar diffusion transverse to $\vec{B}$ increases with collision frequency, while along $\vec{B}$ it decreases (*Chen,* 1984).

3.4 Factors that control the ion distribution

The evolution of ion densities in the upper ionosphere is described by the continuity equation:

$$\frac{\partial n_i}{\partial t} = q_i - l_i - \nabla \cdot (n_i \cdot \mathrm{v}_i) \tag{3.10}$$

Here, q_i is the production rate, l_i is the loss by chemical and photochemical processes, and the last term on the right-hand side $\nabla (n_i \cdot \mathrm{v}_i)$ is the convection term, which is the source or loss of ions due to transport, v_i is the convection velocity (*Brekke*, 2013).

At steady-state condition (dn_i/dt=0) for the continuity equation (3.10), there are two limiting cases:

1) *Photochemical equilibrium:* $q_i = l_i$ (production proceeds due to photoionization process and losses are due to chemical reactions);
2) *Diffusive equilibrium*: $\nabla \cdot (n_i \cdot \mathrm{v}_i) \approx 0$.

3.4.1 Oxygen ions

Since the main neutral species at F-region altitudes is the atomic oxygen O, above 200 km (i.e. in the F_2-region) the dominate ions is O^+ (see Fig. 3.5) and $n_e \simeq n_{O+}$. In "quasi-chemical" photoequilibrium by neglecting convection term in the continuity equation (3.10) will be (see *Brunelli*, 1988):

$$\frac{\partial n_e}{\partial t} = \frac{\partial (\mathrm{O}^+)}{\partial t} = q_{\mathrm{O}^+} - l_{\mathrm{O}^+} \tag{3.11}$$

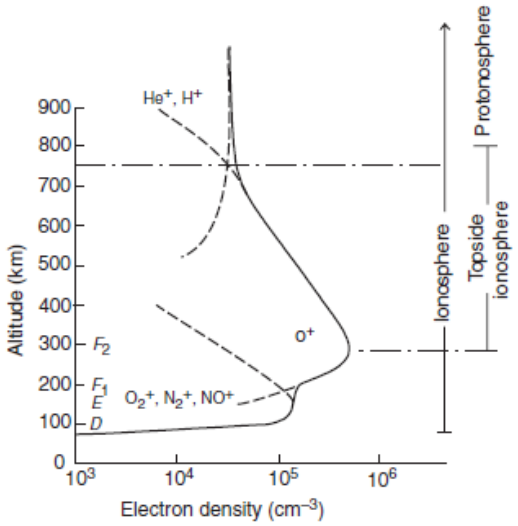

Figure 3.5. The ion density profiles for the daytime mid-latitude ionosphere (Figure from *Schunk* and Nagy, 2009).

O^+ ions in their turn will disappear in the ion-electron and ion-molecular reactions (3.12 – 3.14):

$$O^+ + e \xrightarrow{\alpha_r} O + h\nu \tag{3.12}$$

$$O^+ + N_2 \xrightarrow{k_1} NO^+ + N \tag{3.13}$$

$$O^+ + O_2 \xrightarrow{k_2} O_2^+ + O \tag{3.14}$$

where $\alpha_r = 7.8 \cdot 10^{-14} \sqrt{(\frac{T_e}{300})}$ (m^3/s) is the radiative recombination coefficient, $k_1 = 2 \cdot 10^{-18}$, $k_2 = 2 \cdot 10^{-17} (\frac{T_r}{300})^{-0.4}$ (m^3/s) are the chemical reaction rates. It is obvious, that k_2 is an order of magnitude larger than k_1, but the concentration of N_2 on the altitudes of F_2-region more than O_2. Thus, the contribution of reaction (3.13) near the ionospheric maximum will be the main loss process. Reaction (3.12) is quite slow in contrast to the ion-molecular reactions (3.13) and (3.14). For steady-state conditions, equation (3.11) simplifies:

$$q_{O^+} = l_{O^+} = n_{O^+} \cdot [k_1 \cdot n_{N_2} + k_2 \cdot n_{O_2}] \tag{3.15}$$

It is well known (e.g. *Brekke*, 2013, p. 212) that the continuity equation for electrons simplifies to:

$$q_{O^+} = \frac{k_1 \cdot n_{N_2} + k_2 \cdot n_{O_2}}{1 + \frac{k_1 \cdot n_{N_2}}{\alpha_1 \cdot n_e} + \frac{k_2 \cdot n_{O_2}}{\alpha_2 \cdot n_e}} \cdot n_e \approx \beta \cdot n_e \Rightarrow n_e = \frac{q_{O^+}}{\beta} \tag{3.16}$$

where β – is the effective loss rate.

At altitudes above 200 km q_{O+} decreases proportionally to the concentration of atomic oxygen that is $q(h) \sim \exp(-\frac{h}{H_O})$ (where $H_O = k_B T_n / m_O \cdot g$) and β decreases proportionally to concentration of molecular nitrogen $\beta(h) \sim \exp(-\frac{h}{H_{N_2}})$ (where $H_{N_2} = k_B T_n / m_{N_2} \cdot g$). Since β (h) decreases faster with altitude than q, the electron concentration neglecting transport effects would be (see *Ratcliffe*, 1972):

$$n_e(h) = \frac{\exp(-h/H_O)}{\exp(-h/H_{N_2})} = \exp\left[\frac{m_{N_2} - m_O}{k_B T} \cdot h \cdot g\right] \tag{3.17}$$

Equation (3.17) indicates that the electron concentration (as the atomic oxygen ions) increases with height. Since this is not the case, it shows that transport effects have to be taken in to account.

3.4.2 Hydrogen ions

According to the barometric law, heavier molecules and ions have shorter scale-height than lighter, therefore, the mixing ratio of light ions increase with height. The region, where H^+ and He^+ ions are dominant, is called the protonosphere (or plasmasphere) (*Akasofu*, 1972). The height of the transition from predominantly O^+ to H^+ is usually considered as the beginning of the plasmasphere (Fig. 3.5).

The main source of H^+ is not photoionization of neutral hydrogen atoms, which is a rather slow process. It is the charge exchange process between hydrogen atoms, H, and O^+. The H^+ source and loss reactions are (*Schunk and Nagy,* 2009):

$$O^+ + H \xrightarrow{k_f} O + H^+ \tag{3.18}$$

$$H^+ + O \xrightarrow{k_r} H + O^+ \tag{3.19}$$

where k_f and k_r are the forward and reverse reaction rates ($cm^3\,s^{-1}$) ($k_f = 4.3 \cdot 10^{-11} \sqrt{(T_n + \frac{T_i}{16})}$, $k_r = 2.2 \cdot 10^{-11} \sqrt{(T_i + \frac{T_n}{16})}$), and T_n, T_i is the temperatures of neutral atmosphere and ions respectively.

The protons, which formed during daytime, diffuse upwards and fill the magnetic flux tubes. At nighttime, when the ionization processes in the ionosphere are slow down, both electron density and temperature of charged particles decrease. This, in turn, lead to decreasing plasma pressure at the base of magnetic flux tubes, leading to flux of hydrogen ions from the plasmasphere, and a corresponding increasing the relative concentration of hydrogen ions at heights close to F_2-region and the topside ionosphere (*Akasofu,* 1972). Thus, in the region of the closed geomagnetic field lines the plasmasphere represents the reservoir of plasma filled during daytime and emptied during nighttime.

From chemical equilibrium (applicable below ~500 km), reactions (3.18) and (3.19) lead to a H^+ altitude variations (*Bauer*, 1964):

$$n_{H^+} = \frac{9}{8} \cdot \frac{n_{O_+}\, n_H}{n_O} \sqrt{\frac{T_n}{T_{H^+}}} \tag{3.20}$$

Due to exponential altitude variation of neutral atoms and O^+, equation (3.20) leads to increasing H^+ density:

$$n_{H^+} \propto \exp(\frac{h}{H_7}) \tag{3.21}$$

where h is the geopotential height, H_7 is the height scale of particles with effective mass 7 a.u.m.

In the diffusive equilibrium (when the diffusion velocity v_i=0) the distribution of H^+ (as for He^+) we can write (*Bauer*, 1964):

$$n_{H^+} = n_{0(X^+)} \exp - \left\{ \left[\int_{h_0}^{h} \left(m_{X^+} - \frac{T_e}{T_i + T_e} m^+ \right) \frac{g_0}{k_B T_i} + \frac{\partial\ (T_i + T_e)}{\partial h\ (T_i + T_e)} \right] dh \right\} \tag{3.22}$$

where $n_{0(X^+)}$ is the concentration at the initial height h_0, g_0 is acceleration of gravity at this height, h is the geopotential height, $m^+ = \sum_{i=1}^{n} \frac{n_{X^+}}{n} m_{X^+}$ is the average mass of a mixture of ions, X_i^+ is the ion of i-type.

Analyzing (3.20) (3.22) it worth to note that for T_e=T_i in the diffusion equilibrium $n(H^+)$ increases with altitude where these ions are minor components among the dominant O^+ (see formula 3.22 and Fig. 3.6) and slowly decrease in the region where hydrogen ions are the main ion species (*Bauer*, 1965):

$$n_{H^+} \propto \exp(-\frac{h}{H_{1/2}}) \tag{3.23}$$

In addition, for helium in the diffusive equilibrium:

$$n_{He^+} \propto \exp(-\frac{h}{H_2}) \tag{3.24}$$

where $H_{1/2}$, H_2 are the height scales for particles with effective masses 0.5 and 2 a.u.m.

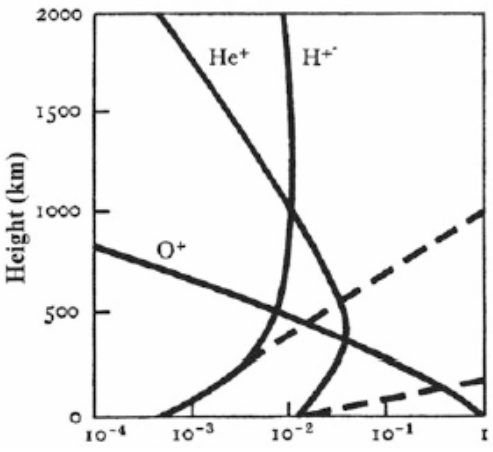

Figure 3.6. Relative ion concentration profiles below 2,000 km altitude for a mixture of H^+, He^+, O^+ and electrons in diffusive equilibrium for isothermal conditions with T_e=T_i 1200 K. The dashed lines correspond to conditions where photochemical equilibrium is predominant (Figure from *Ratcliffe*, 1972).

3.4.3 Helium ions

One of the characteristics of the ionosphere is that there is a continuous upward diffusion of light atoms H and He. They chemically interact with other components of the ionosphere and are produced photoionization of neutral helium and lost due to charge transfer reactions with molecular atmospheric constituents (O_2 and N_2) (*Bauer,*1965):

$$He^+ + N_2 \xrightarrow{k_7} He + N^+ + N \tag{3.25}$$

$$He^+ + O_2 \xrightarrow{k_8} He + O^+ + O \tag{3.26}$$

The chemical equilibrium distribution for He^+ is given by:

$$n_{He^+} = \frac{Q_{He} \cdot n_{He}}{k_7 \cdot n_{N_2} \cdot k_8 \cdot n_{O_2}} \tag{3.27}$$

Here, $Q_{He} = 3 \cdot 10^{-8}$ sec^{-1} is the ionization rate coefficient for helium, $k_7 = 7.8 \cdot 10^{-10}$ (cm^3 sec^{-1}), $k_8 = 9.7 \cdot 10^{-10}$ (cm^3 sec^{-1}) (*Schunk and Nagy*, 2009). As well as for hydrogen the concentration of helium ions will be:

$$n_{He^+} \propto \exp^{\frac{h}{H_{24}}} \qquad \text{if } k_7 \cdot n_{N_2} >> k_8 \cdot n_{O_2}, \tag{3.28}$$

$$n_{He^+} \propto \exp^{\frac{h}{H_{28}}} \qquad \text{if } k_8 \cdot n_{O_2} >> k_7 \cdot n_{N_2} \tag{3.29}$$

The behavior of helium ions from formulas (3.28) and (3.29) shown in Fig. 3.6.

Chapter 4

Instrumentation and method

4.1 Introduction

The possibility to explore the state of the ionosphere based on the analysis of electromagnetic waves scattered on free electrons was experimentally tested and verified in the late of 1950s. The incoherent scatter method gives simultaneous observation of ionospheric parameters for long time periods and with wide altitude coverage. The main parameters of observation are electron density (N_e), ion and electron temperatures (T_i, T_e), plasma drift velocity (V_d), and ion composition. Their altitudinal and temporal dependencies make it possible study heating and cooling of ionospheric plasma, photochemical reactions between electrons, ions, and neutral particles during natural and artificial perturbations in the ionosphere. This method can be used for measurements both above and below the maximum of electron density. Further, the existing radar equipment provides measurements up to 4000 km where, for example, the Incoherent Scatter Radar Facility at Arecibo (Puerto Rico) makes observations using a 300 m diameter antenna (*Isham*, 2000). Thus, IS method gives the researcher an opportunity to observe and learn the evolution of atmospheric and ionospheric processes in a wide range of altitudes from troposphere to exosphere for all geophysical conditions.

4.2 Incoherent scatter theory

In contrast to ionosondes, which measure signals reflected from the ionosphere the method of incoherent scatter uses signals at frequency f_0, typically above 50 MHz, which are significantly higher than the critical frequency of the ionosphere f_{cr}. At such frequency, the transmitted signals will pass through the ionosphere almost without reflection (*Evans*, 1969).

The physics of scattering process is that when the electromagnetic wave interacts with each electron, some energy of the wave is scattered in all directions including in the opposite direction to this wave (see Fig. 4.1). Due to incoherent scattering from many electrons, the energy, which is scattered by each of them, just add together.

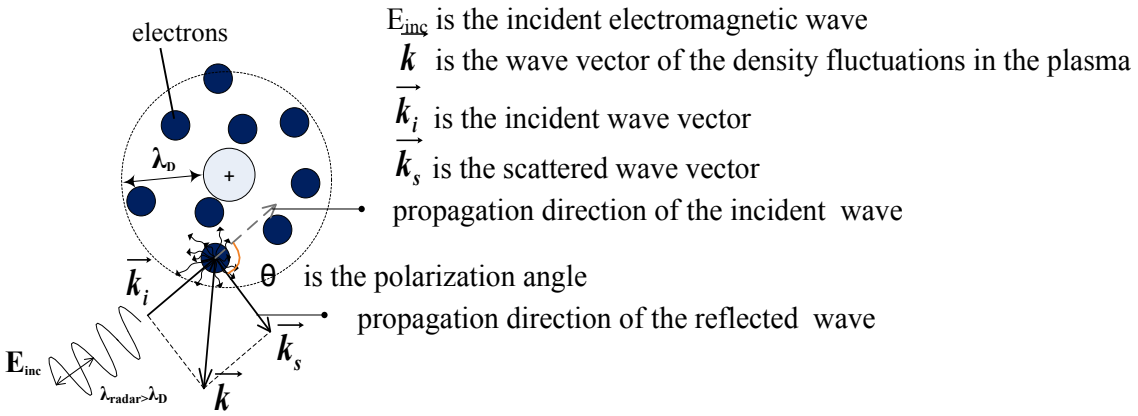

Figure 4.1. Scattering of radio waves with a wavelength $\lambda_{radar}>>\lambda_D$ (here λ_D is the Debye length) on the ionospheric irregularities.

Scattering of radio waves with wavelength in the range of decimeter to meter waves depends on plasma density fluctuations, which are caused by the collective thermal motion of ions and electrons. Due to Coulomb interactions of ions and electrons, there are both ion-acoustic (IAW) and plasma waves in the ionospheric plasma. The ion-acoustic waves are similar to sound waves and propagate with a velocity close to the thermal velocity of major ions. Such plasma waves create density enhancement and depletion (see Fig. 4.2). Radio waves are scattered on these weak inhomogeneities if the Bragg condition is $\lambda_{IAW} = \lambda_{ISR}/2$ which gives the maximum backscatter.

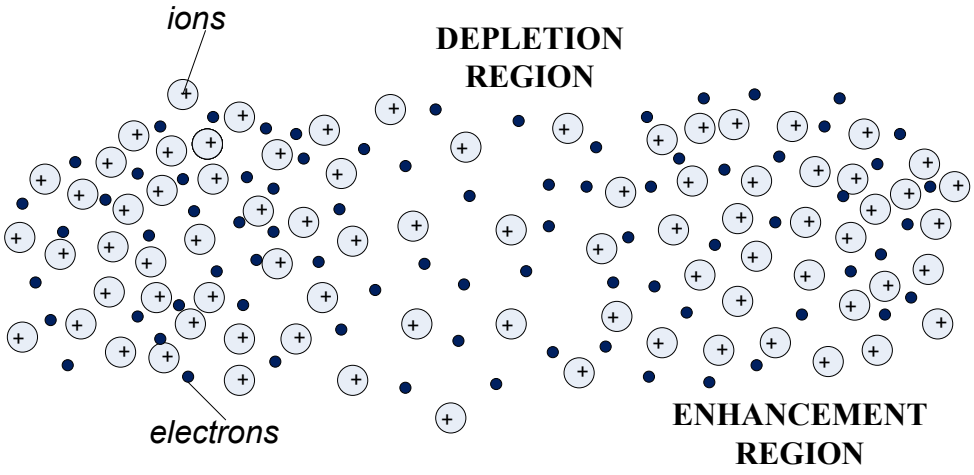

Figure 4.2. Depletion and enhancement density in the plasma.

The radar measures the power of the back-scattered signal from each height interval, which can be converted into the vertical electron density profile (*Evans*, 1969). In addition, estimates of the power density spectrum of the back-scattered signal are obtained. It contains information about the ionospheric plasma. Further, information is extracted from this spectrum or from the autocorrelation function of the received signal,

which is the Fourier transform of the power spectrum how it will be described in section 4.4.

From the theory of plasma physics for Maxwellian plasma distribution conditions the total shape of power density spectrum is composed by two partial spectra's are the electron part and the ion part (see eq. 4.1). Most of the research with incoherent scatter radars utilizes the ion part of spectrum because the plasma lines are more difficult to observe (*Nygren,* 1996).

$$S(\vec{k},\omega) = S_{plasmaline}(\vec{k},\omega) + S_{ionline}(\vec{k},\omega) \tag{4.1}$$

where k is the wave vector, ω is the wave angular frequency

Assuming that electrons and ions in the ionosphere have the Maxwellian velocity distribution, but are characterized by different temperatures, the shape of the ion component of the spectrum will change depending on ionospheric parameters, including the electron to ion temperature ratio T_e/T_i and the ion mass m_i (He^+, H^+, O^+ for our research). The total velocity distribution function for ions in the ionospheric plasma (*Nygren,* 1996):

$$f_{iM}(v) = \left(m_i \big/ 2\pi k_B T_i\right)^{3/2} \exp^{\frac{-(v^2)}{2v_{th}{}^2}} \xrightarrow{for\ v^2 = v_x{}^2 + v_y{}^2 + v_z{}^2} = \left(m_i \big/ 2\pi k_B T_i\right)^{3/2} \exp^{\frac{-m_i(v_x{}^2 + v_y{}^2 + v_z{}^2)}{2k_B T_i}} \tag{4.2}$$

where $v_{th.i} = \sqrt{k_B T_i / m_i}$ is the thermal velocity for ions, m_i is the ion mass, k_B is the Boltzmann constant, T_i is the ion temperature, v is the ion velocity.

Here it is worth to mention, the faster moving of charged particles and higher their temperature, the wider spectrum. Analyzing the last equation is possible to see that the higher T_i, the wider the ion-line spectrum. Due to effect of ion mass, the spectrum is also changed. Decreasing of ion mass, in its turn, leads to a widening of the spectrum. It means that ions with lower mass scatter less power than heavy ions from the same amount of plasma volume. Therefore, the narrower spectra originate at lower altitudes where the average ion mass is larger and the wider spectra at high altitudes. Figure 4.3 shows typical power spectra from the ionosphere.

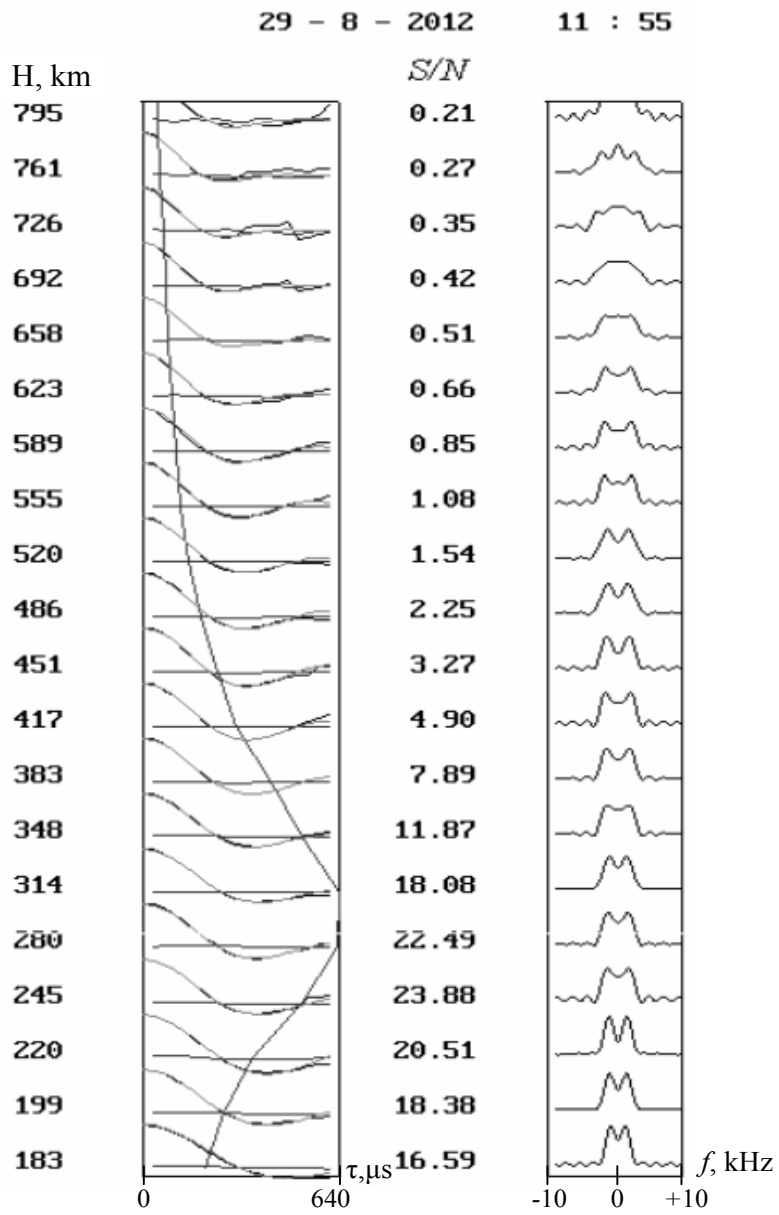

Figure 4.3. The estimation results of ionospheric parameters. Data were obtained by Kharkiv incoherent scatter radar (Figure from *Bogomaz et al.,* 2013).

4.3 Kharkiv Ionospheric Observatory facilities

Kharkiv Incoherent Scatter Radar of Ionospheric Observatory of the Institute of Ionosphere is located 50 km to the south-east from Kharkiv (geographic coordinates: 49.676°N, 36.292°E, geomagnetic coordinates: 45.48°N, 110.29°E). It is the only IS radar in mid-latitude Europe. The capacity and performance of this radar is comparable to the other IS radars around the world. This is one of the four (among more than the dozen existing) IS radar systems in the world which regularly measure the ion composition of the topside ionosphere. The other three radars with such capabilities are (Jicamarca, Peru; Arecibo, Puerto Rico, and Millstone Hill, USA. However, they are located in regions with significantly different geomagnetic coordinates and parameters of McIlvain (*Taran*,

2001). The main characteristics and coordinates of this radar are presented in table 4.1. Consequently, the respective volumes of magnetic flux tubes ($V_m \approx 2/3 \cdot R_e \cdot L^4$) over Jicamarca, Arecibo, and Millstone Hill are: 15 times less, 6 times less and 2.5 times more respectively. Further, the ion distribution in the ionosphere above these radars is considerably different from the situation over Kharkiv radar (*Krinberg*, 1984 and *Brunelli*, 1988).

IS radars	Geographical coordinates	Geomagnetic latitudes	McIlwain L-parameter (at height of 500 km)
Jicamarca, Peru	11.6°S, 76.53° W	1.86°S	1.1
Arecibo, Puerto Rico	18.3° N, 66.7° W	27.82°N	1.4
Millstone Hill, USA	42.6° N, 71.5° W	51.31°N	2.76
Kharkiv, Ukraine	49.6° N, 36.3° E	45.48°N	2.19

Table 4.1. The location of IS radars which explore the ion composition in the upper ionosphere

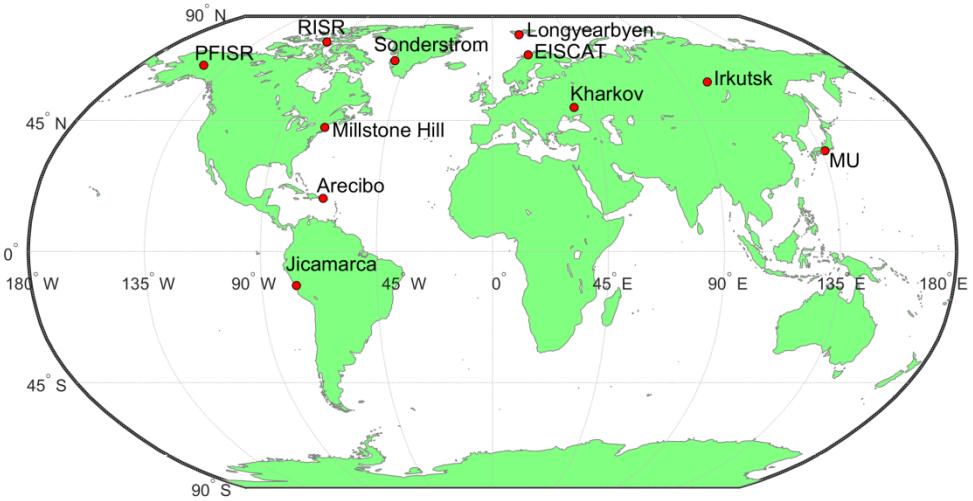

Figure 4.4. Locations of existing incoherent scatter radars.

4.3.1 Kharkiv incoherent scatter radar

The Ionospheric Observatory facilities include VHF IS radar, which is equipped with a 100 m diameter parabolic Cassegrain antenna with a fixed pointing to zenith. The main parameters of the IS radar are as follows: the operating frequency is about 158 MHz, the effective aperture of the 100 m antenna is about 3700 m^2, the half-power antenna beam width is close to 1.3°, the peak pulse power of the transmitter is up to 3.6 MW and the average power is 100 kW, pulse repetition frequency is 24.4 Hz, and the polarization is circular or linear. The noise temperature of the receiver is 120 K and the receiver bandwidth is 11 – 19 kHz. The investigated altitude range is 100 – 1500 km (*Emelyanov*, 2013). Block diagram of IS radar is shown on Fig. 4.5.

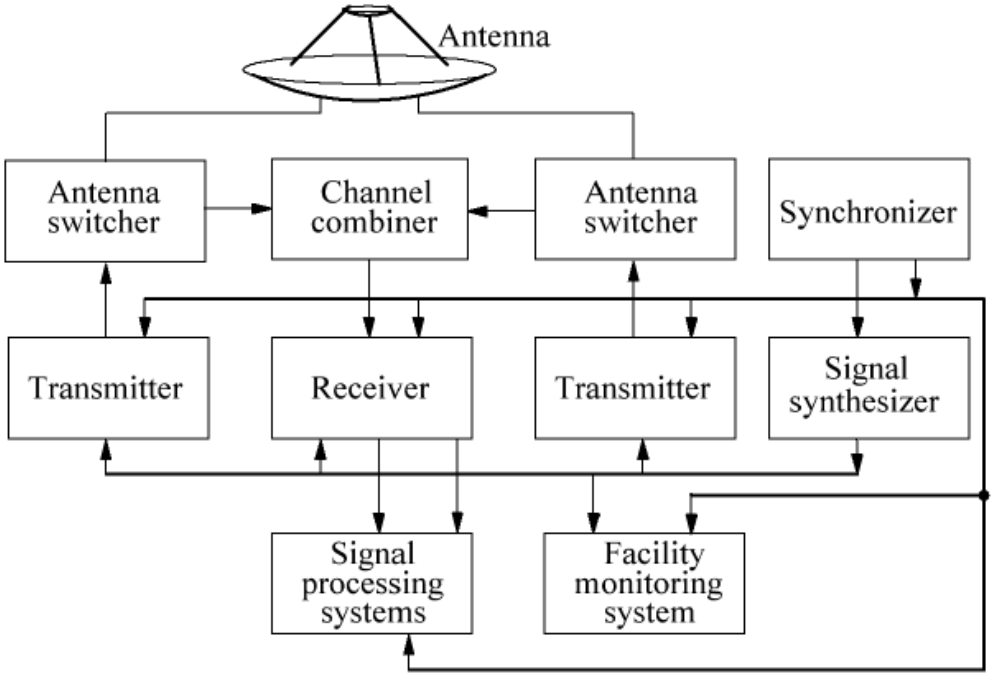

Figure 4.5. Block diagram of KISR ionosphere (Figure from *Domnin et al,* 2014).

Kharkiv IS radar can operate in the following modes (*Rogozhkin et al.,* 2008):

- sounding with a single long pulse with duration time, T_p = 800 μs, for measuring parameters of the topside ionosphere and the ionosphere at the altitudes close to the peak of the ionospheric F-region with altitude resolution 120 km;
- sounding with a cyclic sequence of double pulses (T_p= 65 – 135 μs) with variable delay between pulses from one pulse to another. This mode was actively used during the 23rd solar cycle including the investigated in this work dates: July 01 – 02, 2000 and June 15 – 17, 2004 (see chapter 6);
- sounding with a signal of pulse duration T_p= 135 μs for determination of the electron density.

Since 2006, the main mode of the IS radar operation is radio sounding of the ionosphere using composite two-frequency radio pulse which allows us to improve the resolution of the IS signal parameters measurements. The composite signal is formed by two radio pulses of long duration $T_1 \approx 660$ μs (in July, 2000 and June, 2004 a pulse with T ≈795 μs) was used and short duration $T_2 \approx 135$ μs (see Fig. 4.6). The carrier frequencies for the first pulse, f_0, is 158 MHz and for the second, f_1, is (158 + 0.1) MHz. As a result of receiving and processing of the first signal scattered in the ionosphere, the electron density, the electron and ion temperatures, the vertical component of the plasma velocity, and the ion composition are measured for the altitudes near the peak of the ionospheric F region and in the upper ionosphere (*Emelyanov*, 2013). In the measurement mode of the ion composition in the topside ionosphere the receiver bandwidth of the filter is 9.5 kHz (*Domnin et al.,* 2014).

The specialized correlator of radar gives 19 estimates of the autocorrelation function (ACF) of IS signal with time delays of $\Delta\tau \approx 30$ μs. The autocorrelation functions accumulated with a time-period of one minute are recorded in files with the step of height, which corresponds to the delays step: $\Delta h = c\Delta\tau/2 \approx 4.58$ km. Until 2006, ACF estimations of IS signal which were obtained for the same delays were recorded with the step of height $4\Delta h \approx 18.33$ km. Returned signal from the second pulse element allows us to determine the power of IS signal at heights of 100 to 550 km with altitude resolution 20 km from which the electron density profile is determined. Polarization of both pulse elements is circular (*Rogozhkin et al.,* 2008).

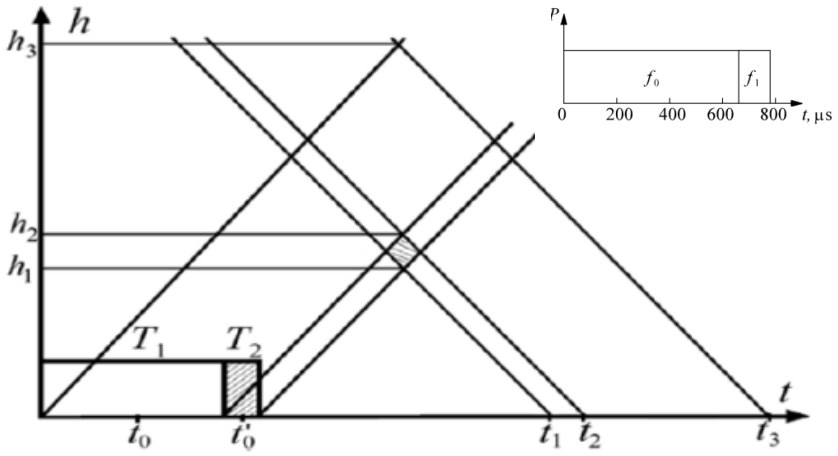

Figure 4.6 The range-time diagram for sounding using composite two-frequency radio pulse (Figure from *Chernyak,* 2013).

4.3.2 The fully steerable VHF IS radar

The effective aperture of the 25-meter antenna is about 290 m^2, the half-power antenna beam width is close to 5.1°. This radar is used to study the dynamics and wave disturbances of the ionosphere. Sometimes the two radars are used simultaneously. This method allows researchers to investigate the spatial structure of the ionosphere over Ukraine, to measure the full vector velocity of the ionospheric plasma motion, and to study the traveling ionospheric disturbances effects in the ionosphere in detail (*Domnin et al.,* 2014).

4.3.3 Ionosonde "Bazis"

The "Bazis" ionosonde is used for calibration of the incoherent scatter radar and for determination the basic parameters of the ionosphere (electron density and critical frequency f_{cr}). The peak electron density, $n_{e,}$ can be calculated from the equation for the ionospheric critical frequency (see (4.3) and (4.4)) (*Emelyanov,* 2011):

$$f_{cr} = \frac{1}{2\pi}\left(\frac{n_e \cdot e^2}{m_e \cdot \varepsilon_0}\right)^{1/2} \tag{4.3}$$

$$n_e \approx 1{,}24 \cdot 10^{10} \cdot f_{cr}^{\ 2} \tag{4.4}$$

Typical value of f_{cr} for ionospheric plasma is 2 −10 MHz.

The main technical characteristics of the "Bazis" ionosonde are as follows as: the operating frequency range in vertical sounding mode is 1− 20 MHz; a number of operating frequencies is 400, pulse repetition frequency is 100 Hz, pulse duration is 100 μs, peak power of transmitter is not less 15 kW, receiver sensitivity is 15μV, the investigated altitude range 100 – 400 km. Transmitting and receiving antennas are identical with orthogonal orientation. Each antenna consists of two rhombs, which work alternately. The large rhomb has frequency range of 0.3 to 7 MHz and for small is 7 − 40 MHz.

4.4 Practical features of ion composition measurements using the IS method

Usually, for research of the ionosphere by the method of incoherent scatter the power spectrum of the backscattered signal is received. It shows the received power per frequency unit (*Nygren*, 1996). The autocorrelation function, which is the Fourier transform of the power spectrum, also carries the information about the ionospheric plasma (see Fig. 4.7).

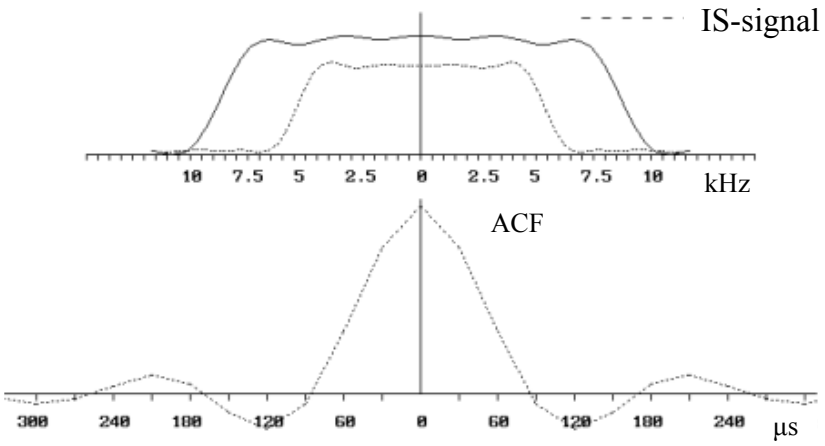

Figure 4.7 Power density spectrum and ACF of the backscattered signal.

The density fluctuations in plasmas with Maxwellian velocity distributions give backscattered signal with power spectra:

$$S(\theta) = \frac{Nr_e^2}{\Omega_0} \frac{|y_e|^2 \sum_n \eta_n \operatorname{Re}(y_{i,n}) + \left|\sum_n \mu_n y_{i,n} + j\gamma^2\right|^2 \operatorname{Re}(y_{i,n})}{\left|y_e + \sum_n \mu_n y_{i,n} + j\gamma^2\right|^2} \frac{1}{\pi\theta} \tag{4.3}$$

where r_e is the classical electron radius; $\theta = \omega/\Omega_0$; ω is the angular frequency; $y_e(\theta_e) = j[1-\theta_e G(\theta_e)]$ and $y_i(\theta_i) = j[1-\theta_e G(\theta_e)]$ are the conductivity functions for electrons and ions, respectively, in the absence of ion-neutral collisions when the angle between the wave vector and the magnetic field is zero; $\theta_e = \omega/\Omega_e$, $\theta_i = \omega/\Omega_i$; $\Omega_e = \frac{4\pi}{\lambda_0}\sqrt{\frac{2\kappa T_e}{m_e}}$, $\Omega_i = \frac{4\pi}{\lambda_0}\sqrt{\frac{2\kappa T_i}{m_i}}$; κ is the Boltzmann constant; m_e , m_i are the masses of electrons and ions respectively; $G(\theta) = j\sqrt{\pi}\exp(-\theta^2) + 2F(\theta)$, $F(\theta) = \exp(-\theta^2)\int_0^\theta \exp(t^2)dt$; $\gamma^2 = \left(\frac{4\pi D}{\lambda_0}\right)^2$, D is the Debye length; $\eta_n = \frac{N_n}{N}$, N_n is the ion concentration of the n-th ion species; $\mu_n = \eta_n\beta$, $\beta = T_e/T_i$. The frequency Ω_0 is the angular frequency normalized to Ω_i for the ion with the smallest mass. In our case this is hydrogen ion H^+ with a.u.m =1.

According to Wiener – Khinchin theorem the Fourier transformation of spectrum is the ACF that makes it possible to calculate theoretical ACF of incoherent scatter signal:

$$R(\tau) = \int_0^\infty S(\theta)\cos(\theta\Omega_0\tau)d\theta \tag{4.4}$$

This equation makes it possible to determine the electron density, n_e, the temperatures of ions, T_i and electrons, T_e, and ion composition (including the relative concentrations of H^+, O^+, and He^+ ions) for a height of the peak electron density and above. These parameters are obtained by solving the inverse problem of radiophysics. Since analytical solution of the inverse problem of radiophysics applied to the method of incoherent scatter does not exist, the solution is a result of comparison of the experimental ACF, $R_{exp}(\tau)$, with each of theoretical functions, $R_{theor}(\tau)$ (which were pre-calculated for the possible combinations of ionospheric parameters) using least-square fitting. The values of the main parameters of the plasma for the theoretical ACF, which has the best agreement with the experimental ACF, may be considered as estimates of measured ionospheric plasma parameters

4.5 Processing of data

The ion composition measurements have been performed during the 23^{d} and 24th solar maximums by using IS radar of Institute of Ionosphere (Kharkiv, Ukraine). During the processing, we used the specialized software package UPRISE (Unified Processing

of the Results of Incoherent Scatter Experiments) developed at the Institute of Ionosphere. The basic features and functions of this software are described in the following section.

4.5.1 Introduction to Kharkiv IS radar data format and the new specialized software package UPRISE

The incoherent scatter radar data processing should be divided into logical stages, which are performed in sequence:

- data filtering (eliminating of interferences of various nature);
- in-painting the pieces of data which correspond to removed interferences;
- calculation the ACF of noise and the received IS signal;
- accounting for hardware characteristics of the radar;
- time averaging of ACF the received IS signal;
- correction of the altitude power spectrum profile of IS signal;
- altitudinal averaging of ACF the received IS signal;
- calculation of ionospheric plasma parameters (ion and electron temperatures, ion composition, plasma velocity).

The *automatic filtering* of data is necessary for elimination of coherent noises (i.e. reflections from satellites and space debris). There are other types of interference in the received signal (impulse noises and spikes) which are more difficult identify and remove. Therefore, they must be filtered by hand. *In-painting of cut out segments* of data is done in two stages. At first, segments with cut out data are interpolated by smooth functions (B-splines of the third degree). Then noise is superimposed which has a normal distribution and standard deviation that corresponds to the average variance of data left and right from the considered data fragment. One of the procedures of *accounting for hardware characteristics of the radar* is the accounting of the transfer characteristic of dischargers which are part of the radar antenna switch. *Temporal averaging of data* is made by the moving average method. Typically the averaging for 5, 15, 30, 45, 60 min with shifts of 1, 2, 3, 5, 15 min is performed. *Correction of vertical profile* of the back-scattered power caused by using long pulses duration (T_n = 663 μs and 795 μs). The meaning of this algorithm is finding such theoretical power distribution which passing through the mathematical model of the measurement channel gives the result which corresponds to the experimental results. Further, the mathematical model of the measuring channel must consider the features of incoherent scattering process and all instrumental characteristics (shapes of the impulse response of the receiver and the envelope of sounding signal). Both *the altitudinal averaging* ACF IS signal and *the temporal averaging* allow reducing noise in the ACF estimates (*Kotov*, 2013).

4.5.2 Data processing using software package UPRISE

The software package UPRISE was written in C and Free BASIC languages. In addition to programs and support files of the software package, which have been included in the installation, the package UPRISE requires libraries of the theoretical auto-correlation functions of IS radar signal. Library of ACF files can be installed on any local disc that has enough free space, 70 GB (*Bogomaz*, 2012).

The libraries of autocorrelation functions were calculated for quasi-optimal steps of the independent parameters: step for the relative density of helium ions $N(He^+)/N$ is 1% (in the range of 0 to 40%), step for the relative density of hydrogen ions $N(H^+)/N$ is 0.5% (in the range of 0 − 100 - $N(He^+)/N$, %), step for ion and electron temperatures is 10 K (in the range of 500 − 4000 K). For different copies of the software package UPRISE one copy of the ACF libraries is enough.

The software package UPRISE includes a set of programs, which implement the main processing stages (*Kotov*, 2013):

- *01_UPRISE_view.exe* is the program for overview and filtering. The working window, before and after filtering, is shown in Fig. 4.8.
- *02 _UPRISE_viewSNew.exe* and *UPRISE_viewSOld.exe* are used for new and old data, respectively.
- *03_UPRISE_processingSNew.exe* and *UPRISE_processingSOld.exe.* The processing of the filtered data is performed according to a time of accumulation, a step of the moving window, interpolation, and trapezoidal summation.
- *04_UPRISE_estimate.exe.* The estimation of ion and electron temperatures and ion plasma composition is performed.

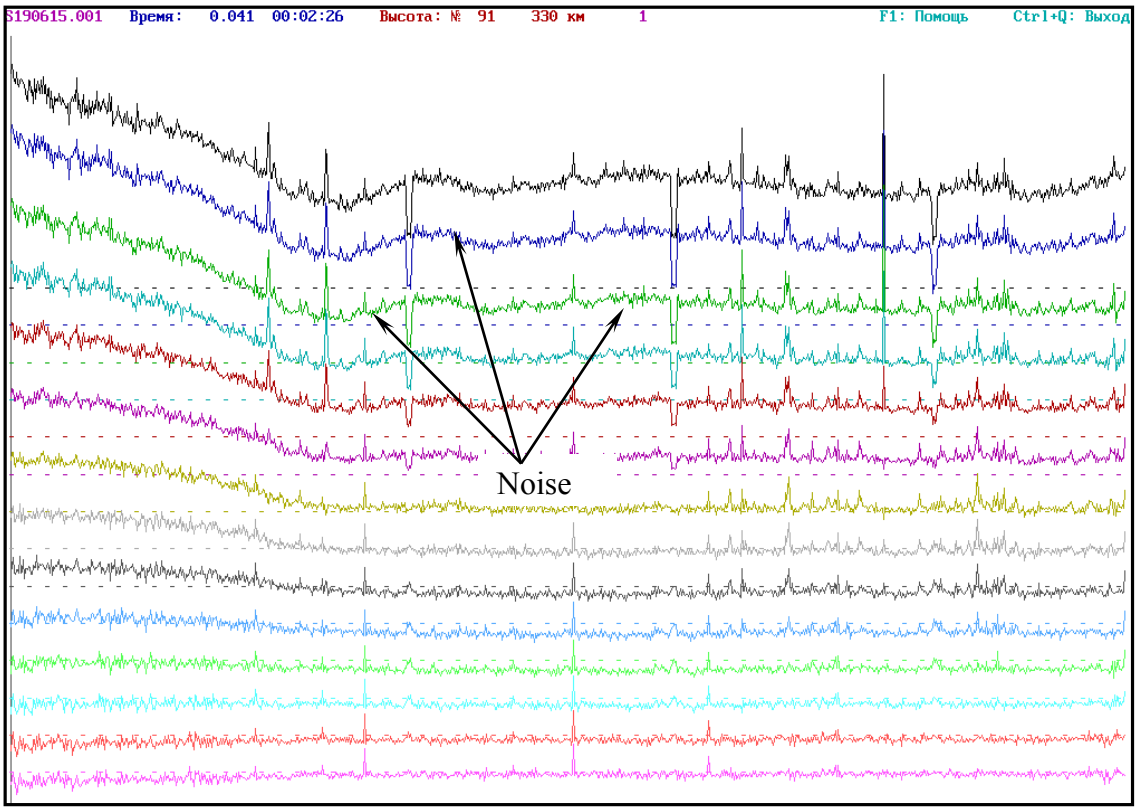

a

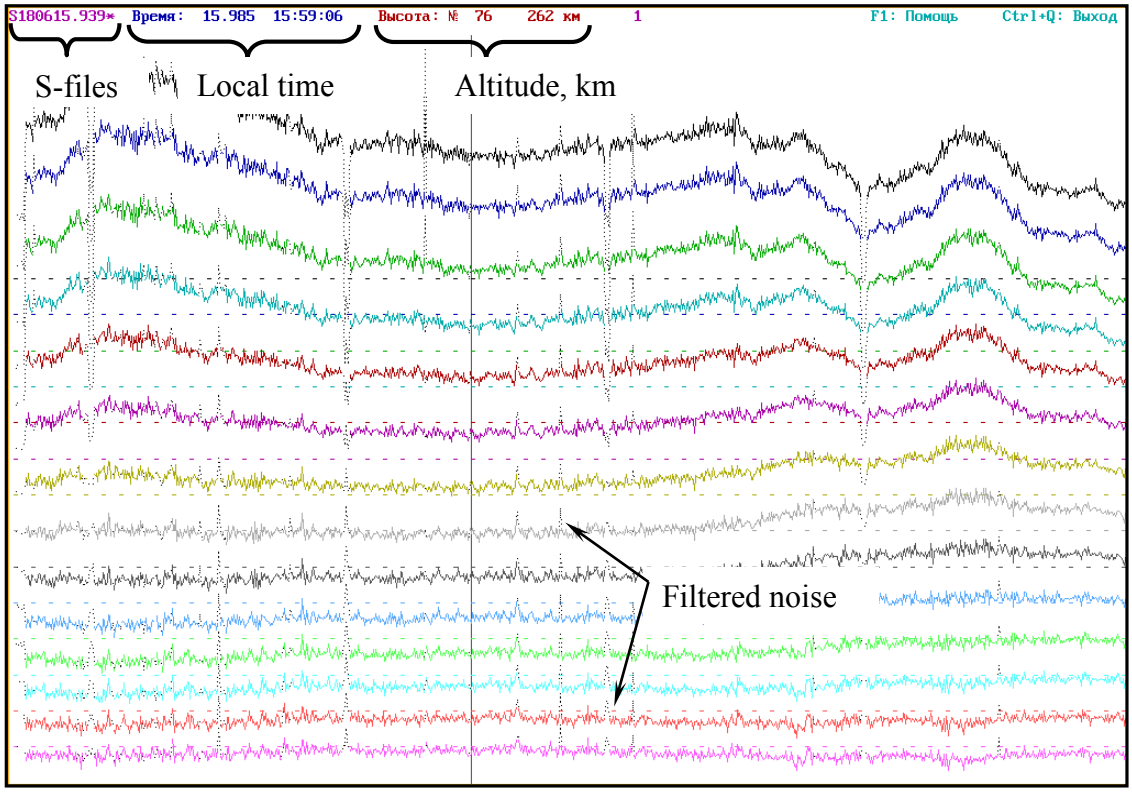

b

Figure 4.8 The program of view data: a - before filtering of interferences, b - after filtering.

Chapter 5

The empirical and physical models of the ionosphere (IRI and SAMI3)

5.1 Ionospheric models as main data sources of ion composition in the topside ionosphere

Modeling of the ionosphere is a process, which leads to a generalized and quantitative description of spatial and temporal variations of ionospheric parameters. These include the electron density, ion composition, ion and electron temperatures, and bulk motion of ion drift (*Ivanov-Kholodnyi et al.,* 1980). Since the ionospheric parameters change with altitude depending on the geomagnetic and geographic coordinates, a central task during modeling is accounting of dependencies of the ionospheric parameters on location, altitude, time, as well as solar and magnetic activity. The ionospheric models can be divided into three groups: empirical, semi-empirical, and physical.

1) Empirical (also known as statistical) ionospheric models are created by assimilation of a large number of observations from different locations and represent a description of the physical-chemical characteristics of the space environment.
2) Semi-empirical models (or hybrid models) are a combination of empirical and theoretical models (in other words, the method calculation of parameters, characteristics and properties of the ionosphere are based on experimental data).
3) Physical models are based on systems of momentum, continuity, energy equations etc., which describe the totality of chemical transformations of the charged particles, their interaction with particles of the neutral atmosphere, the electric and magnetic fields. The solution of these equations determines the state of the ionosphere for predetermined conditions. The implementation of such models requires significant computational resource.

The basic models of the ionosphere which provide information about high altitude variations of the ions investigated in this work are IRI (International Reference Ionosphere) (*Bilitza*, 2014), SAMI2 (SAMI2 is Another Model of the Ionosphere), SAMI3 (SAMI3 is Also a Model of the Ionosphere) (*Huba*, 2000 and 2008).

5.2 Empirical model of the ionosphere IRI

Empirical models play an important role in all regions of the Sun-Earth environment. They provide an opportunity for easy access to a "compressed form" of empirical data for a certain parameter based on all compiled data sources that exist for this parameter. One of the most important data sources for the IRI model is a global network of ionosondes, which monitor the state of the ionosphere since the 1930-ies. In addition to ionosondes, there are other sources of data for the development of the IRI model such as incoherent scatter radars, rockets, and satellites. The advantage of this model is that it provides estimates of the altitude profiles ionospheric parameters such as electron density, electron and ion temperatures, ion composition (O^+, H^+, N^+, He^+, O_2^+, NO^+ and Cluster ions) for the altitude range 50 − 2000 km. These parameters are given as functions of date, season, year, location, time of day (LT or UT), and required range of heights with random step (*Bilitza*, 2014).

5.2.1 Ion composition

Ion composition has always been the most uncertain part of IRI due to scarcity of data (in particular well-calibrated global measurements of ion composition) and discrepancies between ground-based and satellite observations. The earliest version of the IRI was based on the work of Danilov & Smirnova, 1995 in the lower ionosphere and Danilov & Yaichnikov, 1985 in the upper ionosphere. At the same time, IRI has used results of satellite measurements (Electron-2, Electron-4, S3-1) and rocket observations for the topside ionosphere (*Danilov*, 1985).

The model of Danilov & Yaichnikov, 1985 has provided estimates of the ion composition (O^+, H^+, N^+, He^+, O_2^+, NO^+ and Cluster ions) as a function of solar zenith angle, latitude, season and solar activity. A new version of the ion composition model of the upper ionosphere is TTS (the abbreviation consists of the first letters of surnames model developers − Třísková L., Truhlík V., Šmilauer J.). This model uses the best global coverage that is provided by the measurements of satellite mass spectrometers (Intercosmos – 24 and Atmospheric Explorer - C, - E). TTS consists of sub models for individual range of altitudes and seasons. The data were grouped by season (90-day periods those are symmetric according to equinoxes and solstices that provides coverage over all values of the local time) and for the following altitude ranges: 350 ± 40 km 550 ± 50 km, 850 ± 90 km, 1400 ± 150 km and 2000 ±300 km (*Truhlik et al*., 2012). Significant progress of the latest version of IRI-2012 (in contrast to the previous IRI - 2007) was an improvement of ion composition using tested data about photochemistry in the lower ionosphere which is provided by the physical model FLIP (Field Line Interhemispheric Plasma) (*Richards et al.,* 2010) for computation the concentrations of main ions in this region (*Bilitza*, 2014).

5.3 Physical model of the ionosphere

The physical (or theoretical) models are based on physical conservation laws and are intended for study and understanding of physical processes occurring in the ionosphere. SAMI3 is a three-dimensional global ionospheric model based on two-dimensional model SAMI2. This models calculate the plasma dynamics and changes of the chemical composition for seven ion species (H^+, He^+, N^+, O^+, NO^+, N_2^+ and O_2^+) in the low and middle latitude ionosphere in the altitude range 85 km to 20000 km by solving the ion momentum and continuity equations (*Huba et al.,* 2000). The energy equations are solved for H^+, He^+, and O^+ and electrons. In addition, the **E x B** drift of plasma motion is included for both zonal electric fields (vertical drifts) and meridional electric fields (zonal drifts). The neutral composition and temperature for SAMI3 are provided by NRLMSISE-00 model and the neutral winds are obtained from the Horizontal Wind Model (HWM) (*Huba*, 2008). The input parameters to these models are the value $F_{10.7}$ (daily and 3 months average) index; A_P index and **E x B** drift velocity. The output parameters are ion densities, ion temperature, ion velocity and electron temperature.

5.4 Advantages and disadvantages of theoretical modeling the ion composition

The advantage of theoretical approach in the modeling of the ionosphere is that physical model allows modeling of all required ionospheric parameters with any desired spatial and temporal resolution. Further, there is a fundamental opportunity to take into account the specific helio-geophysical conditions for a certain time in contrast to empirical approach where the monthly averaged conditions are described. However, at the same time, there are many difficulties associated with limiting of our understanding of the physics as such and the computational simplifications. This imposes restrictions on the accuracy of the modeled parameters (*Sojka*, 1984). Thus, theoretical models represent a very successful basis for describing the state of the ionosphere under different geophysical conditions and, in consequence, for one of the main tasks of the ionospheric service — ionospheric prediction. In practice, theoretical models are still too complex and bulky for operative work with applied problems.

5.5 Advantages and disadvantages of satellite methods of observations the ion composition

From the works of *Truhlik*, *Triskova*, and *Smilauer*, where comparison between IRI model estimates and results of various experimental observations were made, it is worth to mention that the IRI provides estimates only for an averaged and “smoothed ionosphere”. As a result, the accuracy of estimated concentrations values is low. This, in my opinion, is a considerable disadvantage for the real understanding of day-to-day variations, which control the behavior of the ionosphere for the region of interest.

The ionosphere undergoes very complex spatial and temporal variations, which depend on effects of solar activity, electric and magnetic fields, thermosphere circulation, and meteorological formations in the lower and middle atmosphere. In the consequence of this, formation mechanisms of the ionosphere at various heights are different, and even such an important parameter as the electron density can vary in different regions of the ionosphere. Since in the IRI model the required for estimations data are grouped within 90 days, it is natural that for such period the state of geospace and in particular the ionosphere varies even for quiet helio-geophysical condition. Thus, model estimates often have discrepancy with experimental results into several times.

Kharkiv incoherent scatter radar is able to provide continuous experimental data on the ion composition for midlatitude region of the topside ionosphere. Therefore, important stage of this work is comparison of IS radar data with estimates of IRI and SAMI3 models for clarification, correction, and obtaining reliable results in the future.

Chapter 6

Results

6.1 Introduction

This chapter is devoted to the description and analysis of altitudinal and temporal variations of the three main topside ion species (atomic oxygen O^+, hydrogen H^+, and helium He^+), which were obtained using KISR of Institute of Ionosphere during the 23rd and 24th solar cycles (see Fig. 6.1). Further, will be presented data provided by empirical and physical models (IRI-2012 and SAMI3 respectively) and analysis of comparison their estimates with experimental results. Observations were performed for dates close to the summer solstices with a relatively quiet state of space weather for 2000, 2004 and 2012 – 2015. The characteristics of solar activity by observation periods are presented in table 6.1 including the daily values of solar radio flux $F_{10.7}$, the values of the planetary and geomagnetic activity indices: K_p and A_p.

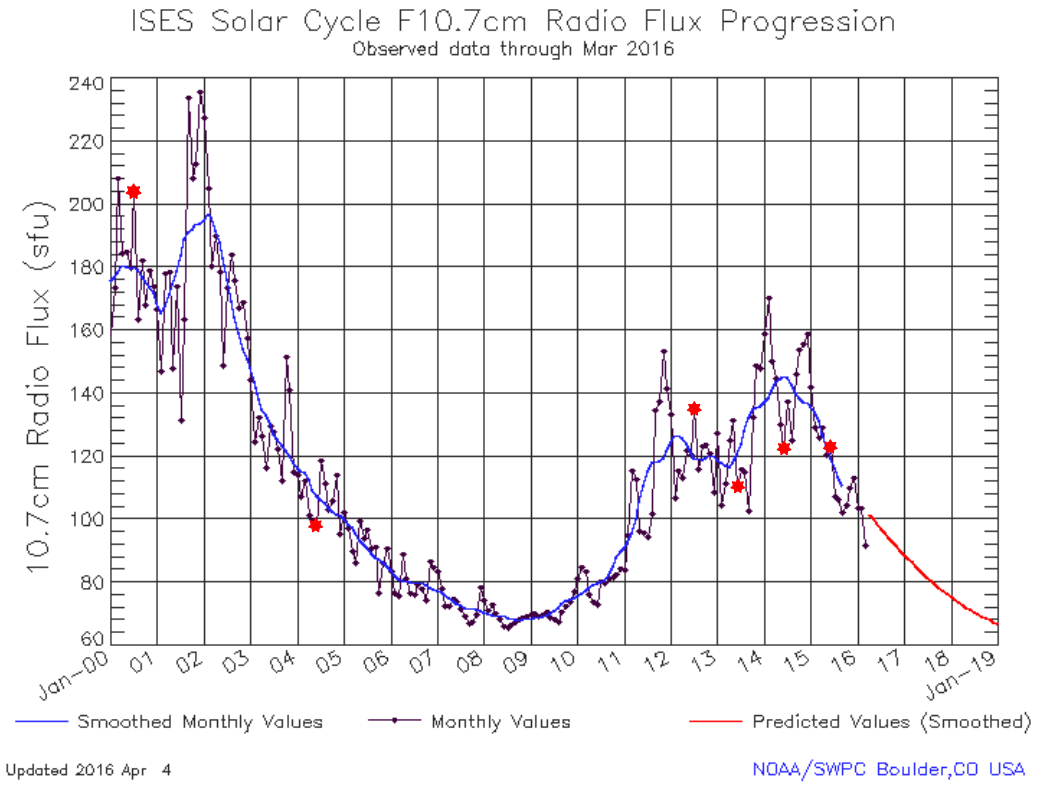

Figure 6.1 Solar cycle progression (Figure from Space weather prediction center NOAA).

Date of measurements	$F_{10.7}$	K_p	A_p, nT
July 01, 2000	164	2	9
July 02, 2000	162	2	6
July 03, 2000	166	3	10
June 15, 2004	109	3	16
June 16, 2004	112	2	7
June 17, 2004	111	2	7
June 19, 2012	110	1	3
June 20, 2012	104	1	4
June 21, 2012	98	1	3
June 22, 2012	88	1	5
June 18, 2013	123	1	5
June 19, 2013	126	1	5
June 20, 2013	133	2	11
June 21, 2013	130	3	17
June 25, 2014	174	1	6
June 26, 2014	178	1	5
June 18, 2015	126	2	7
June 19, 2015	130	1	5

Table 6.1 Dates of ion composition measurements by using incoherent scatter radar and corresponding values of solar and geomagnetic activity indices.

Since the relative concentration of atomic nitrogen ions N^+ in the mid-latitude ionosphere usually does not exceed a few percent of the total ion concentration, the IS method does not allow to distinguish ions N^+ and O^+, due to their small mass difference (*Evans*, 1969). Thus, the IS method provides information about the total concentration of O^+ and N^+, although we should always remember that the concentration accurate to a few (at the most ten) percent the same as the concentration of O^+. In this work, for calculation the relative concentrations of oxygen ions, we assumed that plasma consists of three ions: O^+, H^+, He^+. We neglected by the nitrogen ions N^+ and used simple formula for calculations $N(O^+)/N = 100\ \% - N(H^+)/N - N(He^+)/N$. Here and in all the following cases N in the denominator is the electron density.

The following sections will be divided into several paragraphs for different types of sources, which give appropriate results. For the first phase of the 24th solar cycle – June 18 – 21, 2013, for the period of solar maximum phase – June 24 – 26, 2014, and for the initial phase of solar activity recession – June 18 – 19, 2015. For the maximum of the 23rd solar cycle – July 01 – 03, 2000, and for the phase of solar activity recession – June 15 – 17, 2004.

6.2 The main results of investigation using Kharkiv Incoherent Scatter Radar

6.2.1 19 – 20 and 21 – 22 June, 2012

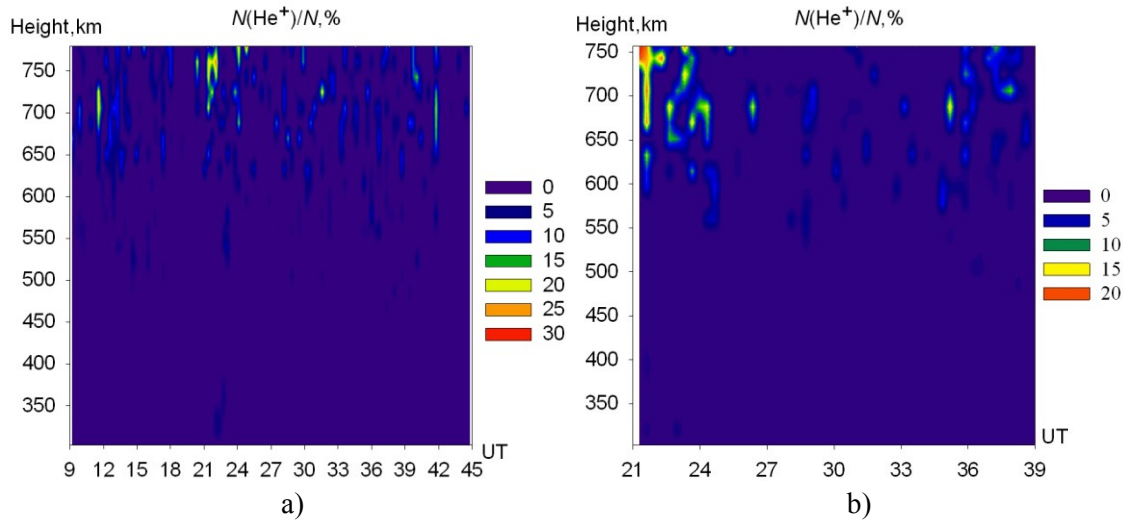

Figure 6.2 Daily variations of $N(He^+)/N$ for a) 19.06 – 20.06. 2012, b) 21.06 – 22.06. 2012.

Helium ions. The maximum values of $N(He^+)/N$ are observed at night and increase with height (see Fig. 6.2). At a height of 750 km, the maximum daily value $N(He^+)/N$ for June 19, 2012 is about 30% at 24:00 UT and is 20% for June 21, 2012 at 22:00 UT at the same altitude. Below 600 km, $N(He^+)/N$ is almost absent over the entire measurement period in the summer of 2012.

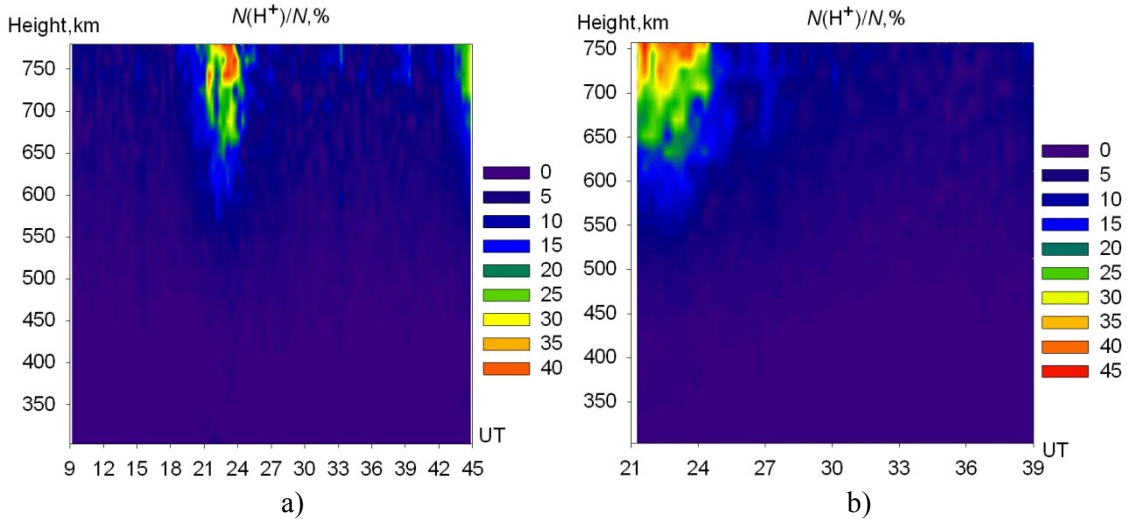

Figure 6.3 Daily variations of $N(H^+)/N$ for a) 19.06 – 20.06. 2012, b) 21.06 – 22.06 2012.

Hydrogen ions. Analogously to the previous case with helium ions $N(H^+)/N$ increases with height. Maximum values of $N(H^+)/N$ were registered during

(21:00 − 24:00) UT for June 19 and 21, 2012 at a height of 750 km for both dates and were about 40% (see Fig. 6.3). The lowest values of hydrogen ions (no more than 10%) were observed at noon below 700 km altitude. At an altitude range of 303 – 450 km, H^+ throughout the entire measurement period mostly is absent.

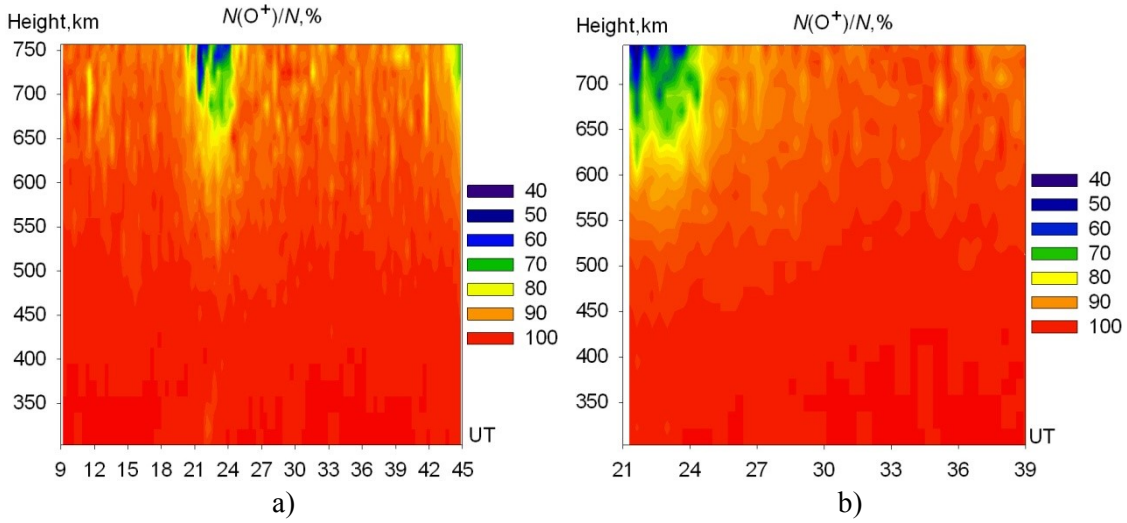

Figure 6.4 Daily variations of $N(O^+)/N$ for a) 19.06 – 20.06. 2012, b) 21.06 – 22.06. 2012.

Oxygen ions. The relative concentration of $N(O^+)/N$ on June 19 – 22, 2012 has retained its maximum values from 90% to 100% for most of the day. But at night, between 21:00 UT and 01:00 UT (on June 19 and 21, 2012) beginning from a height of 650 km, the number of O^+ is decreased to 40% (see Fig. 6.4).

6.2.2 18 – 19 and 20 – 21 June, 2013

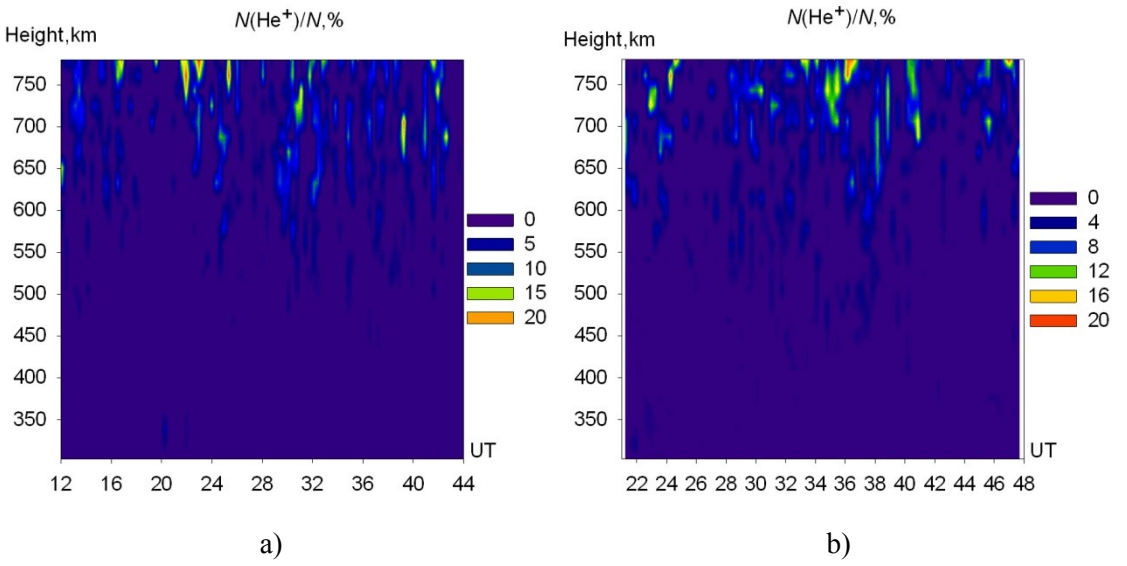

Figure 6.5 Daily variations of $N(He^+)/N$ for a) 18.06 – 19.06. 2013, b) 20.06 – 21.06. 2013**.**

Helium ions. The relative concentration of helium ions in June 18 – 19, 2013 reaches its maximum (about 20%) at altitudes close to 750 km both in the evening and

nearly midnight (see Fig. 6.5). Here, it is also worth noting the presence of helium ions in the morning (about 07:00 UT) on June 19, 2013. The 15% at an altitude of ~ 700 km and up to 10% at the altitude range 600 – 700 km. On June 21, 2013, estimate of $N(He^+)/N$ ≈ 12% at noon near the height of 700 km. Below 600 km, $N(He^+)/N$ basically does not exceed 4%.

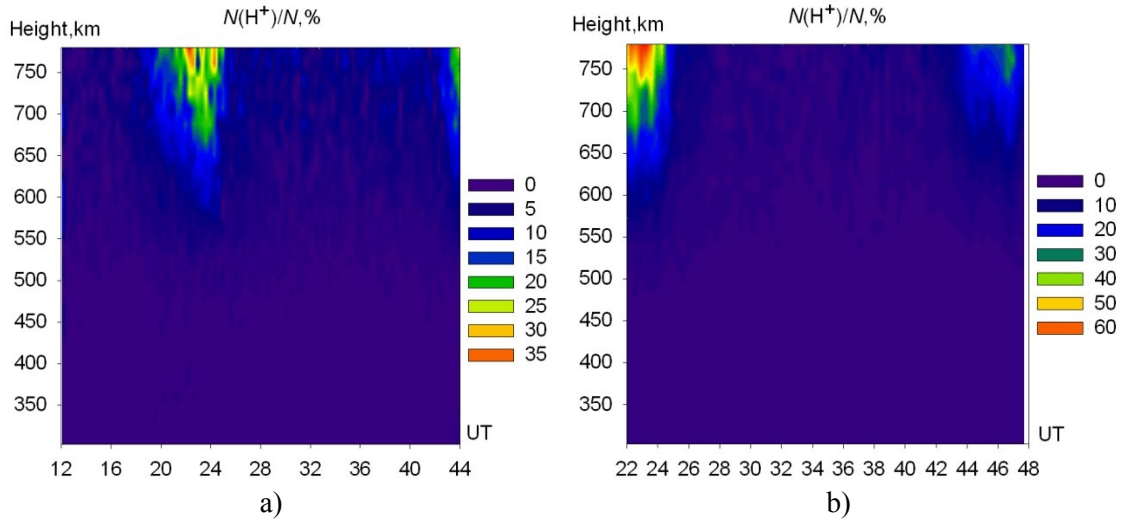

Figure 6.6 Daily variations of $N(H^+)/N$ for a) 18.06 – 19.06. 2013, b) 20.06 – 21.06 2013.

Hydrogen ions. On June 18 – 19, 2013, the maximum concentration of hydrogen ions is observed during 22:00 – 24:00 UT and $N(H^+)/N$ is about 35% for altitudes above 750 km (see Fig. 6.6), whereas on June 20 – 21, 2013 at similar altitude and time $N(H^+)/N$ is about 60%.

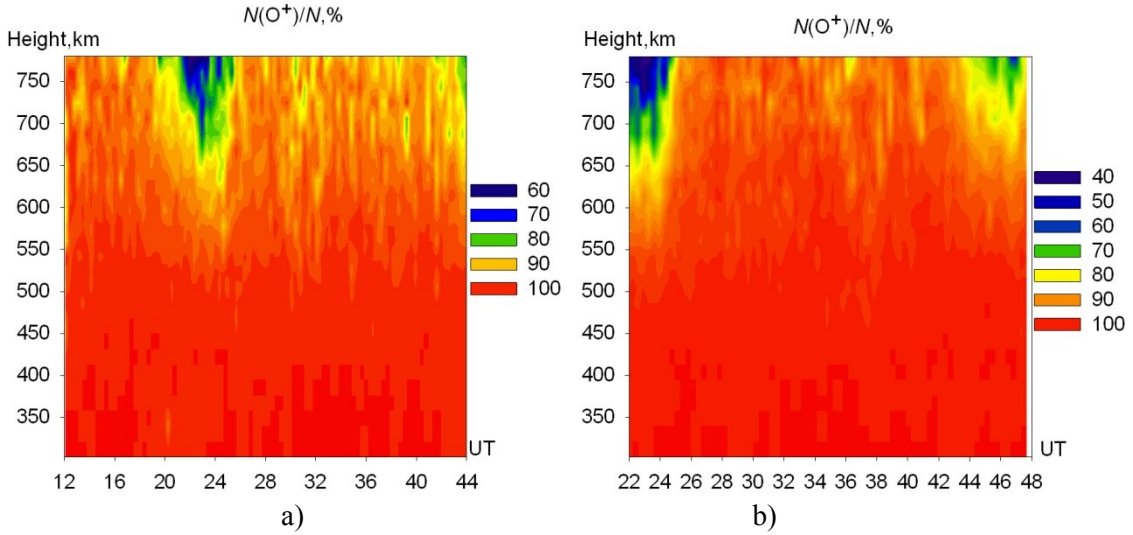

Figure 6.7 Daily variations of the $N(O^+)/N$ for a) 18.06 – 19.06. 2013, b) 20.06 – 21.06 2013**.**

Oxygen ions. In June 18-19, 2013, a significant amount (90% to 100%) of atomic oxygen ions is concentrated at the altitude range of 300 – 600 km. Only at nighttime 21:00 – 01:00 UT it is possible to notice a decrease to 60% at a height of 700 km and above (see Fig. 6.7). During June 20–21, 2013, there is a significant decrease of $N(O^+)/N$

at nighttime (from 80% to 40%), starting from a height of 650 km and above. Another picture was observed for the hydrogen ions. The $N(H^+)/N$ was increased to 60% over the same period. In the rest of the day, there is the maximum amount of O^+ about 100 % at an altitude range 600 – 780 km. Below of this range, the region of ions accumulation to 100% is observed, and lower 450 km O^+ are the dominant.

6.2.3 25 – 26 June, 2014

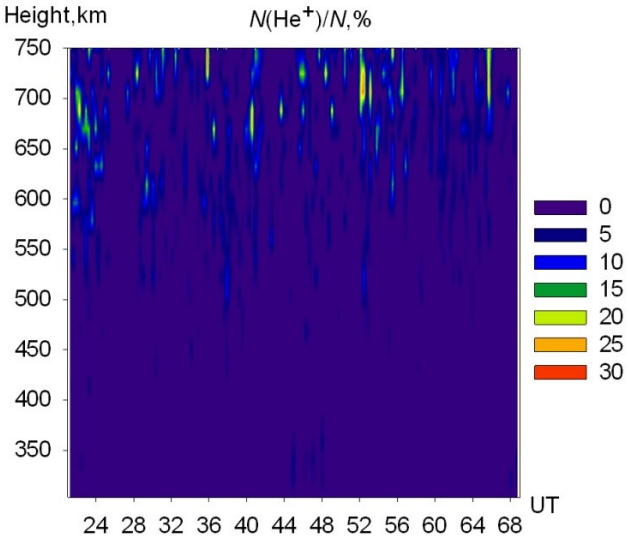

Figure 6.8 Daily variations of $N(He^+)/N$ for 25.06 – 26.06. 2014**.**

Helium ions. Figure 6.8 shows that $N(He^+)/N$ reaches maximum values during the pre-dawn hours on June 26, 2014 (around 04:00 UT) close to 700 km. During June 25 – 26, 2014, the presence of helium ions is observed in the form of short-term emissions, which look like sharp increase of concentration or like small "bursts". At the altitude range 500 – 650 km, $N(He^+)/N$ does not exceed 10%. Below 500 km, He^+ is almost absent.

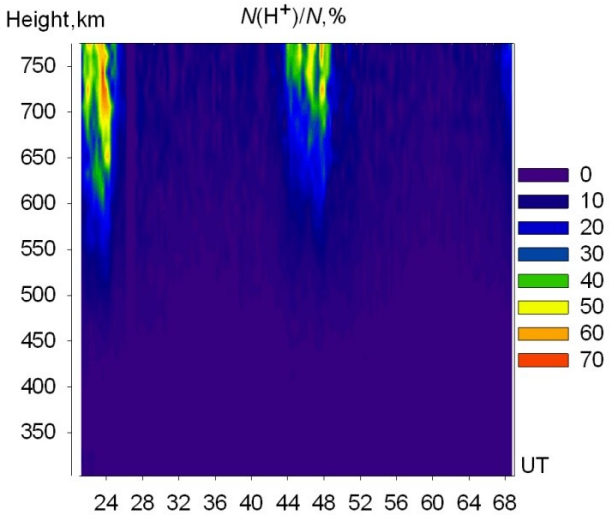

Figure 6.9 Daily variations of $N(H^+)/N$ for 25.06 – 26.06. 2014**.**

Hydrogen ions. The relative concentration of hydrogen ions during June 25 – 26, 2014 increases with height (see Fig. 6.9). This is especially noticeable during 22:00 − 01:00 UT. Here, $N(H^+)/N$ is about 50% at a height of 650 km (June 25, 2014). During daytime, $N(H^+)/N$ does not exceed 10% above 500 km. On June 26, 2014, at night, $N(H^+)/N$ is about 40% above 650 km.

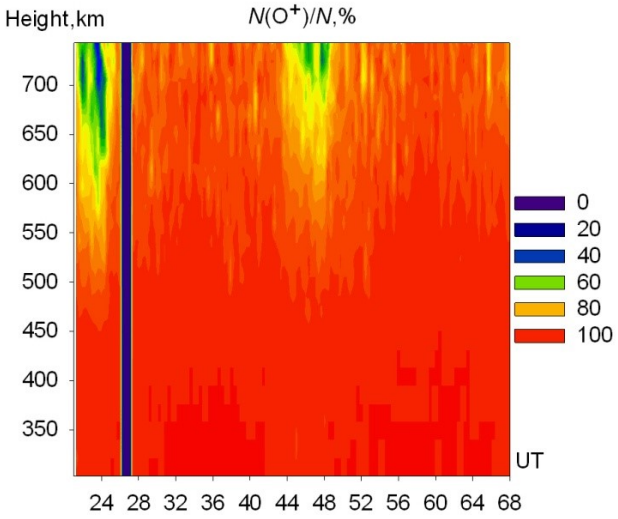

Figure 6.10 Daily variations of $N(O^+)/N$ for 25.06 – 26.06. 2014**.**

Oxygen ions. The $N(O^+)/N$ at all heights is within of 90 – 100 %. Especially, large number of O^+ is registered during daytime. Only a small decrease (down to 60%) of the $N(O^+)/N$ is observed close to midnight at a height of 700 km (see Fig. 6.10).

6.2.4 18 – 19 June, 2015

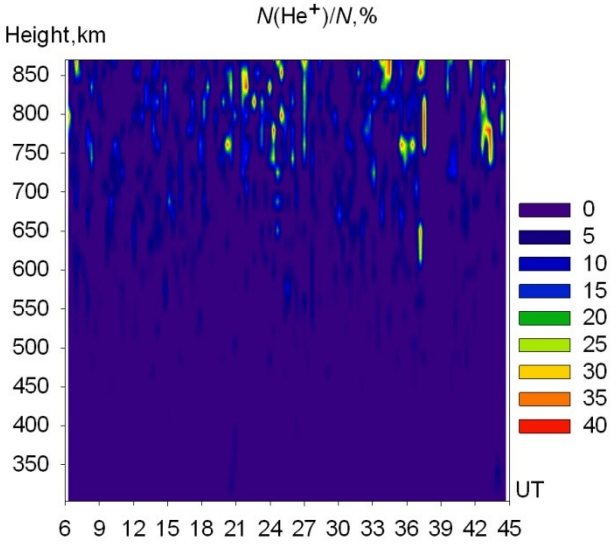

Figure 6.11 Daily variations of $N(He^+)/N$ for 18.06 – 19.06. 2015.

Helium ions. In the summer of 2015, during 21:00 – 01:00 UT, $N(He^+)/N$ is about 35% in the altitude range 750 – 850 km. In the daytime, $N(He^+)/N$ does not exceed 15%. Below 700 km altitude, the relative concentration of He^+ gradually starts to decrease and below 600 km, He^+ are almost absent (see Fig. 6.11).

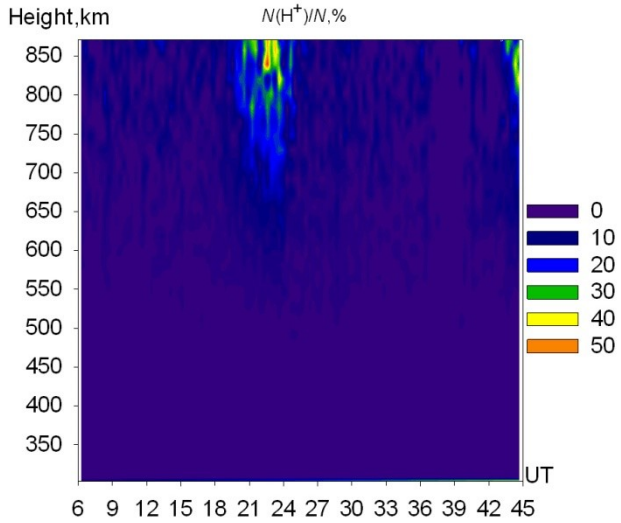

Figure 6.12 Daily variations of $N(H^+)/N$ for 18.06 – 19.06. 2015.

Hydrogen ions. On June 18 – 19, 2015, the maximum relative concentration of ions H^+ (about 50%) is observed during 21:00 – 24:00 UT approximately at 850 km and above. From 800 km to 650 km $N(H^+)/N$ does not exceed 20% for the same time interval. The lowest number of H^+ is registered during daytime and does not exceed 10%. Below 550 km, H^+ almost are not observed (see Fig. 6.12).

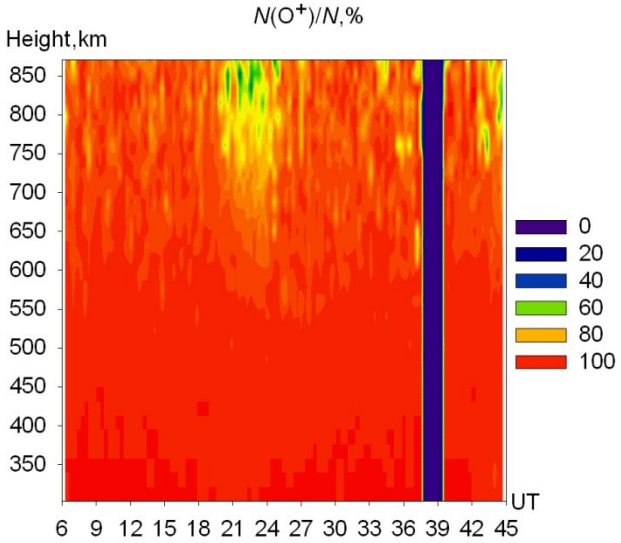

Figure 6.13 Daily variations of $N(O^+)/N$ for 18.06 – 19.06. 2015.

Oxygen ions. The relative concentration of atomic oxygen ions for all the considered altitudes is changed from 90 % to 100%. Only at night, 21:00 – 01:00 UT $N(O^+)/N$ is reduced to 60% at altitudes close to 850 km. Below 550 km, O^+ is a predominant ion (see Fig. 6.13).

6.2.5 01 – 03 July, 2000

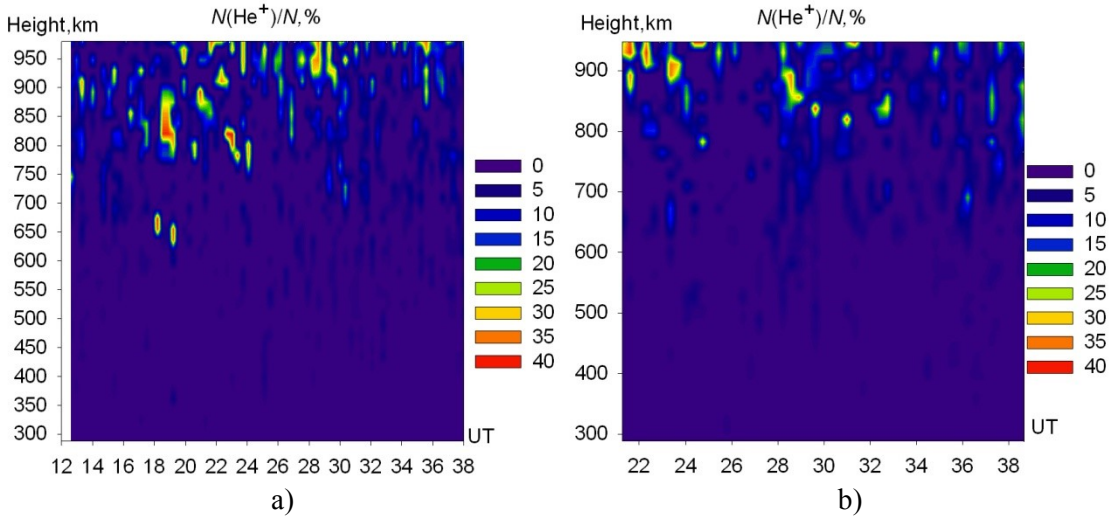

Figure 6.14 Daily variations of $N(He^+)/N$ for a) 01– 02.07. 2000 b) 03.07. 2000**.**

Helium ions. During the of 23rd solar cycle (July 01 – 03, 2000) $N(He^+)/N$ had reached the maximum values in the evening and midnight. It is possible to observe the rapid increase of the relative concentrations helium ions to 35 % and 40% (July 01, 2000) from 18:30 to 19:30 UT close to 650 km. On July 03, 2000 is observed a slight increase of $N(He^+)/N$ in the morning hours about 06:00 − 08:00 UT at a height of ~ 850 km. The minimum values of $N(He^+)/N$ is registered about noon. At the altitude range 700 − 800 km it does not exceed 15%. Below 600 km, the probability of presence of helium ions is very low and the relative concentration of He^+ decreases from 5% to ~ 0% at lower altitudes (see Fig. 6.14).

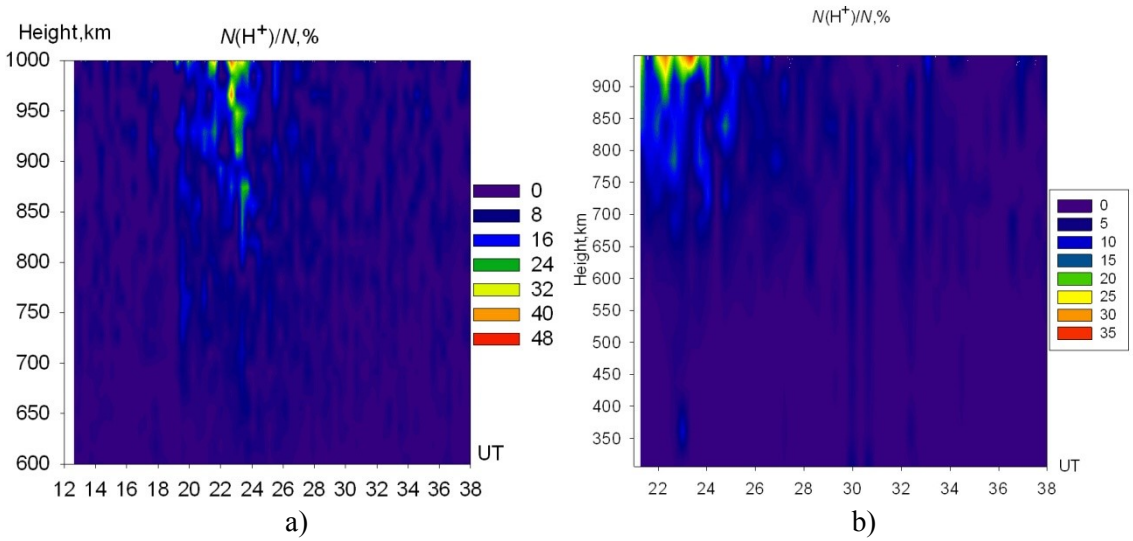

Figure 6.15 Daily variations of $N(H^+)/N$ for a) 01 – 02.07. 2000 b) 03.07. 2000**.**

Hydrogen ions. During July 01 – 03, 2000, maximum values of $N(H^+)/N$ is observed close to midnight and minimum at noon (see Fig. 6.15). At the altitude a bit higher of 700 km $N(H^+)/N$ is about 20%, whereas above 850 km it increases to 48 % (on July 01, 2000) and to 35% (on July 02, 2000) during 22:00 – 24:00 UT. During the rest of the day (from 02:00 to 20:00 UT) $N(H^+)/N$ does not exceed 10% .

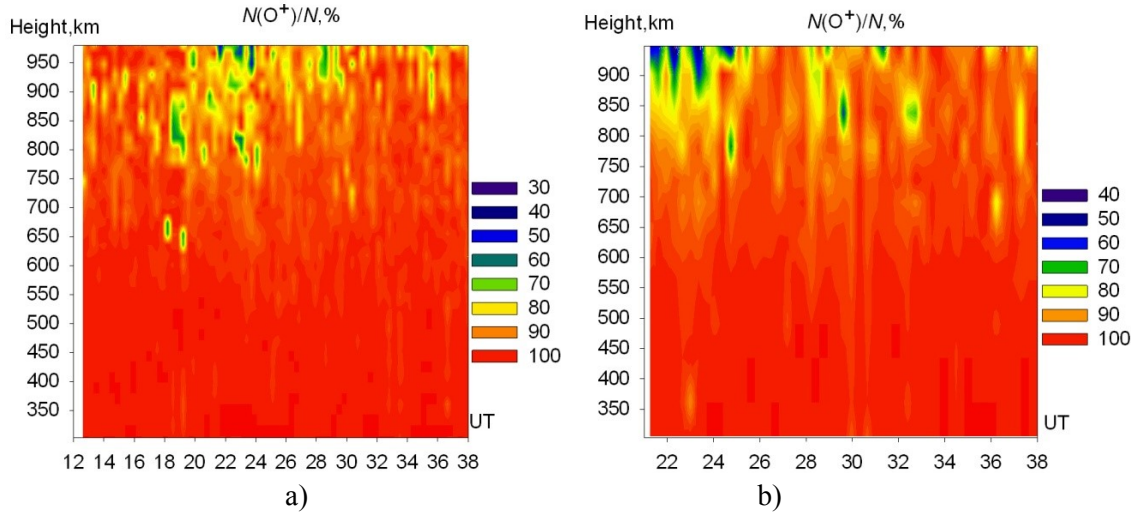

Figure 6.16 Daily variations of $N(O^+)/N$ for a) 01 – 02.07. 2000 b) 03.07. 2000.

Oxygen ions. The relative concentration of atomic oxygen ions on July 01 − 03, 2000 is within 90 − 100%. This is especially noticeable beginning from a height of 300 km up to the 750 km for the most part of the day (see Fig. 6.16). Slight decrease of O^+ is observed only in the evening and at nighttime. Starting from 20:00 UT the estimate of $N(O^+)/N$ is decreased to 70% close to 850 km and to 30% (on July 01 − 02, 2000) above 850 km at 24:00 UT.

6.2.6 15 – 17 June, 2004

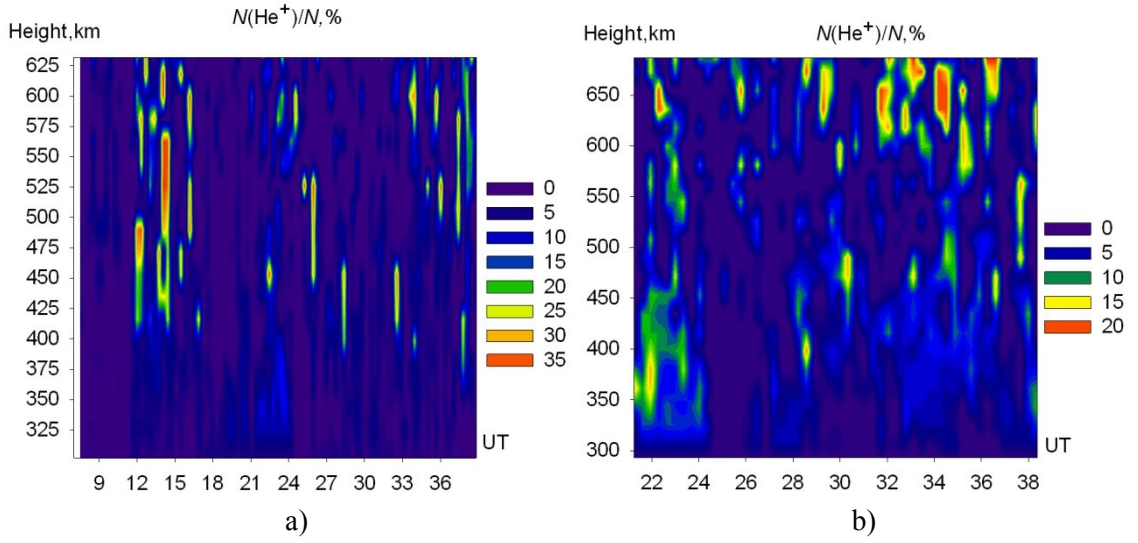

Figure 6.17 Daily variations of $N(He^+)/N$ for a) 15 – 16.06.2004 b) 17.06. 2004.

Helium ions. During the period from 15th to 16th of June 2004 had been registered abnormally maximum values of the $N(He^+)/N$ during daytime. $N(He^+)/N$ is about 35% at heights of 480 km and 600 km (June 15, 2004) at about 12:00 UT and 14:00 UT respectively. Figure 6.17 shows increase (which look like small "bursts") of $N(He^+)/N$ from 23% to 35% in the altitude range 400 – 600 km during daytime (09:00 – 14:00 UT). At night, $N(He^+)/N$ also reaches about 35% (approximately at 22:00 UT) at a height of 450 km (June 15, 2004), at 2:00 UT at the altitude range 450 − 540 km, and at 4:30 UT from 400 to 435 km on June 16, 2004. Throughout the rest of the day $N(He^+)/N$ does not exceed 15%.

On June 17, 2004, the relative ion concentration reaches a maximum values (~15%) in the altitude range 360 − 400 km at 22:00 UT. At noon, helium ions are also registered. The parameter $N(He^+)/N$ varies from 08:00 to 13:00 UT in kind of "bursts" with duration from 30 min to 1 hour and consists ~ 20% above 600 km.

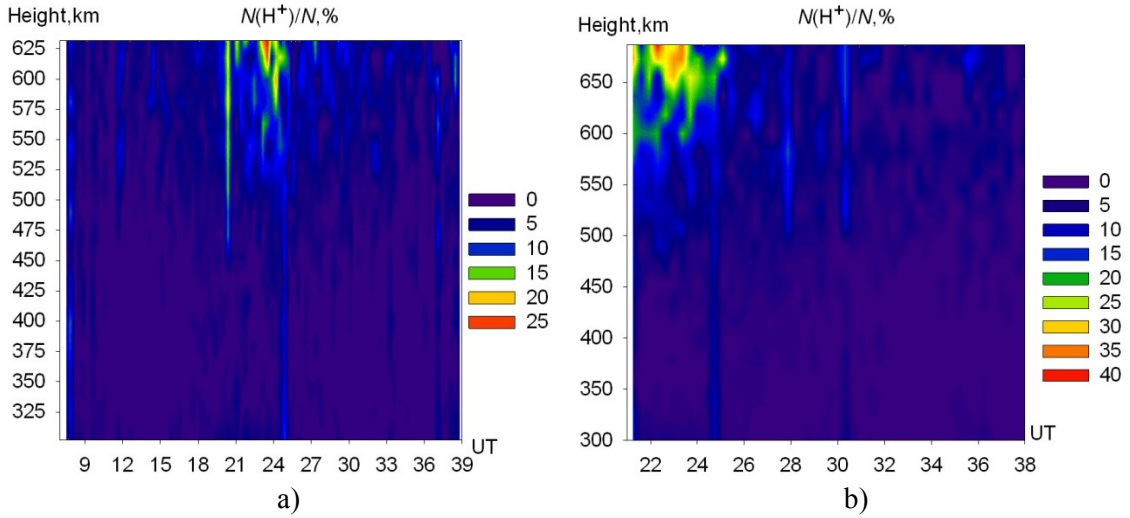

Figure 6.18 Daily variations of $N(H^+)/N$ for a) 15 – 16.06.2004 b) 17.06. 2004.

Hydrogen ions. On June 15-16, 2004, $N(H^+)/N$ increases with height and close to midnight reaches 25% at the height about 620 km. Decrease of $N(H^+)/N$ is observed in the daytime (06:00 to 20:00 UT) from the height of 500 km (where the amount of hydrogen about 10%) down to 300 km (where H^+ completely disappear).

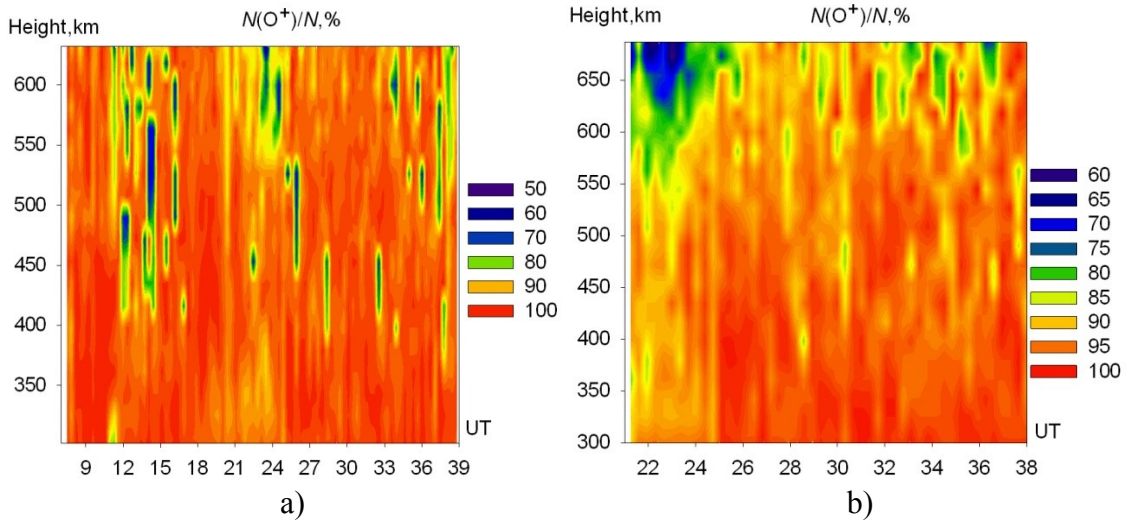

Figure 6.19 Daily variations of $N(O^+)/N$ for a) 15 – 16.06.2004 b) 17.06. 2004.

Oxygen ions. On June 15 – 17, 2004 the relative concentration of O^+ is varies from 90% to 100% in the altitude range 300 − 550 km. However, at noon, the height of maximum values for $N(O^+)/N$ is 650 km. During 22:00 − 24:00 UT, above 550 km, $N(O^+)/N$ decreases from 80% to 60%. On June 15 – 16, 2004 is observed small decrease of $N(O^+)/N$ near midday 12:00 − 16:00 UT to 50% at a height of 450 km and above.

6.3 The main results of investigation using empirical model IRI-2012

According to estimates of $N(H^+)/N$, $N(He^+)/N$ and $N(O^+)/N$, which provides the IRI model, it was found that variations of relative concentrations in almost all cases have a symmetrical nature regarding noon compared to experimental data. The largest amount of helium ions were observed in the evening time (between 16:00 – 20:00 UT) starting from a height of ~ 600 km and $N(He^+)/N$ did not exceed 1%. During the 24th solar cycle, helium ions are absent in the daytime. Only on June 18 – 21, 2013 $N(He^+)/N$ reaches 0.1% at a height of 750 km (see Fig. 6.21). During the 23rd solar cycle He^+ is also absent in the daytime at the lower altitudes, but above 650 km (July 01– 03, 2000) $N(He^+)/N$ reaches 0.1% (see Fig. 6.24).

The maximum values of $N(H^+)/N$ were observed in the evening and at nighttime (especially around midnight) above 600 km. The estimates of $N(H^+)/N$ did not exceed 10% for all investigated dates during the 24th solar maximum. On July 01 – 02, 2000 (the maximum phase of solar activity), $N(H^+)/N$ was significantly reduced and did not exceed 3%. During daytime, up to 700 km H^+ was absent for all investigated dates. Above 700 km $N(H^+)/N$ did not exceed 2% (June 25 – 26, 2014).

Variations of $N(O^+)/N$ compared to He^+ and H^+ have an opposite behavior. The maximum values of $N(O^+)/N$ are about 92% in the daytime (up to 650 km) during the 24th solar cycle, and about 96% in July 01 – 02, 2000 (see Fig. 6.24). The minimum values of the relative concentrations were observed at nighttime above 650 km. $N(O^+)/N$ was reduced to 80% in June 25–26, 2014 (see Fig. 6.22).

6.3.1 19 – 20 and 21– 22 June, 2012

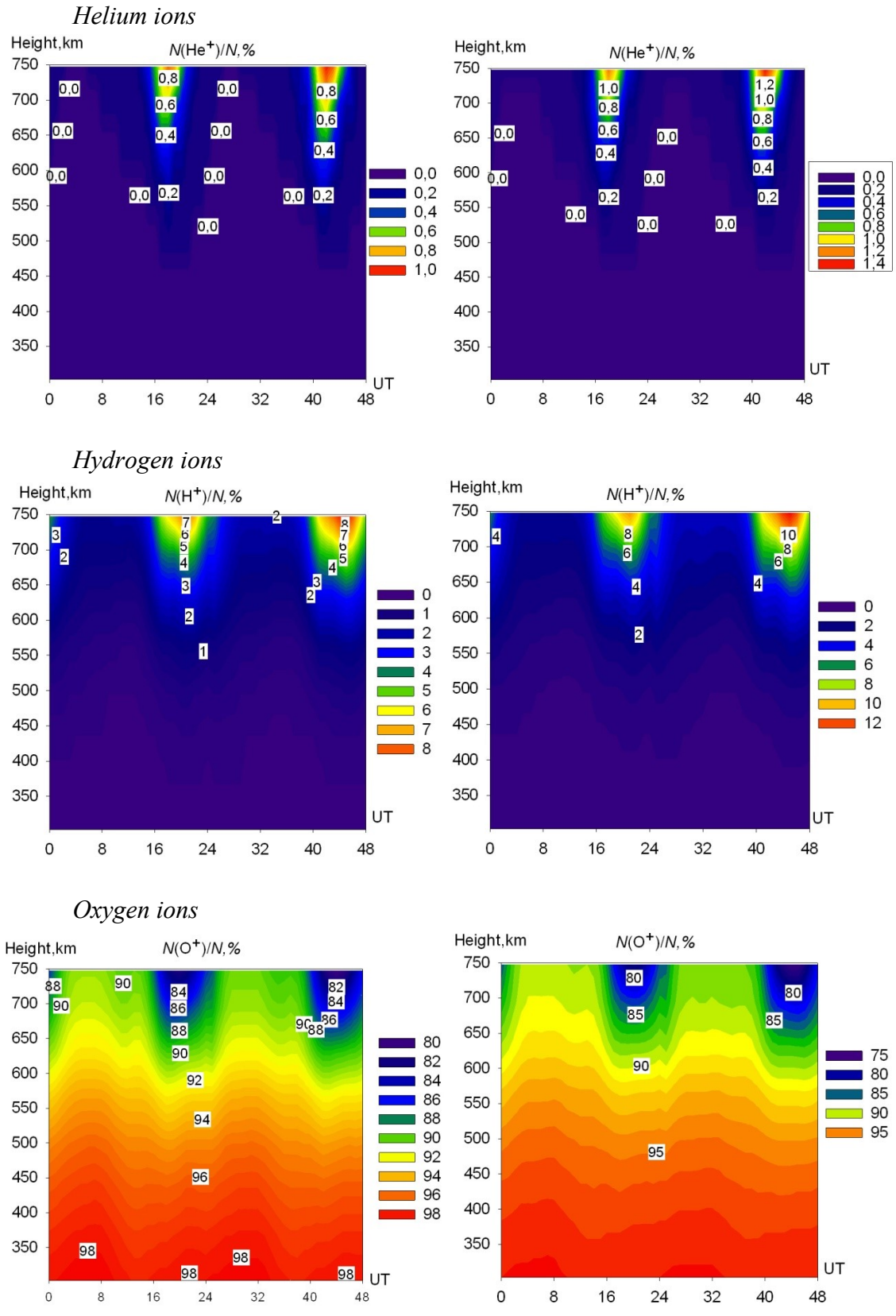

Figure 6.20 Daily variations of the relative concentrations He^+, H^+, O^+ ions for 19 – 20.06.2012 (left panel), 21.06.2012 – 22.06.2012 (right panel).

6.3.2 18 – 19 and 20 – 21 June, 2013

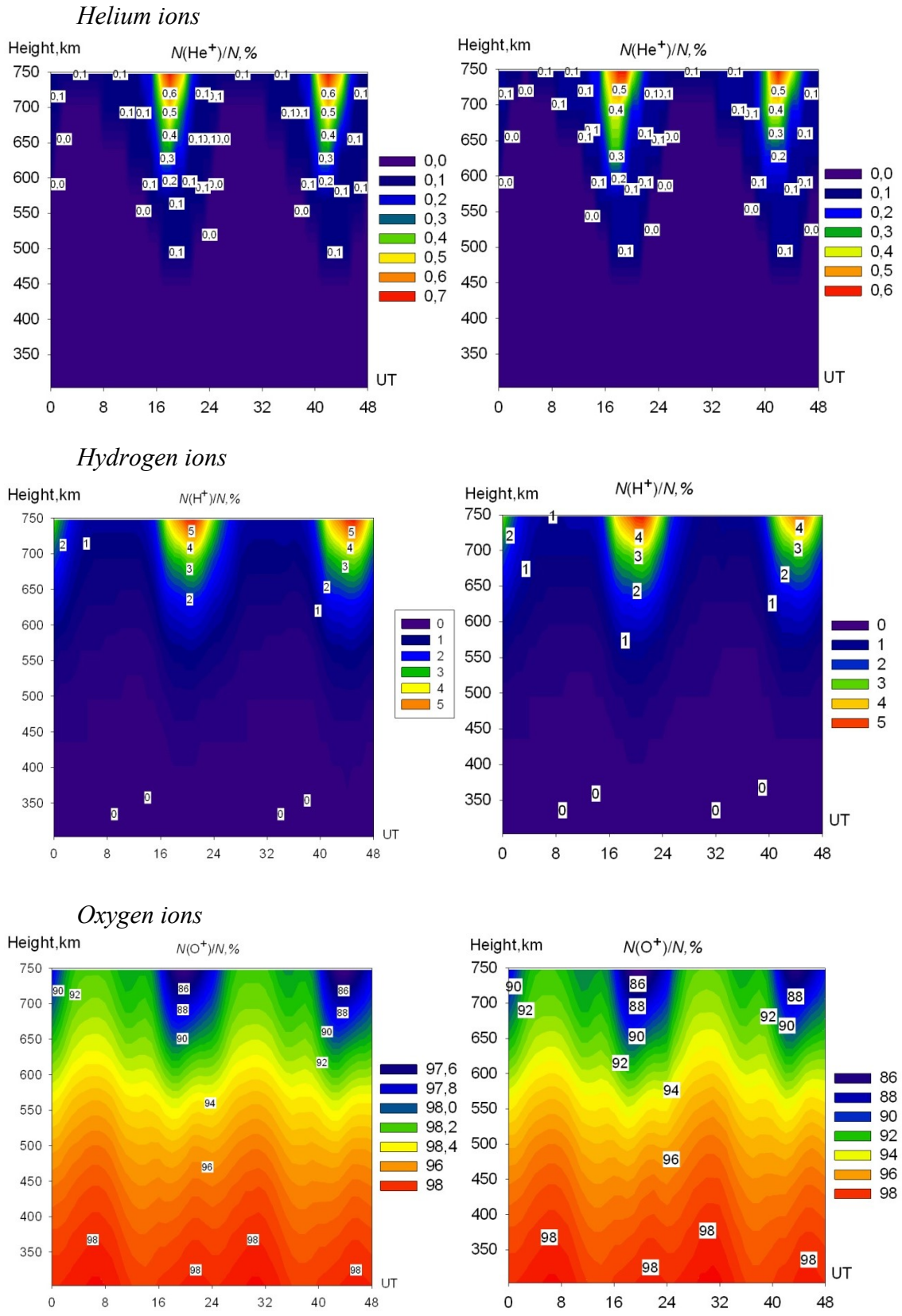

Figure 6.21 Daily variations of the relative concentrations He^+, H^+, O^+ ions for 18 – 19.06.2013 (left panel), 20.06.2012 – 21.06.2012 (right panel).

6.3.3 25 – 26 June, 2014

Helium ions

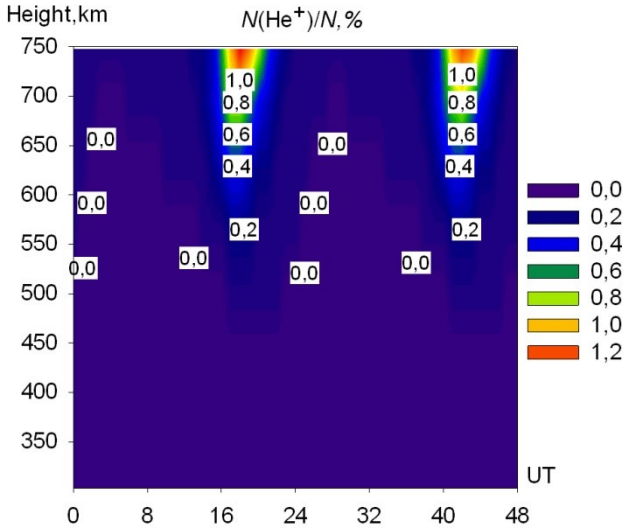

Hydrogen ions

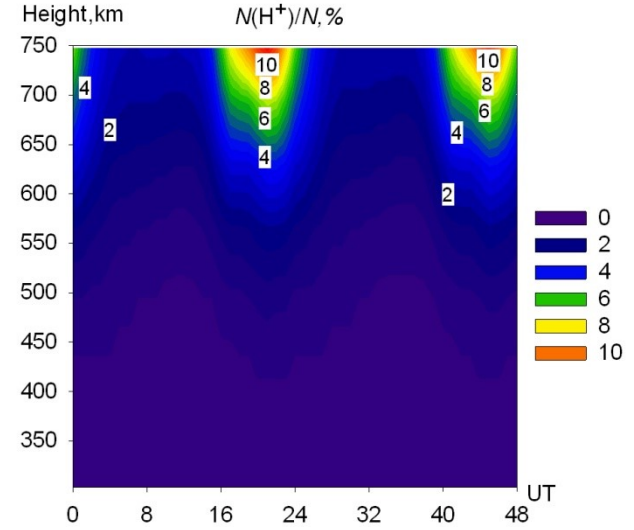

Oxygen ions

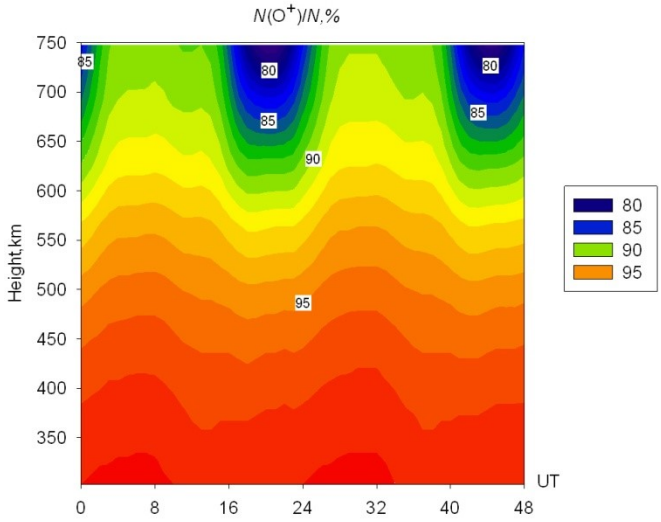

Figure 6.22 Daily variations of the relative concentrations He^+, H^+, O^+ ions for 25 – 26.06.2014.

6.3.4 17 – 19 June, 2015

Helium ions

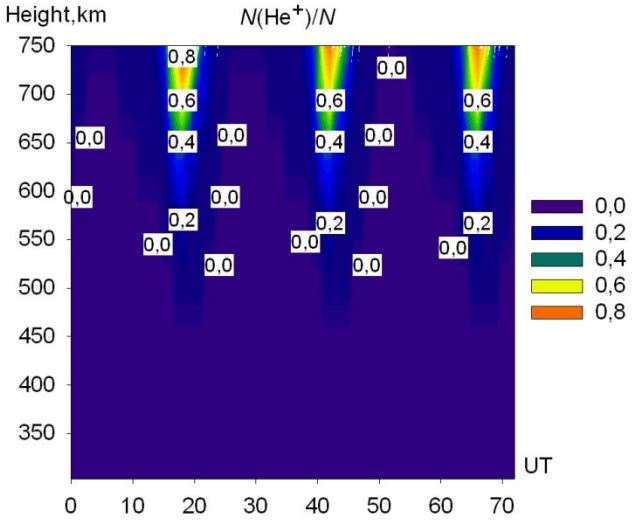

Hydrogen ions

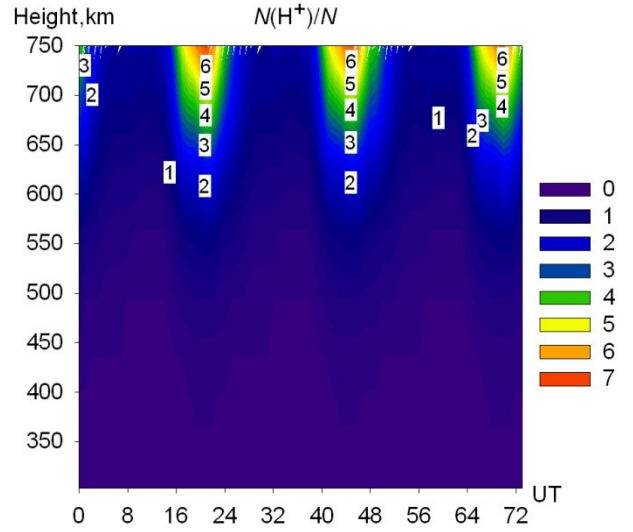

Oxygen ions

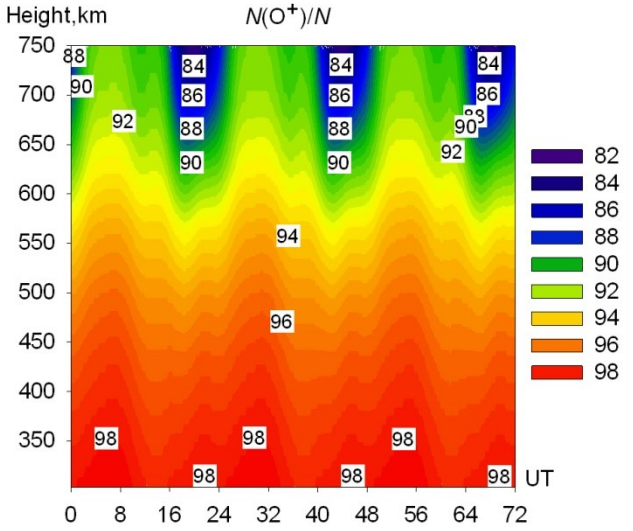

Figure 6.23 Daily variations of the relative concentrations He^+, H^+, O^+ ions for 17 – 19.06.2015.

6.3.5 01-03 July, 2000

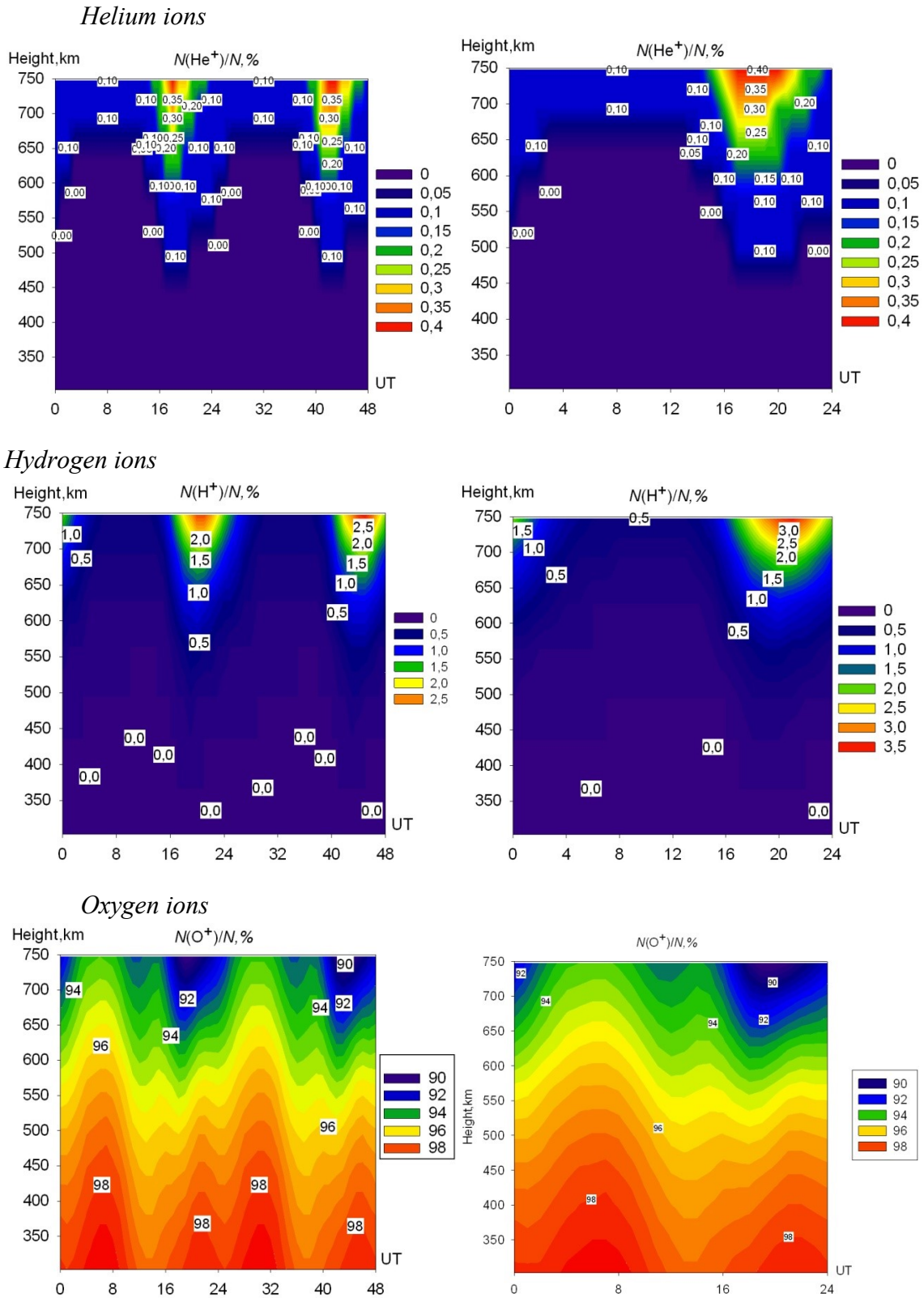

Figure 6.24 Daily variations of the relative concentrations He^+, H^+,O^+ ions for 01 – 02.07.2000 (left panel), 03.07.2000 (right panel).

6.3.6 15 – 17 June, 2004

Helium ions

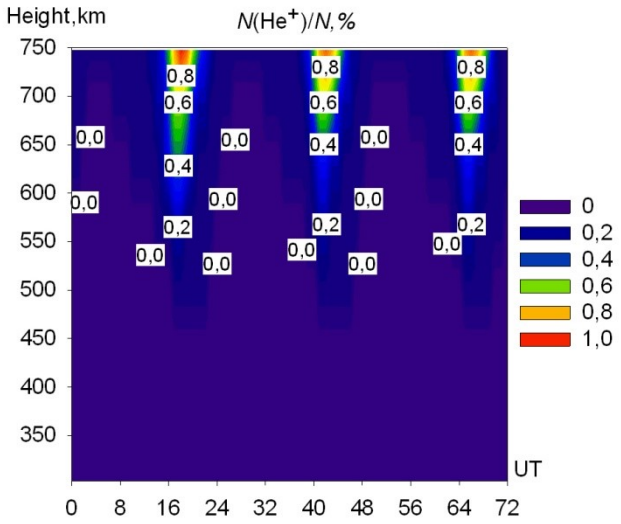

Hydrogen ions

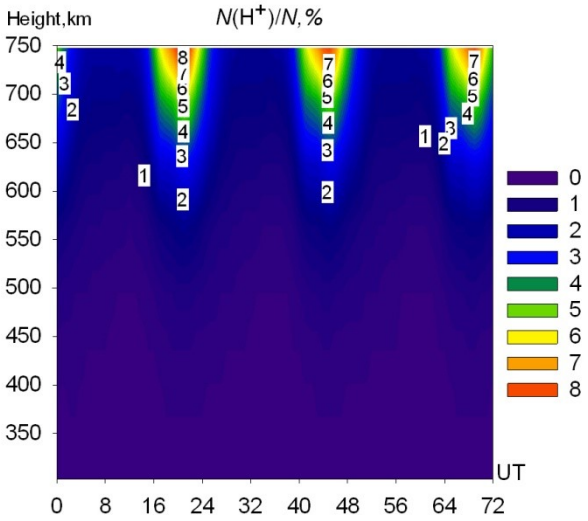

Oxygen ions

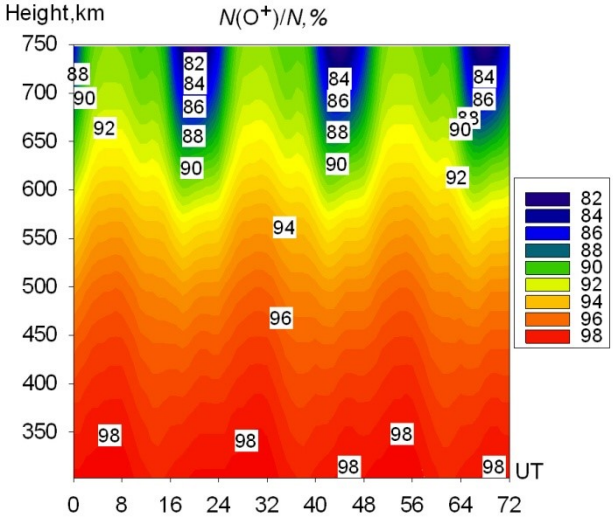

Figure 6.25 Daily variations of the relative concentrations He^+, H^+, O^+ ions for 15 – 17.06.2004.

6.4 The main results of investigation using physical model SAMI3

6.4.1 19 – 20 and 21 – 22 June, 2012

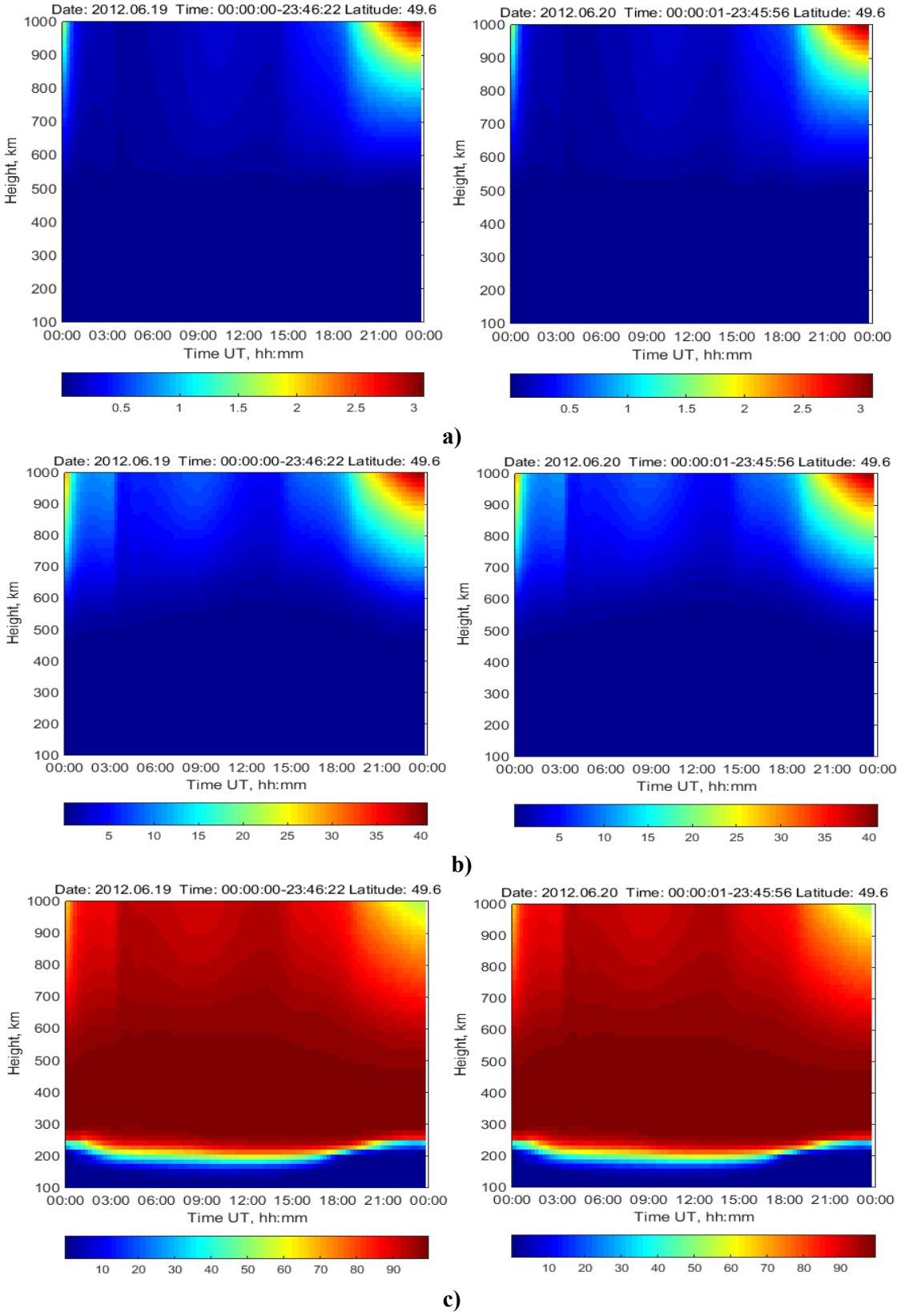

Figure 6.26 Altitudinal and temporal variations of the relative concentrations a) He^+, b) H^+, c) O^+ ions for 19.06.2012 (left panel) and 20.06.2012 (right panel).

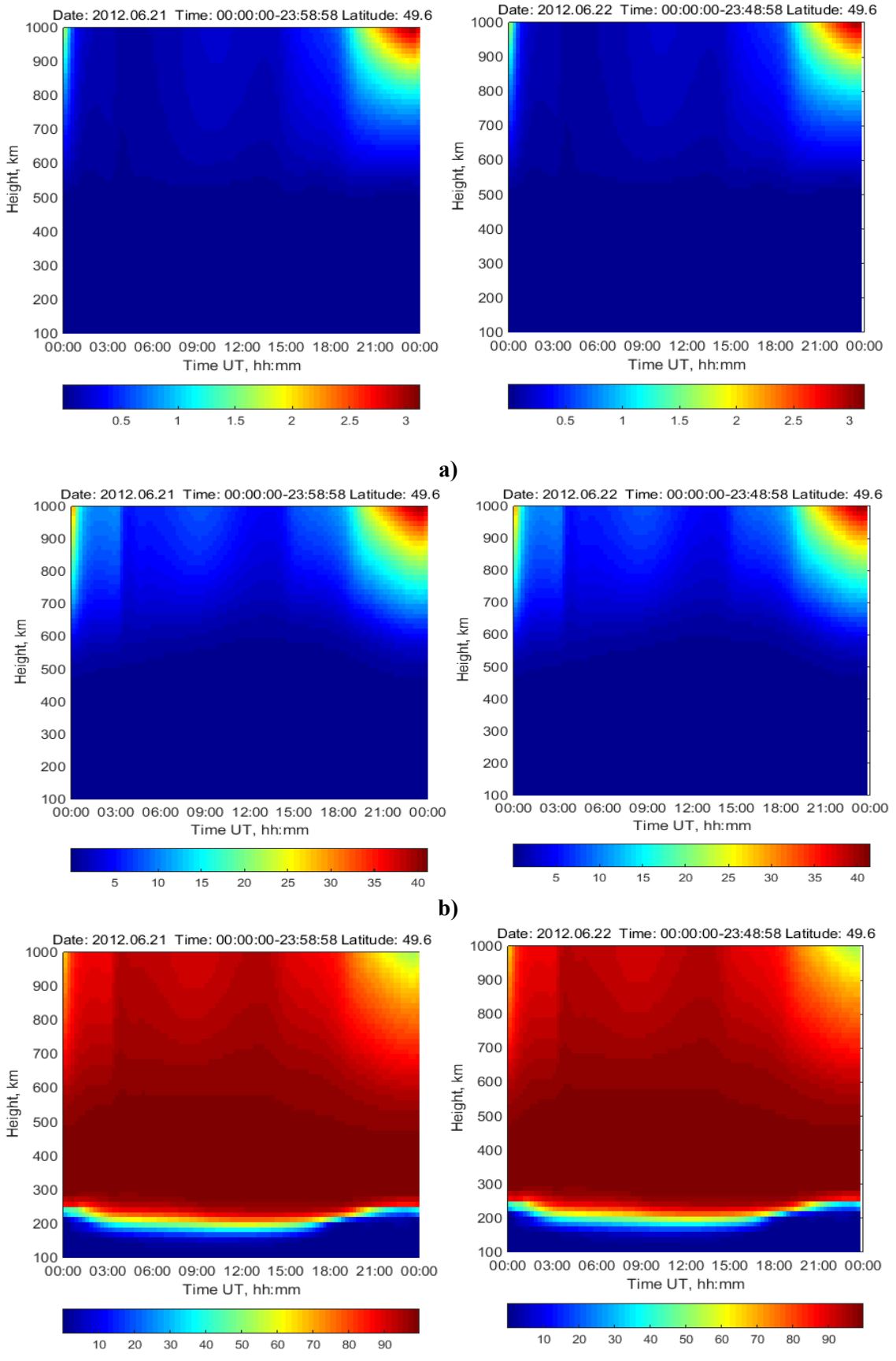

Figure 6.27 Altitudinal and temporal variations of the relative concentrations a) He^+, b) H^+, c) O^+ ions for 21.06.2012 (left panel) and 22.06.2012 (right panel).

6.4.2 18 – 19 June, 2013

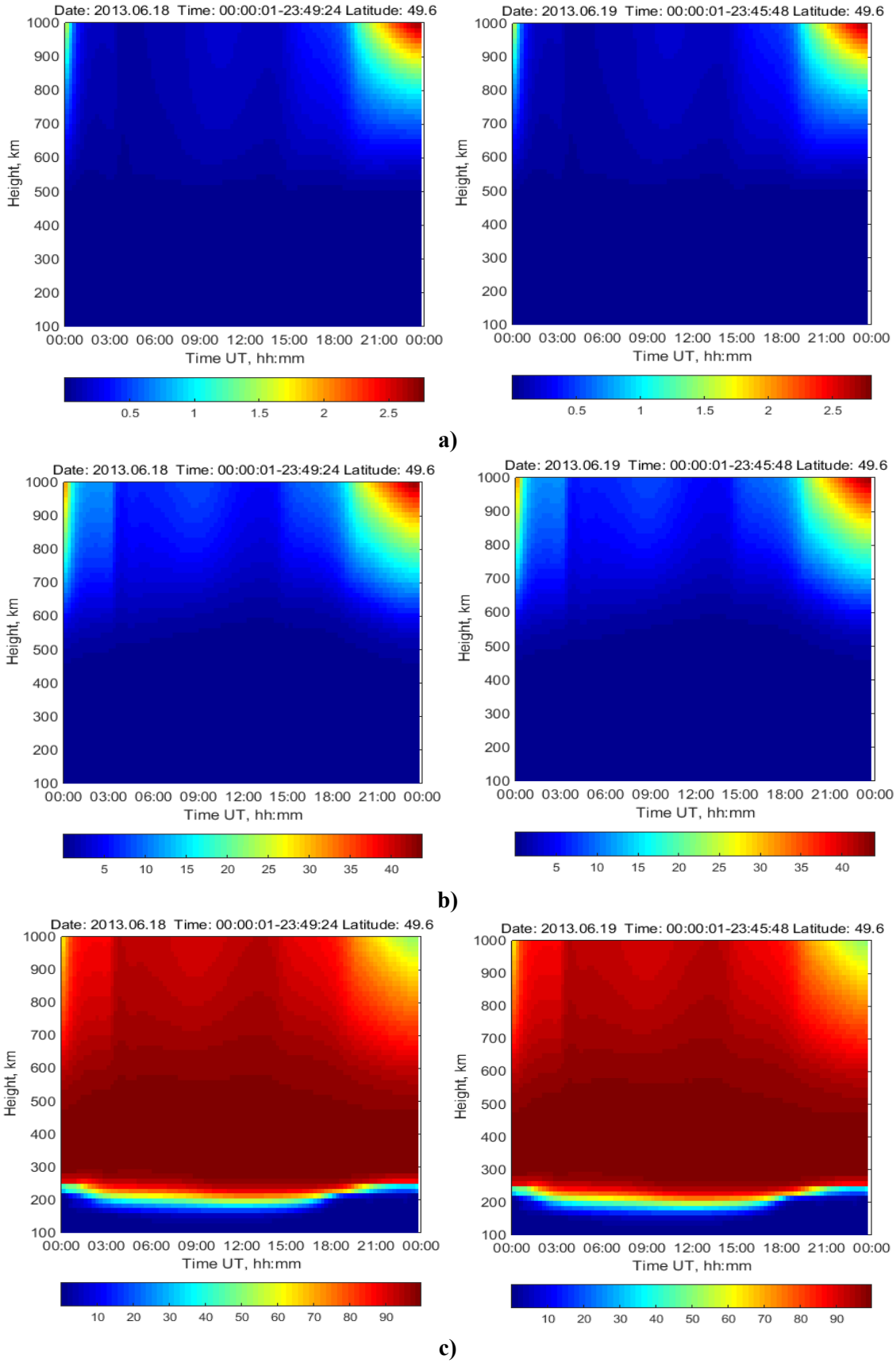

Figure 6.28 Altitudinal and temporal variations of the relative concentrations a) He^+, b) H^+, c) O^+ ions for 18.06.2013 (left panel) and 19.06.2013 (right panel).

6.4.3 25 – 26 June, 2014

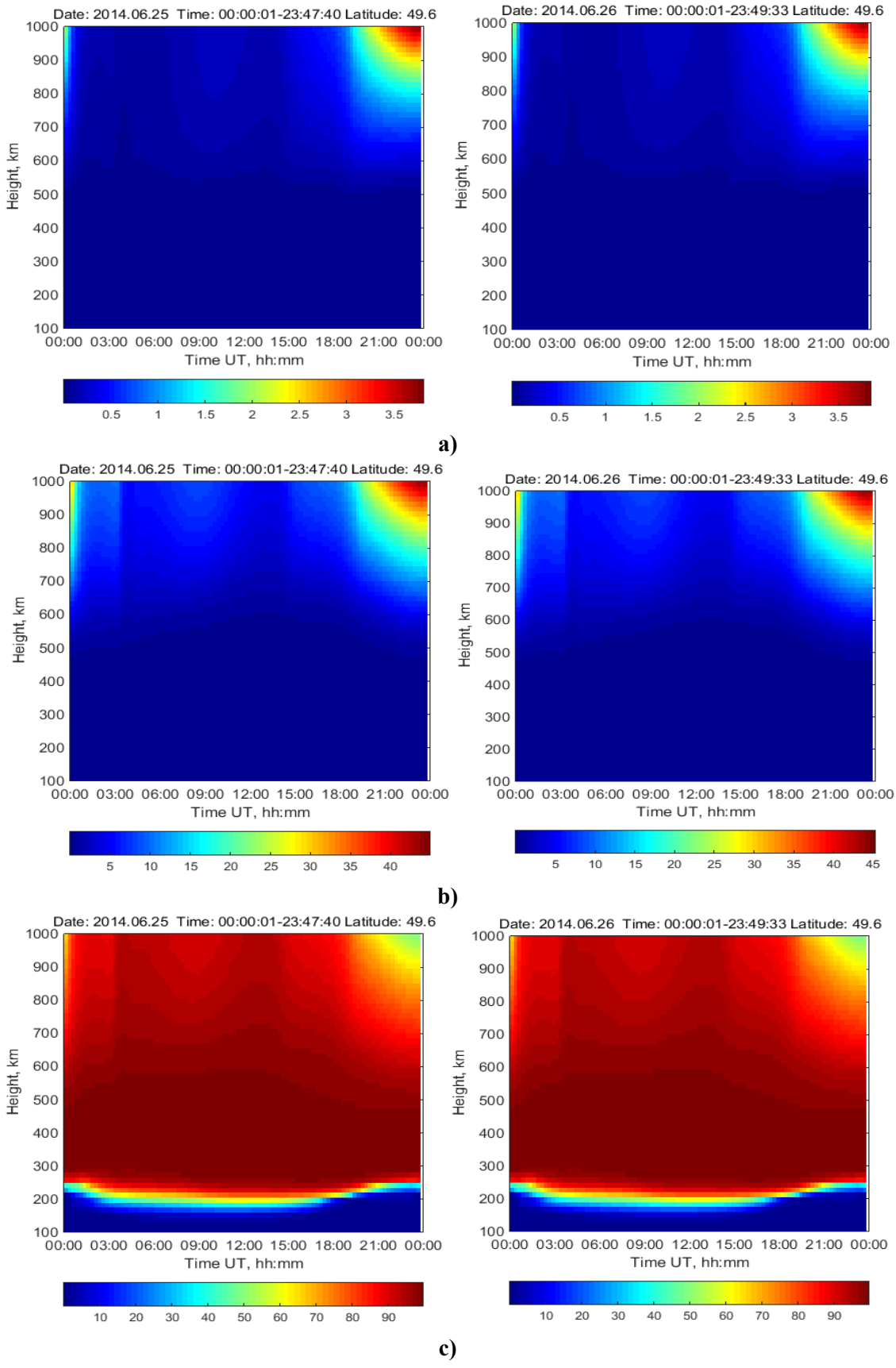

Figure 6.29 Altitudinal and temporal variations of the relative concentrations a) He^+, b) H^+, c) O^+ ions for 25.06.2014 (left panel) and 26.06.2014 (right panel).

6.4.4 18 – 19 June, 2015

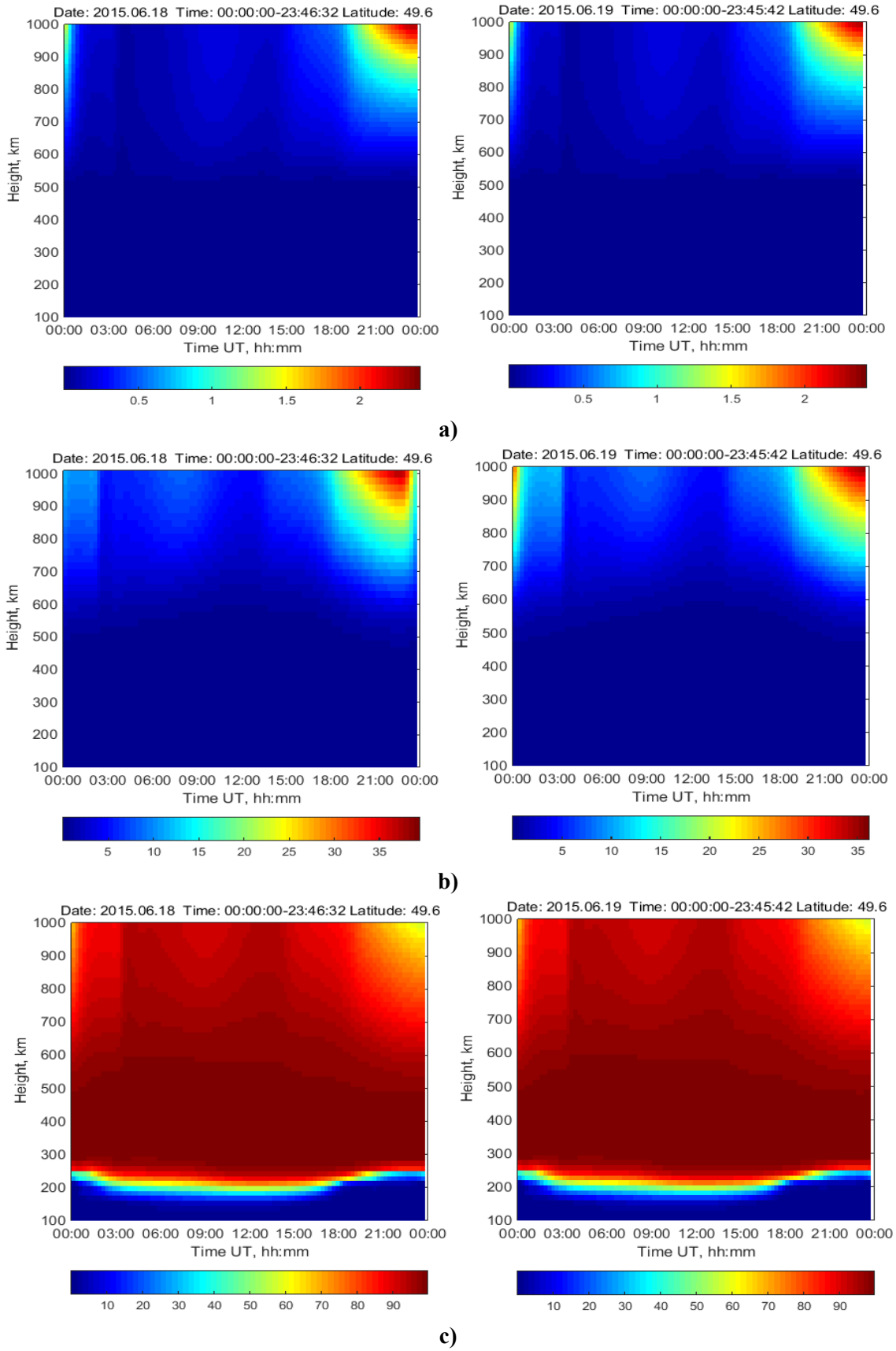

Figure 6.30 Altitudinal and temporal variations of the relative concentrations a) He^+, b) H^+, c) O^+ ions for 18.06.2015 (left panel) and 19.06.2015 (right panel).

6.4.5 01 – 02 July, 2000

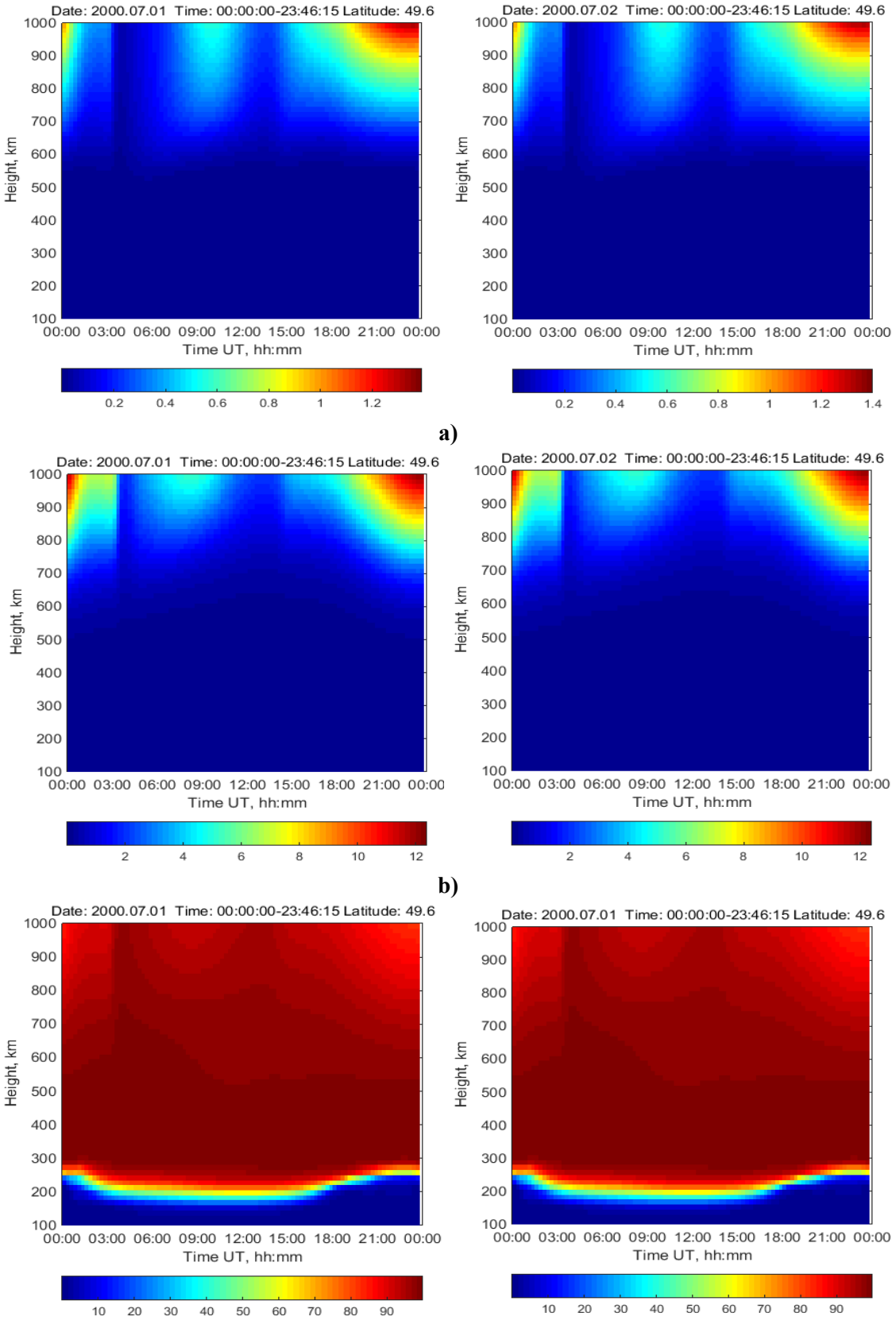

Figure 6.31 Altitudinal and temporal variations of the relative concentrations a) He^+, b) H^+, c) O^+ ions for 01.07.2000 (left panel) and 02.07.2000 (right panel).

6.4.6 15 – 16 June, 2004

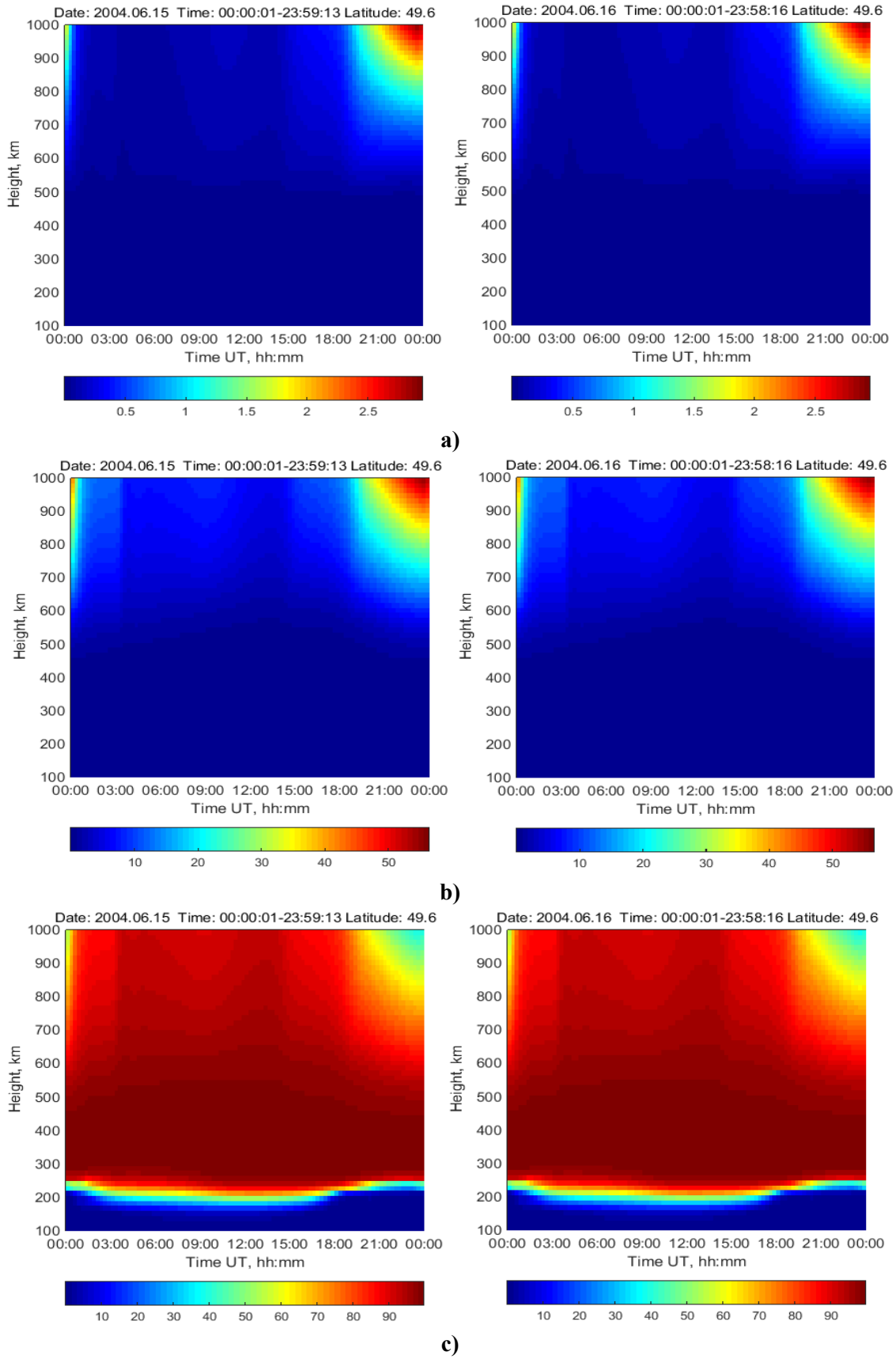

Figure 6.32 Altitudinal and temporal variations of the relative concentrations a) He^+, b) H^+, c) O^+ ions for 15.06.2004 (left panel) and 16.06.2004 (right panel).

The main results of investigation using physical model showed that the maximum amount of helium ions are mainly observed between 21:00 UT and 24:00 UT starting from 800 km altitude and $N(He^+)/N$ did not exceed 4%. Below 600 km, helium ions are absent both during daytime and nighttime. Above 600 km, during daytime $N(He^+)/N$ does not exceed 0.6% for all investigated dates. Only in July 01 – 03, 2000 estimates of $N(He^+)/N$ are reduced to 1.5% at nighttime.

The hydrogen ions according to SAMI3 model also mainly are observed at nighttime above 700 km (from 21:00 to 24:00 UT) where $N(H^+)/N$ is about 40% for the 24th solar cycle. On July 01– 03, 2000 the maximum value of $N(H^+)/N \approx 12\%$ and in June 15 – 17, 2004 $N(H^+)/N \approx 50\%$. During daytime, below 500 km, $N(H^+)/N$ does not exceed 5% and above 500 km $N(H^+)/N$ is ~ 10%.

Compared to hydrogen and helium ions, O^+ are mainly observed in the daytime. During the 24th solar cycle $N(O^+)/N$ is almost 100% below 600 km in the daytime and below 500 km in the nighttime. Above 600 km, $N(O^+)/N$ is reduced to ~ 90% and at night, to ~ 60%. Only in June 15 – 17, 2004, estimate of $N(O^+)/N$ is reduced to 50 % from 20:00 to 24:00 UT above 800 km. The maximum amount of O^+ is observed in July 01 – 03, 2000 both at daytime and at nighttime. $N(O^+)/N$ is not less than 85% for this period.

6.5 Comparison of observational results with estimates of IRI-2012 and SAMI3

Comparative analysis of variations light ions in the upper atmosphere using empirical (IRI-2012) and physical (SAMI3) models as well as observation results of incoherent scatter radar show the following main discrepancies.

Hydrogen ions.

For all dates and the considered heights (see Fig. 6.33 − 6.38) the model values of $N(H^+)/N$ are lower than the experimental results. The absolute magnitude of the observed discrepancies is minimal at daytime and increases during transition to nighttime. For example, during June 19 – 20, 2012 about 24:00 UT at a height of 565 km (Fig. 6.35) the experimental estimates of $N(H^+)/N \approx 7\%$ whereas the corresponding values for SAMI3 are 3 % and IRI (TTS03, NeQuick) only give 1%. Thus, data discrepancies between SAMI3 and IS radar are almost a factor of 2 and 7 for IRI and IS radar respectively. Here it also worth to mention that the maximum value of $N(H^+)/N \approx 30\%$ at nighttime at a height of 743 km, whereas the model values of SAMI3 and IRI is about 10 % and does not exceed 6 % respectively.

Figure 6.36 (June 18 – 19, 2013) shows that the IS radar estimate of $N(H^+)/N$ is about 0.6 % at 385 km (23:00 UT) and increase to 21% at 743 km altitude. During daytime, the relative concentration of H^+ does not exceed 7 % for all altitudes. For the corresponding temporal condition the model values from SAMI3 is 0.2 % at 385 km (discrepancies from IS radar data a factor of 3) and about 16 % at 743 km (discrepancies a factor of 1.5).

The IRI model gives $N(H^+)/N \approx 0.2\%$ during (21:00 – 22:00 UT) at a height of 385 km and close to midnight $N(H^+)/N$ is 0.1 % as during the rest of the day. At a height

of 743 km $N(H^+)/N \approx 6\%$ at 22:00 UT (discrepancies with IS radar data a factor of 2.5) but during the day does not exceed 1 % .

For June 25 – 26, 2014 (see Fig. 6.37) during 21:00 – 01:00 UT, at height 743 km the experimental estimate $N(H^+)/N \approx 40\%$ and in the daytime it is about 8 %. According to model SAMI3, the corresponding values are 15 % at nighttime and not more than 5% in the daytime. Significant discrepancies are observed in the nighttime (to 25 %) and in the daytime, they are less pronounced. Here, it is worth to mention that agreement between IRI model and experimental results is worse at high altitudes than at low. For example, at a height of 743 km discrepancy between IRI data and IS radar is about 20 % at 24:00 UT, whereas at heights 385 km and 431 km no more than 0.5 % at nighttime and good agreement is observed during daytime.

In the summer of 2015 (see Fig. 6. 38) at a height of 624 km the relative concentration of hydrogen ions is about 5 % (at 01:30 UT June 19) and about 2 % at the midday time. The model values for the analogous altitude and temporal conditions are $N(H^+)/N \approx 3$ and 5 % for SAMI3 and about 1 % (both nighttime and daytime) for IRI. At higher altitudes, SAMI3 data insignificantly differ from the experimental results during June 19, whereas the IRI density is a factor of 7 lower at midnight and approximately a factor of 2 in the daytime (at 565, 624 and 743 km). At lower altitudes, the model data in good agreement with observation results. Only at nighttime SAMI3 and IRI estimates (about 01:00 UT at a height of 385 km) differ from experimental results almost a factor 2.

On July 01 – 02, 2000 (see Fig. 6.33) almost at all altitudes, during daytime, SAMI3 and IRI estimates differ from experimental observations by less than 2%. During nighttime (at midnight) at higher altitudes, the model estimates do not differ by more than 3%, while at lower altitudes (at 20:00 UT) by only 1%. The situation is similar in the daytime during June 15 – 16, 2004 (experimental and modeling values only slightly different). At night, discrepancies increase (particularly between IRI and IS radar data). For example, at a height of 624 km on June 15, 2004, at 23:00 UT (see Fig. 6.34) the relative density of H^+ for IS radar $N(H^+)/N = 12\%$ while the corresponding value of IRI is about 3% (discrepancies a factor of 4). At height of 565 km, this difference is about 7%, at 431 and 385 km is 1.5%, and at 312 km is about 2.5%.

Helium ions.

Figures 6.33 – 6.38 show that both physical and empirical models give lower densities that what is observed. The absolute magnitude of discrepancies from the observations increases at high altitudes (above 400 km). For example, during June 19 – 20, 2012 at altitudes 565, 624, and 743 km the maximum value of $N(He^+)/N$ on June 20 are 1.5% (around noon UT), 2% (about 06:00 UT), and 5% at 21:00 UT respectively. From the model results for all altitudes and time $N(He^+)/N$ does not exceed 1%. A similar tendency is observed for another dates. Below 400 km, helium ions is almost absent according to data of models and IS radar. Further, here it worth to mention that variation of He^+ are complicated and depend on the altitude range. From the experimental results, it is possible to see different variation of He^+ for daytime and nighttime conditions. For example, during June 19, 2015 the relative concentration of He^+ reaches the maximum values (about 8 %) at a height of 743 km at 01:00 UT and the minimum (to 1 %) before

and after noon (see Fig. 6.38). For another case (19 June, 2015 at a height of 624 km), the maximum values of $N(He^+)/N$ is about 4 % at noontime and the minimum is close to evening (no more than 1 %).

Atomic oxygen ions.

O^+ density for all dates decreases from day to night (see Fig. 6.33 – 6.38). However, according to IRI there is a tendency of reduced ratio $N(O^+)/N$ below 500 km from 08:00 UT to afternoon (see Fig. 6.35 for 385 km) after which it increases again. According to IS radar, data observations of $N(O^+)/N$ does not change its maximum value throughout the day and starts to decrease closer to midnight. The SAMI3 model is not much different from the daytime at low altitudes, but at night, the model is a bit overestimated whereas the concentration of O^+ should decrease (see Fig. 6.35 for 385 km).

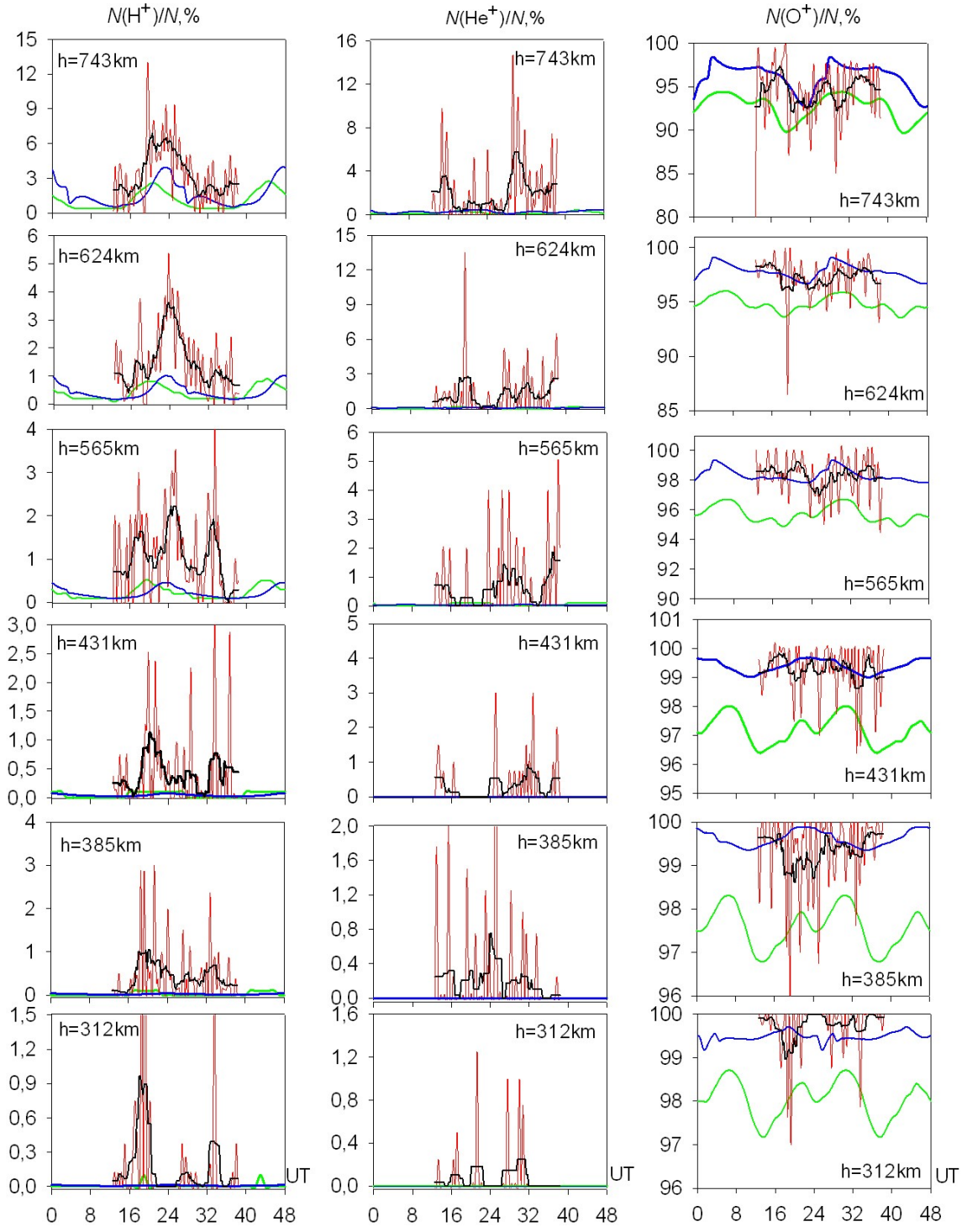

Figure 6.33 Altitude and diurnal variations the relative concentrations of H^+, He^+, O^+ ions 01 – 02 July, 2000. Here and further the red line shows data of Kharkiv incoherent scatter radar, green line – data of model IRI-2012, blue line – data of SAMI3 model, and black line shows the averaged IS radar data.

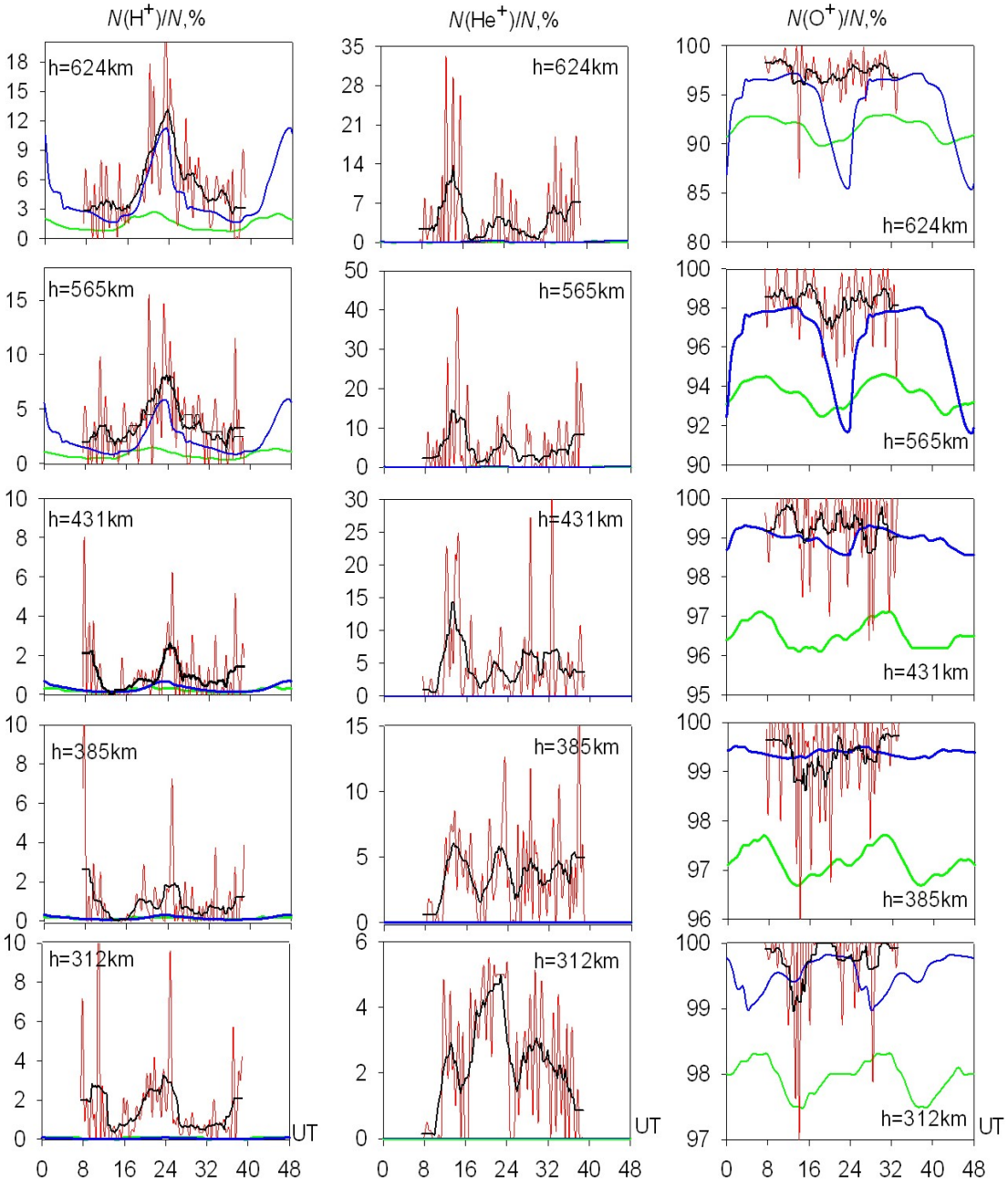

Figure 6.34 Altitude and daily variations the relative concentrations of H^+, He^+, O^+ ions 15 – 16 June, 2004.

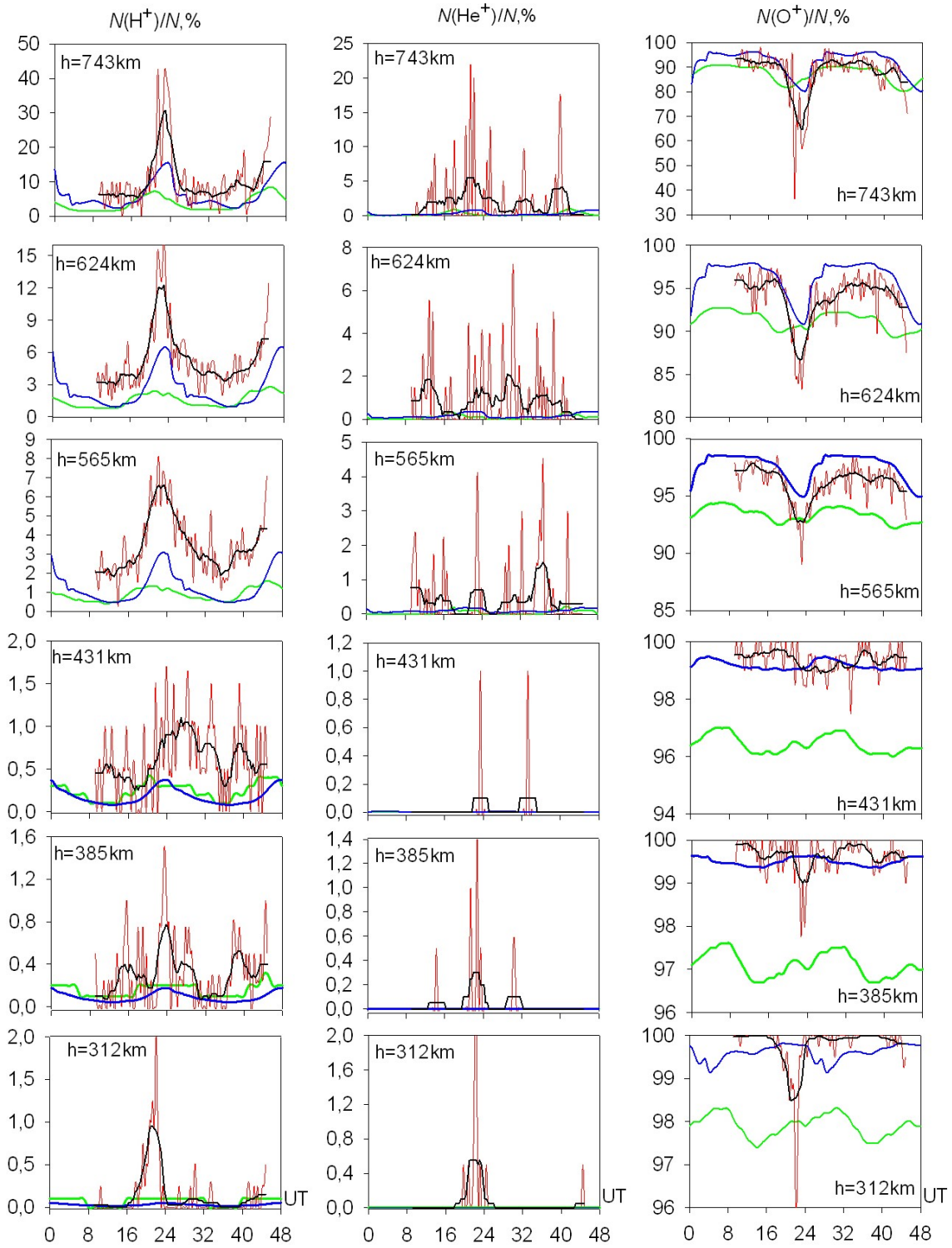

Figure 6.35 Altitude and daily variations the relative concentrations of H^+, He^+, O^+ ions 19 – 20 June, 2012.

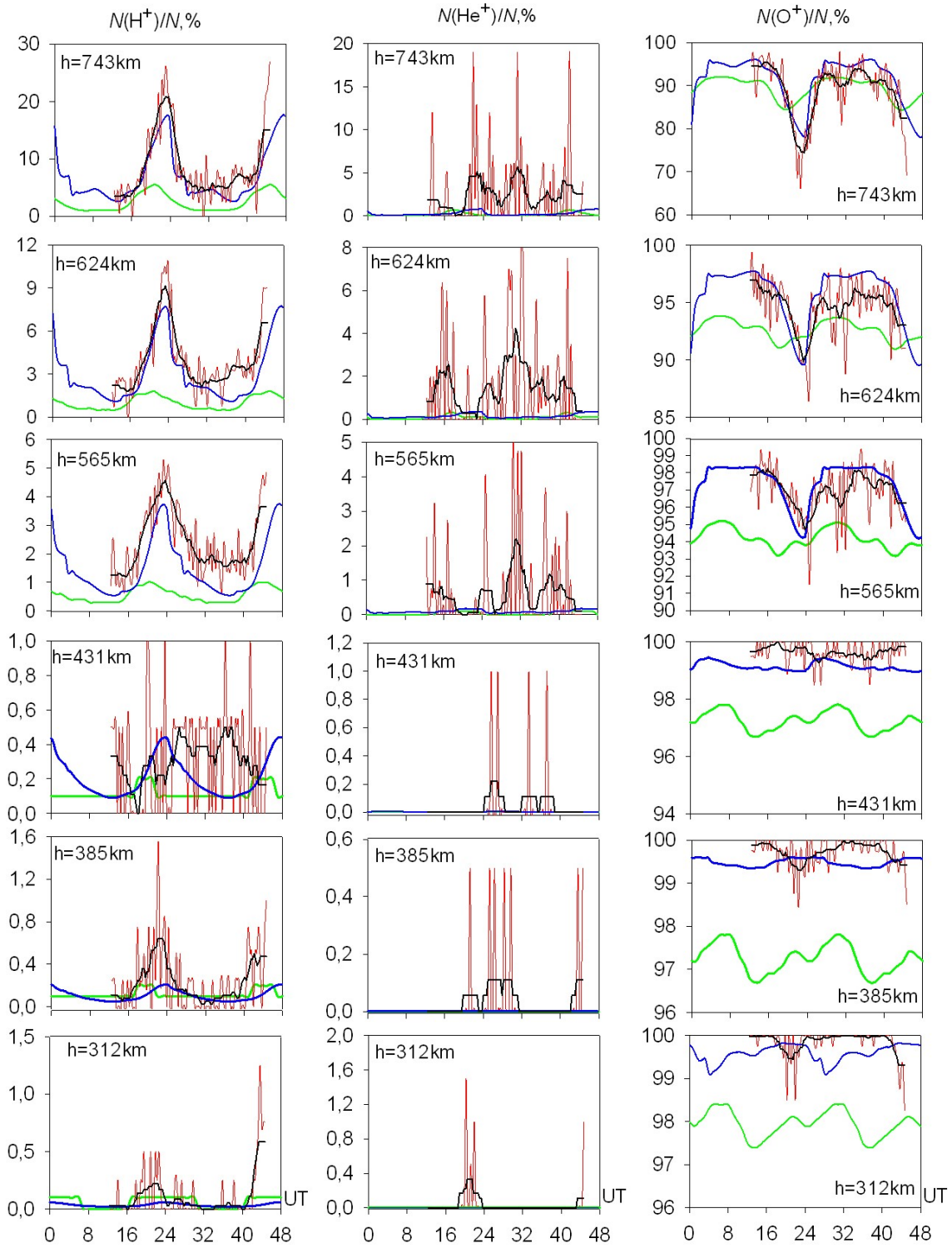

Figure 6.36 Altitude and daily variations the relative concentrations of H^+, He^+, O^+ ions 18 – 19 June, 2013.

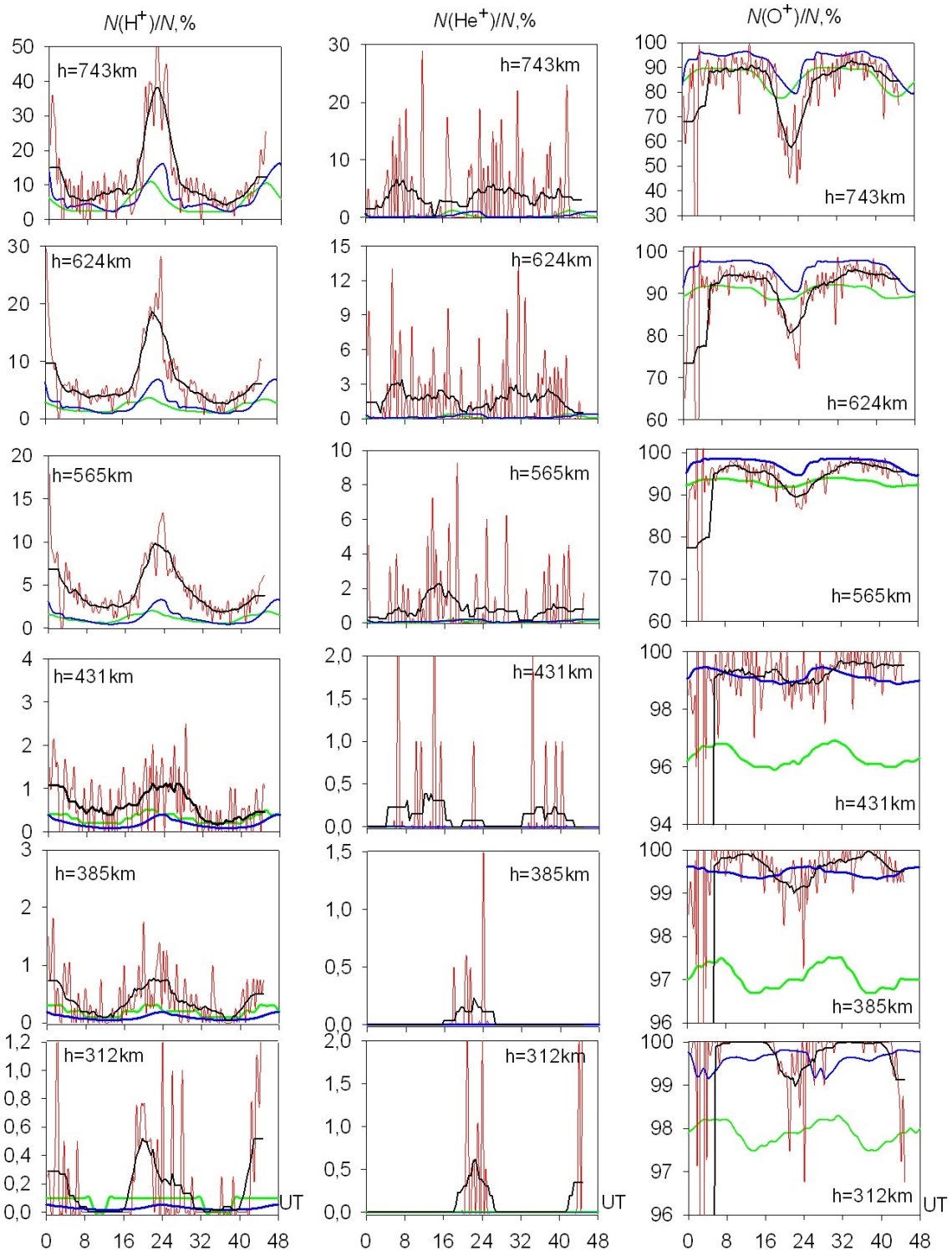

Figure 6.37 Altitude and daily variations the relative concentrations of H^+, He^+, O^+ ions 25 – 26 June, 2014.

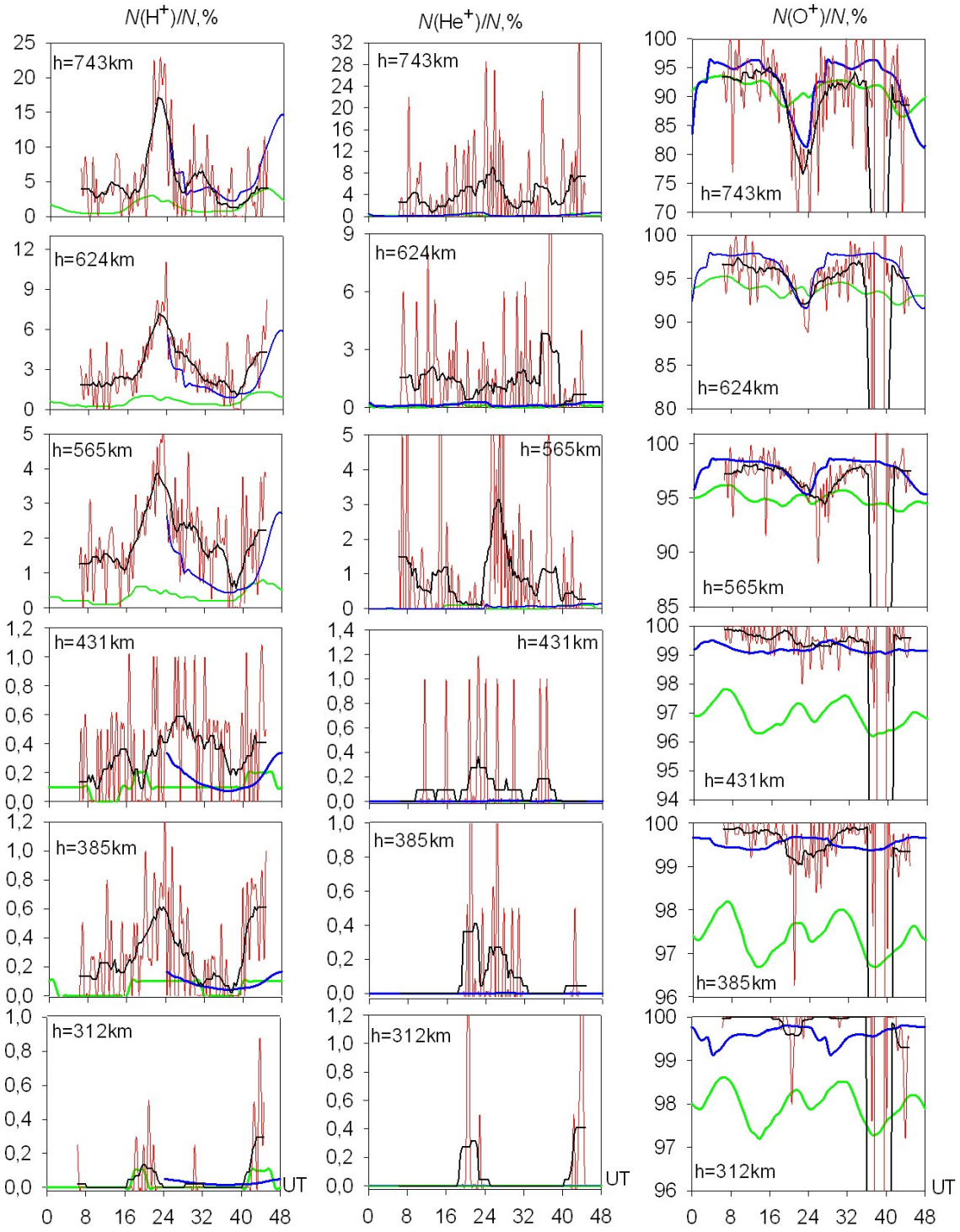

Figure 6.38 Altitude and daily variations the relative concentrations of H^+, He^+, O^+ ions 18 – 19 June, 2015.

Chapter 7

Discussion

7.1 Observation results

The observed relative concentrations of the main topside ion species, which are presented in this thesis, show the behavior of H^+, He^+ and O^+ in the upper ionosphere. In the daytime, estimate of $N(H^+)/N$ is low during the 24th solar cycle (does not exceed 10%). This is because the main source of hydrogen ions is not photoionization of neutral hydrogen atoms, but the charge exchange reaction between O^+ and hydrogen atoms, which during daytime are present in small quantities at lower altitudes. At night, $N(H^+)/N$ reaches maximum values, just before sunrise (local time) when the thermosphere is cooled. The processes, which are described in chapter 3 allow figuratively explain the observed growth of the relative hydrogen ion concentration with increasing height during nighttime conditions

Atomic oxygen ions have an opposite behavior compared to hydrogen ions. Their relative concentration increases during daytime and decreases at night due to recombination processes close to the F_2 - region (see equations 3.12 – 3.14). But $N(O^+)/N$ does not decrease to extremely low values, since the downward plasma velocity is increased at night. This leads to more active transport of H^+ to lower altitudes compared to daytime conditions when $N(O^+)/N$ is increased according to 3.12 –3.14. As a result, losses of H^+ are increased (see reaction 3.19) which lead to enhancement of O^+ density at these altitudes.

Variations of helium ions are more complex. At altitudes up to 600 km, in most cases, there is an increased concentration of He^+ both at night and in the daytime. At higher altitudes, the situation is different. It is possible to observe the daytime maximum in June 20, 2012 (see Fig. 6.1 a and 6.35) or in the morning in June 19, 2013 at a height of 565 km (Fig 6.36 and 6.4 a). The maximum at night can coincide with the maximum in the daytime, as it was in June 18 – 19, 2013 at a height of 743 km (Fig 6.36.), simply absent (June 25 – 26, 2014) or exceeds the daytime maximum (June 19, 2015). Such complicated altitudinal and temporal dependence the distribution of He^+ is associated with altitude-temporal variations of ionization, chemical, and dynamical processes.

Here it is also worth to note from experimental results for the 23rd cycle of solar activity that values of parameter $N(He^+)/N$ are slightly overestimated during daytime while among the dense oxygen plasma it should not be observed (June 15 – 17, 2004).

Such behavior of helium ions for the corresponding dates during daytime caused by the fact that from 2000 to 2006 data have been obtained in the old format. During this period, the step height of signal was about 18.3 km, while after 2006 is about 4.6 km. It can be seen that better results are obtained for the 24th solar cycle.

Thus, the results of this study confirm the influence of dynamic processes (especially at night), on the distribution of light ions. For the midlatitude ionosphere, the main factors, which lead to existence flows of hydrogen ions from ionosphere to plasmasphere (and vice versa) are ambipolar diffusion and neutral winds (*King*, 1965; *Salah,* 1974 and *Danilov*, 1989).

7.2 Comparison the altitudinal and diurnal variations of light ions based on ISR measurements during the 23rd and 24th solar cycles

From the observations presented in chapter 6 about the behavior of O^+, H^+, and He^+ have been found the following differences during the 23rd and 24th solar maximums:

1. During the 23rd solar maximum, the density of O^+ increases with solar activity both during daytime and at night. Particularly noticeable was increase of $N(O^+)/N$ with increasing altitude. Figure 6.16 shows for July 2000 that the maximum concentration of O^+ is observed up to 700 km at nighttime and to 900 km in the daytime, whereas for the 24th solar cycle the maximum values of $N(O^+)/N$ were observed at lower altitudes. For example, in June 2015 the largest numbers of O^+ is observed up to 550 km at night and to 700 km in the daytime (see Fig. 6.12).
2. There are more helium than hydrogen ions in the daytime during the 23rd solar maximum (see Fig. 6.13 and 6.17). Such cases have also been described before by *Heelis*, (1990), *Bauer*, (1965) and *Gonzalez et al.,* (2004). This fact is important and it should be taken into account to improve a model of the ion composition. During the 24th solar maximum the concentration of helium ions in the daytime is less than during the 23rd cycle. Only at higher altitudes is there a slight increase of $N(He^+)/N$ in the daytime conditions. Such behavior of helium ions can be explained as follows: due to increased photoionization rates during a period of enhanced solar activity, particularly during daytime, the relative concentration of He^+ also increases (even at low altitudes). This allows He^+ to be transported to higher altitudes by ambipolar diffusion. At night, the helium ions can not diffuse rapidly through the O^+ to lower altitudes where they would be lost by the charge exchange reaction with N_2 (*Heelis*, 1990). Therefore, they remain at higher altitudes.
3. The relative concentration of hydrogen ions decreases with increasing of solar activity. For the investigated dates during the 23rd and 24th solar maximums, it can be seen that values of parameter $N(H^+)/N$ significantly differ above the 500 km (particularly at nighttime). Figures 6.33 and 6.34 show that in July 01 – 02, 2000 the maximum value of $N(H^+)/N$ is about 6% at 24:00 UT at a height of 743 km and 12% at a height of 624 km in June 15 – 16, 2004. For analogous altitudinal

and temporal conditions in June 25 – 26, 2014 the $N(H^+)/N$ is about 40% and in June 19 – 20, 2012 is about 30% (see Fig. 6.35 and 6.37).

7.3 Comparison between observations and models

The next task was a comparative analysis experimental data and estimates of empirical and physical models. These comparisons show that the IRI model describes only the average and smoothed ionosphere with low accuracy for the relative concentration of all ions considered in this report. It can be seen that it is lower at night but agrees well during daytime. In addition, IRI model shows a good agreement for O^+ but a significant discrepancy in the case of light ions (especially He^+). Discrepancies between experimental results and IRI model can be caused due to the fact that model does not take into account the specific situation which occurs in the certain geophysical conditions.

Thus, the model of ionic composition IRI does not allow to make reliable conclusions about the impact of dynamic and chemical processes on light ions as well as to determine their common features for the mid-latitude ionosphere. The incoherent scatter radar of Institute of Ionosphere make it possible to obtain more reliable data of ionospheric parameters for specified heights, taking into account effect of transport processes and changes in solar activity.

The physical model SAMI3 has a slightly better agreement with experimental results for almost all investigated dates, especially for hydrogen ions at higher altitudes both day and night. Only for atomic oxygen ions at heights below 500 km at night is observed excess of parameter $N(O^+)/N$ and for helium ions a significant decrease of $N(He^+)/N$ for all dates and heights of the 24th solar maximum. Perhaps this is due to neglecting the complexities of interrelated processes in calculations, which have an effect on the behavior of ions in the upper ionosphere.

Chapter 8

Conclusions

Report an investigation of the main features daily variations of the ion composition in the midlatitude topside ionosphere during the 23rd and 24th cycles of solar activity is presented. In addition, a comparative study of these variations with empirical (IRI) and physical (SAMI3) models was performed. The most significant scientific results are following:

- In the analysis of altitude-temporal variations of the relative concentrations H^+, He^+ and O^+, which were obtained using Kharkiv incoherent scatter radar was show changes both throughout the day and with altitude. The concentration of H^+ in the investigated range increases with altitude and reaches maximum values at nighttime. The relative content of O^+ undergoes variations of the opposite nature. During daytime, $N(O^+)/N$ reaches maximum values and at night, minimized. In contrast to the variation of the concentrations of H^+ and O^+ daily variations in the concentration of ions He^+ are more complex. Daily maximum $N(He^+)/N$ significantly depends on altitude and time of day.
- Analysis of the obtained results confirms significant effect of dynamic processes on the concentration distribution of light ions in the upper ionosphere.
- For the obtained results, a comparative analysis of the altitude and diurnal variations of light ions was carried out based on KISR measurements during the 23rd and 24th solar cycles. In the analysis, it was found the characteristic discrepancies and discussed the most probable reasons for such behavior of light ions.
- Further, a comparison of the observed variations the ion composition with estimates of model IRI and SAMI3 was performed. As a result, it was found that the concentrations of H^+, He^+ and O^+ over Ukraine significantly differ from the model estimates. The greatest discrepancies are observed between ISR and IRI. In most cases at night time the model estimates of parameter $N(H^+)/N$ and $N(He^+)/N$ significantly lower. Slightly better agreement is observed for $N(O^+)/N$. Comparison of estimates the SAMI3 model with experimental results showed only a slight overestimation of the parameter $N(O^+)/N$ at altitudes below 500 km and a considerable underestimation of $N(He^+)/N$ for all studied dates, heights and time of day. For hydrogen ions, a better agreement is observed.

Thus, according to the results of this study, it can be concluded that data about the ion composition, which provides ISR of Institute of Ionosphere could be used for the creation of the regional ionosphere model. This model will improve the accuracy of prediction of the altitude-temporal variations of the upper atmosphere parameters over Central Europe.

A. Matlab code

A.1 Script for “Main_Read_txt_SAMI3”

This script calls functions “read_sami_txt” which extracts data from the .txt files of physical model SAMI3 and “plot_sami_txt” which creates plots and .xls files.

```
%% Script for reading Pointdata txt SAMI3 files
% Read txt files of model SAMI3, plot figures with relative density
% and creating .xls files with relative density for software package SigmaPlot
% (Systat Softwhare Inc.)
%%
calc=input('Do you want calculate new date?\n 0 - NO\n 1 - YES\n');
if calc==1, % if we want calculate new date of SAMI3 data;
    clear; % clear old data;
    clc;
    % Calling function for reading text SAMI3 data files:
    [data_array,time_arr_fr_filename,n_h,year,month,day]=read_sami_txt();
elseif calc == 0;
    [FileName,PathName]=uigetfile('*.mat','Open .mat data file');
    load([PathName,'\',FileName]);% load already calculated .mat data files;
end;
% time_arr_fr_filename - time array from filenames;
% n_h - quantity of heights;
%%
% Manual set of parameters:

height_plot_mode = 1; % mode for plot figures:
% 0 - plot figure only for one chosen height;
% 1 - plot for range_heights;
% 2 - plot both figures;

create_xls = 0; % mode for creating .xls files for extract data to program SigmaPlot:
% 0 - don't create .xls files;
% 1 - create .xls files;

In_latitude = 49.6; % [deg], input required latitude;
range_heights = [100,1000]; % [km], input range of heights;
one_height = 430; % [km], or use only one this height,
                  % if 'height_plot_mode' = 1 or 2;

% Calling function for plotting figures of relative dansity and creating
% xls files with relative density (if need):
plot_SAMI3(data_array,time_arr_fr_filename,height_plot_mode,create_xls,...
                        In_latitude,range_heights,one_height);
```

A.2 Function “read_sami_txt”

This function makes it possible to extract the absolute concentrations of H^+, He^+ and O^+ and calculate their relative concentrations $N(X^+)/N$. All data are saved in the array “data_array”.

```
function[data_array,time_arr_fr_filename,n_h,year,month,day]=read_sami_txt()
% function for reading txt files of model SAMI3 and splittig them by
% heights. Main script: "Main_Read_txt_SAMI3".
%
% Input: no input arguments;
```

```
%
% Output:
%  data_array - main total array cells, where each line is one point of time
%            cell columns: 1-file name; 2-Lon [deg]; 3-Lat [deg]; 4-H [km];
%                          5-N_e [cm^-3]; 6-N_ion [cm^-3]; 7- N_ion./N_e [%]
%            arrays in each cell is n x m, where n - line of different latitudes,
%                                          m - column of different heights;
%  time_arr_fr_filename - time array from names of files;
%  n_h - quantity of heights in each file;
%  year,month,day - date for current file;
%================================================================================

%% Get file name:
[~,File_Pth] = uigetfile('*.t*','Open txt data files');
list = dir(File_Pth); % get list of files in selected directory;

%% Removing line-folder in "list"
k=1;
for i=1:length(list) % i is line "list";
 % if line in the "list" is a folder OR not txt file:
   if ((list(i).isdir)==1)||( (isempty(strfind(list(i).name,'.txt')))||...
            ((isempty(strfind(list(i).name,'pointdata')))) ),

        n_empt_line(k)=i; % write this line number in array;
       k=k+1;
   end;
end;
list(n_empt_line)=[]; % delete line in "list" which is folder or not txt file;

%% Extract data from txt SAMI files:
% Initialization variables:
data_array=cell(length(list),7); % array for data;

for n_file=1:length(list)% n_file - file number in list;
    % Reading data from txt file:
    fid = fopen([File_Pth list(n_file).name],'r');
    Data = textscan(fid,'%f %f %f %f %f','commentStyle','#');
% columns of Data: 1-Longit,deg| 2-Latitud,deg| 3-H,km| 4-N_e,cm^-3| 5-N_ion,cm^-3.

% array of cells: each line is one point of time
% columns: 1-file name; 2-Lon,deg; 3-Lat,deg; 4-H,km; 5-N_e,cm^-3; 6-N_ion,cm^-3.
    fclose(fid);

%% Splitting the file by the heights:
h_count=0;% set counter of change of the height H;
n_h=0; % set counter of number heights (array number for one height);

    for line=1:length(Data{1,3})-1 % line - line number in file;
        h_count=h_count+1; % increase counter of change of the height H;

        % definition boundaries of the same heights in file:
         if (Data{1,3}(line+1)>Data{1,3}(line)), % if H2>H1
             n_h=n_h+1; % increase number heights;
             line_begin=line-h_count+1; % the begin one height;
             Longit(:,n_h)= Data{1,1}(line_begin:line);
             Latitude(:,n_h)= Data{1,2}(line_begin:line);
             Heights(:,n_h) = Data{1,3}(line_begin:line);
             N_e(:,n_h) = Data{1,4}(line_begin:line);
             N_ion(:,n_h) = Data{1,5}(line_begin:line);
             h_count=0;
         end;

        if(line==length(Data{1,3})-1),% the last "piece" of one height in the txt file;
            n_h=n_h+1;
            line_begin=line-h_count+1;
            Longit(:,n_h)= Data{1,1}(line_begin:line+1);
            Latitude(:,n_h)= Data{1,2}(line_begin:line+1);
```

```
            Heights(:,n_h) = Data{1,3}(line_begin:line+1);
            N_e(:,n_h) = Data{1,4}(line_begin:line+1);
            N_ion(:,n_h) = Data{1,5}(line_begin:line+1);
        end;

    end;

% Calculation of the relative density in "%" = N(ion)/Ne *100%:
Relat_dens=(N_ion./N_e)*100;

%% Time array from filenames:
time_arr_fr_filename(1,n_file)=datenum([str2double(list(n_file).name(24:27)),...
    str2double(list(n_file).name(28:29)), str2double(list(n_file).name(30:31)),...
    str2double(list(n_file).name(33:34)), str2double(list(n_file).name(35:36)),...
    str2double(list(n_file).name(37:38))]); % format(Year,Month,Day, HH,MM,SS);

%% Create total array:
    % array of cells: each line is one point of time;
    % columns of cells: 1-file name; 2-Longitude [deg]; 3-Latitude [deg];
    % 4-Height [km]; 5-N_e [cm^-3]is the electron density;
    % 6-N_ion [cm^-3]is the ion density; 7- N_ion./N_e [%]is the relative density.
    % Columns in internal arrays are for heights from txt data file...
    % (see 4th column cell in data_array)
    % Rows in internal arrays are latitude;
data_array{n_file,1}= list(n_file).name;
data_array{n_file,2}= Longit; % 2nd column cells in data_array;
data_array{n_file,3}= Latitude; % 3d column cells in data_array;
data_array{n_file,4}= Heights; % 4th column cells in data_array;
data_array{n_file,5}= N_e; % 5th column cells in data_array;
data_array{n_file,6}= N_ion; % 6th column, electron density;
data_array{n_file,7}= Relat_dens; % relative density;

end; % the end of extract data from .txt SAMI files;
%%
% Date of current file:
year = data_array{1,1}(24:27);
month = data_array{1,1}(28:29);
day = data_array{1,1}(30:31);
total_file_name=['Data_SAMI3_',year,month,day,'_',data_array{1,1}(33:34),...
     data_array{1,1}(35:36),data_array{1,1}(37:38),...
     '-',data_array{n_file,1}(33:34),data_array{n_file,1}(35:36),...
     data_array{n_file,1}(37:38)]; % total file name from name txt SAMI file.

%% Save total array to mat file:
   [tot_file_nam2,tot_file_pth]=uiputfile([total_file_name,'.mat'],...
'Selct folder for save file');
 % tot_file_nam2 - file name with user corrections;
 save(sprintf('%s\\%s',tot_file_pth,tot_file_nam2),'data_array',...
     'time_arr_fr_filename','year','month','day');
end % the end of function;
```

A.3 Function “plot_SAMI3”

This function is responsible for plotting the relative concentrations for the required altitude range. In addition, this function create .xls files with data.

```
function[year,month,day]=plot_SAMI3(data_arr,time_arr,height_plot_mode,...
            create_xls,In_latitude,range_heights,one_height)
% function for main program "Main_Read_txt_SAMI3" for plot figures
% for one or range heights and creates xls files for SigmaPlot.
%
% Output:
%   year,month,day - date for current files
%
```

```
% Input:
%   data_arr - main total array cells, where each line is one point of time;
%            cell columns: 1-file name; 2-Lon [deg]; 3-Lat [deg]; 4-H [km];
%                          5-N_e [cm^-3]; 6-N_ion [cm^-3]; 7- N_ion./N_e [%]
%            arrays in each cell is n x m, where n - line of different latitudes,
%                                          m - column of different heights;
%   time_arr - time array from files name;
%   height_plot_mode - mode for plot figures:
%       0 - plot figure only for one chosen height;
%       1 - plot for range_heights;
%       2 - plot both figures;
%   create_xls - mode for creating xls files for extract data to program SigmaPlot:
%       0 - don't create xls files;
%       1 - create xls files;
%   In_latitude - [deg], input latitude;
%   range_heights - [km], heights for plot, [H_begin, H_end];
%   one_height - [km], required height, height for plot for the mode one height.
%=========================================================================================
%
qty_line=length(data_arr); % numbers of lines in data_array
n_h = length(data_arr{1,4}(1,:)); % numbers of heights
%
% index of latitude in array of latitudes form data_array:
[~,ind_LAT]=min(abs(In_latitude(1)-data_arr{1,3}(:,1)));

N_e=zeros(1,n_h);% set array for electron density;
N_H_p=zeros(1,n_h);% set array for ion density;
Relat_dens=zeros(1,n_h);% set array for relative density;

  for i_plot = 1:qty_line, % i_plot - line number (or time) from "data_array"
% (see 1-st column)
      % columns in arrays correspond to heights from "heights_line":
      % reading data from "data_array":
      N_e(i_plot,:) = (data_arr{i_plot,5}(ind_LAT,:));
      N_H_p(i_plot,:) = (data_arr{i_plot,6}(ind_LAT,:));
      Relat_dens(i_plot,:) = (data_arr{i_plot,7}(ind_LAT,:));

  end;
%
heights_line= data_arr{1,4}(1,:); % the one-line array with heights;
% Current date:
year = data_arr{1,1}(24:27);
month = data_arr{1,1}(28:29);
day = data_arr{1,1}(30:31);

%% Plot for one height:
if (height_plot_mode ==0) || (height_plot_mode ==2)
% index of required height:
[~,ind_height]=min(abs(one_height-heights_line));

figure('Units', 'centimeters','position', [0 3 17 12]);
plot(time_arr,Relat_dens(:,ind_height));

 str_title1 =['Date: ',year,'.',month,'.',day,'  ','Time: ',...
 data_arr{1,1}(33:34),':',data_arr{1,1}(35:36),':',data_arr{1,1}(37:38),...
 '-',data_arr{qty_line,1}(33:34),':',data_arr{qty_line,1}(35:36),...
 ':',data_arr{qty_line,1}(37:38),'  H = ', num2str(heights_line(ind_height)),...
 ' km',' Latitude: ',num2str(data_arr{1,3}(ind_LAT,1))];
title(str_title1);

grid on;
xlabel('Time UT, hh:mm');
datetick('x',15);
ylabel('Relative density, [%]');

end; % the end Plot for one height;
```

```
%% Plot for many heights (color):
if (height_plot_mode ==1) || (height_plot_mode ==2)

[~,ind_height1]=min(abs(range_heights(1)-heights_line));
[~,ind_height2]=min(abs(range_heights(2)-heights_line));

figure;
 pcolor(time_arr,heights_line(ind_height1:ind_height2),...
                            (Relat_dens(:,ind_height1:ind_height2))');
 shading flat;
 colormap('jet');
 colorbar('southoutside');
 xlabel('Time UT, hh:mm');
 ylabel('Height, km');
 ax1=gca;
 datetick('x',15);
 fig=gcf;

 str_title2 =['Date: ',year,'.',month,'.',day,'  ','Time: ',...
 data_arr{1,1}(33:34),':',data_arr{1,1}(35:36),':',data_arr{1,1}(37:38),...
 '-',data_arr{qty_line,1}(33:34),':',data_arr{qty_line,1}(35:36),...
 ':',data_arr{qty_line,1}(37:38),' ','Latitude: ',num2str(data_arr{1,3}(ind_LAT,1))];

 t=title(str_title2);
 t.FontSize=11; % size font for title;
 t.FontWeight = 'normal';
 ax1.Position = [0.15 0.25 0.5 0.7];
 ax1.FontSize = 11; % size font for axes;
 fig.PaperUnits = 'centimeters';
 fig.PaperPositionMode = 'manual';
 fig.PaperPosition = [0 0 19 13];
 % Save figure:
 [figfile_nam,figfile_pth]=uiputfile(['*','.*'],...
                                'Select folder for save figure');
 % figfile_nam - figure name with user corrections;
 if figfile_nam~=0, % save fugure if it is selected name;
 saveas(fig,[figfile_pth,figfile_nam],'fig'); % save in MATLAB format;
 print([figfile_pth,figfile_nam],'-dpng','-r0'); % save in png format;
 end;
end; % the end of Plot for many heights (color);

%% Save data in XLS files:
%%
if create_xls==1;
time_hour_arr = (time_arr - datenum(str2double(year),str2double(month),...
    str2double(day),00,00,00))/(1/24); % array of hours;
   [tot_file_nam3,tot_file_pth3]=uiputfile(['*','.*'],...
                                'Select folder for save relat density');
 % tot_file_nam3 - file name with user corrections;

 % Save variables to file to path:tot_file_pth3 with name: tot_file_nam3:
 save(sprintf('%s\\%s',tot_file_pth3,tot_file_nam3),'Relat_dens',...
   'heights_line','one_height','year','month','day','time_arr'); % save to mat file;
 xls_name_path = [tot_file_pth3,'\',tot_file_nam3]; % name and path for xls file;
 % Save to xls file:
 xlswrite(xls_name_path,[[NaN,heights_line];[time_hour_arr',Relat_dens]]);
end;

end % the end of function;
```

Bibliography

Acasofu, S. I. and S. Chapman (1972), *Solar–Terrestrial Physics*, Oxford, U.K.: Clarendon Press.

Apponte, N., C.G.M. Brum, M.P. Sulzer, S. A. Gonzalez (2013), Measurements of the O^+ to H^+ transition height and ion temperatures in the lower topside ionosphere over Arecibo for equinox conditions during the 2008–2009 extreme solar minimum, *Journal of Geophysical Research: Space Physics, 118*(7), P. 4465-4470, DOI: 10.1002/jgra.50416.

Bauer, S. J. (1964), Some implications of a direct measurement of the hydrogen and helium ion distribution in the upper atmosphere, *Journal of Geophysical Research, 69*(3), P. 553-555, DOI: http://dx.doi.org/10.1029/JZ069i003p00553.

Bauer, S. J. (1965), Hydrogen and helium ions-NASA-TM-X-55329, *Sponsoring Organization*: *NASA Goddard Space Flight Center*.

Bilitza, D. (2014), The International Reference Ionosphere: Rawer's IRI and its status today, *Advances in Radio Science: Kleinheubacher Berichte, 12*, P. 231–236, DOI: 10.5195/ars-12-231-2014.

Bilitza, D., D. Altadill, Y. Zhang, C. Mertens, V. Truhlik, P. Richards, L-A. McKinnel, and B. Reinisch (2014), The International Reference Ionosphere 2012-a model of international collaboration, *Journal of Space Weather and Space Climate, 4*(A07), DOI:10.1051/swsc/2014004.

Bogomaz, A. V. (2012), Model of the processing system of incoherent scatter radar data, *Bulletin of the National Technical University "Kharkiv Polytechnic Institute". Series*: *Radiophysics and Ionosphere, 57*(963), P. 18 – 24 (in Russian).

Bogomaz, A. V. (2013), The results of the signal processing IS considering the width of the probe pulse spectrum. *Journal of NTU "KhPI". Series: Radio and ionosphere, 28*(1001), P. 21-24, (in Russian).

Brekke, A. (2013), *Physics of the Upper Polar Atmosphere,* (2-nd ed.), Springer.

Brunelli, B., and A. A. Namgaladze (1988), *Physics of ionosphere,* Moscow: Nauka (in Russian)

Chen, F. F. (1984), *Introduction to Plasma physics and Controlled Fusion,* (2-nd ed.), V.1: Plasma physics), Springer.

Chernogor, L. F. (2007), The Earth-Atmosphere – Ionosphere – Magnetosphere as an Open Dynamic Nonlinear Physical System. 2, *Nonlinear World, 5*(4), P. 198-231, (in Russian).

Chernyak, Yu. V., and V.N. Lysenko (2013), Measurements of the Ionosphere Plasma Electron Density Variation by the Kharkov Incoherent Scatter Radar, *Acta Geophysica, 61*, P. 1289-1303, DOI: 10.2478/s11600-013-0118-0.

Committee on Solar-Terrestrial research for the 1980's. NASA-CR-169258 (1981)*, Geophysics Research Board, Assembly of Mathematical and Physical Sciences National Research Council*, Washington: NATIONAL ACADEMY PRESS.

Danilov, A., and A. Yaichnikov (1985), A new model of the ion composition at 75 km to 1000 km for IRI, *Advances in Space Research, 5*(7), P. 75–79, DOI: 10.1016/0273-1177(85)90360-6.

Danilov, A. D. (1989), *Popular Aeronomy,* (2-nd ed.). Leningrad: Gidrometeoizdat, (in Russian)

Domnin, I. F., Ya.N. Chepurny, L.Ya. Emelyanov, S.V. Chernyaev, A.F. Kononeko, D.V. Kotov, O.V. Bogomaz, and D.A. Iskra (2014), Kharkiv Incoherent Scatter Facility, *Bulletin of the National Technical University "Kharkiv Polytechnic Institute". Series*: *Radiophysics and Ionosphere, 47*(1089), P. 28-41.

Emelyanov, L. Ya., and A. A. Kononenko (2011), Ionosonde "Bazis" of the Institute of Ionosphere as a tool for monitoring the state of the ionosphere, *Radiotekhnika: All-Ukr. Sci. Interdep. Mag*, 167, P. 30-33, (in Russian).

Emelyanov, L. Ya., and T. G. Zhivolup (2013), History of the development of IS radars and founding of the Institute of Ionosphere in Ukraine, *History of Geo- and Space Sciences*, (4), P. 7-17, DOI:10.5194/hgss-4-7-201.

Evans, J. (1969), Theory and practice of ionosphere study by Thomson Scatter radar, *Proceedings of the IEEE, 57*(4), P. 496-530, DOI: 10.1109/PROC.1969.7005.

Evans, J. (1975), High-power radar studies of the ionosphere, *Proceedings of the IEEE, 63*(12), P. 1636–1650, DOI:10.1109/PROC.1975.1003.

Frank-Kamenetzky, D. (1975), *Plasma - the fourth state of matter,* (4-th ed.), Moscow: Atomizdat, (in Russian).

González, S. B. (1992), Ion Composition of the Topside Equatorial Ionosphere during Solar Minimum, *Journal Geophysical Research, 97*, P. 4299.

González, S. A., M. P. Sulzer, M. J. Nicolls, and R. B. Kerr (2004), Solar cycle variability of nighttime topside helium ion concentrations over Arecibo, *Journal of Geophysical Research: Space Physics, 109*(A07302), P.n/a-n/a, DOI: 10.1029/2003JA010100.

Hargreaves, J. (1982), *The Solar-Terrestrial Environment: An Introduction to Geospace – The Science of the Terrestrial Upper Atmosphere, Ionosphere, and Magnetosphere,* New York: Cambridge University Press.

Heelis, R. A, W. B. Hanson, and G.J. Bailey (1990), Distribution of He^+ at middle and equatorial latitudes during solar maximum, *Journal of Geophysical Research, 95*(A7), P. 103113-10320, DOI:10.1029/JA095iA07p10313.

Heelis, R.A., W.R Coley, A.G. Burrell, M.R. Hairston, G.D. Earle, M.D. Perdue, R.A. Power, L.L. Harmon, B.J. Holt, C.R. Lippincott (2009), Behavior of the O^+/H^+ transition height during the extreme solar minimum of 2008, *Geophysical Research Letters, L00C03*, DOI: 10.1029/2009GL038652 .

Huba, J. D., G. Joyce, and J. A. Fedder (2000), SAMI2 (Sami2 is Another Model of the Ionosphere): A New Low-Latitude Ionosphere Model, *Journal Geophysical Research: Space Physics, 105*(10), P. 23035-23053.

Huba, J. D., G. Joyce, and J. Krall (2008), Three-dimensional equatorial spread F modeling, *Geophysical Research Letters, 35*(10), P. n/a-n/a, DOI: 10.1029/2008GL033509.

International Reference Ionosphere (2015), http://iri.gsfc.nasa.gov

Ivanov-Kholodnyi, G. S. (1980), Predicting the state of the ionosphere. A deterministic approach, Leningrad: Gidrometeoizdat, (in Russian).

Isham B., C. A. Tepley, M.P. Sulzer, Q. H. Zhou, M.C. Kelley, J.S. Friedman, and S.A. Gonzalez (2000), Upper atmospheric observations at the Arecibo Observatory: Examples obtained using new capabilities, *Journal of Geophysical Research: Space Physics, 105*(A8), P. 18609-18637, DOI: 10.1029/1999JA900315 .

Kazimirovsky, E. S. (1973), Wind and drifts in the ionosphere, *Scientific reviews and reports,*(7), P. 52, (in Russian).

King J.W. and H. Kohl (1965), Upper atmospheric winds and ionospheric drifts caused by neutral air pressure gradients, *Nature, 206*(4985), 699 – 701, DOI: 10.1038/206699a0.

Kotov, D. V. (2013), Seasonal variations of the relative concentration of hydrogen ions in the upper ionosphere over Ukraine according to the method of incoherent scattering and their comparison with estimates of model IRI-2012. 1. Maximum of solar activity, *Radio physics and radio astronomy, 18* (1), P. 43-48.

Kotov, D.V., and A.V. Bogomaz (2013), New generation program for data processing Incoherent Scatter Radar (UPRISE), *Radiophysics and Ionosphere*, (28), P.29-37, (in Russian).

Kotov, D V., V. Truhlík, , P. G. Richards, S. Stankov, O. V. Bogomaz, L. F. Chernogor, and I. F. Domnin (2015), Night-time light ion transition height behaviour over the Kharkiv (50°N, 36°E) IS radar during the equinoxes of 2006–2010, *Journal of Atmospheric and Solar-Terrestrial Physics, 132*, P. 1-12, DOI: 10.1016/j.jastp.2015.06.004.

Kotov, D. and Y. Kleynosov (2010), Modeling the effect of neglect the presence of helium ions on the accuracy of estimates of the ionospheric plasma parameters by incoherent scattering, *"Kharkiv Polytechnic Institute". Series: Radiophysics and Ionosphere, 48*, http://archive.kpi.kharkov.ua/View/22387/

Krinberg, I.A. and A.V. Tashchilin (1984), *Ionosphere and Plasmasphere*, Moscow: Nauka (in Russian).

Nygren, T. (1996), *Introduction to Incoherent Scatter Measurements*, Invers.

Pulyaev, V. A., D. A. Dzyubanov, and I. F. Domnin (2011), *Determination of the ionospheric parameters using the incoherent scattering technique*, Kharkiv: NTU "KhPI", (in Russian).

Raitt, W.J., R.W. Schunk, and P.M. Banks (1978), Helium ion outflow from the terrestrial ionosphere, *Planetary and Space Science, 26*(3), P. 255-268, DOI: 10.1016/0032-0633(78)90091-0.

Ratcliffe, J. (1972), *An Introduction to the Ionosphere and Magnetosphere*, London: Cambridge University Press.

Rogozhkin, E.V., V.A. Pulyaev, and V.N. Lysenko (2008), *Sounding signals to study the ionosphere by the incoherent scattering,* Kharkiv: NTU "KhPI" (in Russian).

SAMI3 (Sami3 is Also Model of the Ionosphere),
http://ccmc.gsfc.nasa.gov/models/modelinfo.php?model=SAMI3

Salah, J.E., and J.M. Holt (1974), Midlatitude thermospheric winds from incoherent scatter radar data, *Radio Science, 9*(2), P. 301—313, DOI: 10.1029/RS009i002p00301.

Schunk, R., and A. Nagy (2009), *Ionospheres: Physics, Plasma Physics, and Chemistry*, Cambridge atmospheric and space sciences series, Cambridge University Press.

Sojka, J. (1989), Global scale, physical models of the F region ionosphere, *Reviews of Geophysics, 27*(3), P. 371–403, DOI:10.1029/RG027i003p00371.

Solomon, S.C., T.N. Woods, L.V. Didkovsky, J.T. Emmert, L. Qian (2010), Anomalously low solar extreme-ultraviolet irradiance and thermospheric density during solar minimum, *Geophysical Research Letters, 37*(16), DOI: 10.1029/2010GL044468.

Taran, V. (2001), The investigations of ionosphere in naturally and artificially perturbed states by incoherent scatter method, *Geomagn. Aeronomy, 41*(5), P. 659–666, (in Russian).

Taylor, H. (1971),. Evidence of solar geomagnetic seasonal control of the topside ionosphere. *Planetary and Space Science, 19*(1), P. 77-93, DOI: 10.1016/0032-0633(71)90068-7.

Triskova, L., V. Truhlik, and J. Smilauer (2003), An empirical model of ion composition in the outer ionosphere, *Advances in Space Research, 31*(5), P. 653–663, DOI: 10.1016/S0273-1177(03)00040-1.

Triskova, L., V. Truhlik, and J. Smilauer (2004), New advances in empirical modeling of ion composition in the outer ionosphere, *Advances in Space Research, 33*(6), P. 844–849. DOI: 10.1016/j.asr.2003.06.006.

Truhlik, V, L. Triskova, Rf. Benson, D. Bilitza, J. Grebowsky, and P.G Richards (2014), Comparison of H^+ and He^+ plasmapause locations based on the resurrected and reevaluated OGO-5 ion composition data base, *Journal of Atmospheric and Solar-Terrestrial Physics, 119*, P/ 27-34, DOI: 10.1016/j.jastp.2014.06.007.

Wilford, C.R., R.J. Moffett, and J. M. Rees (2001), Modelling helium ions in the earth's upper atmosphere, *Dynamics of Atmospheres and Oceans,, 34*(2),P. 383-397. DOI: 10.1016/S0377-0265(01)00076-8.

Zang, S., J. M. Holt, and A. M. Zalucha (2004), Midlatitude ionospheric plasma temperature climatology and empirical model based on Saint Santin incoherent scatter radar data from 1966 to 1987, *Journal of Geophyical Research: Space Physics, 109*(A11), P. 1– 9.

Zhang, S., J. M. Holt, A. P. Eyken, M. McCready, C. Amory-Mazaudier, S. Fukao, and M. Sulzer (2005), Ionospheric local model and climatology from long-term databases of multiple incoherent scatter radars, *Geophysical Research Letters, 32*(20), P.n/a-n/a, DOI: 10.1029/2005GL023603.